

AD-A105 189

HUGHES RESEARCH LABS MALIBU CA

ANISOTROPIC AND ELECTRO-OPTICAL EFFECTS IN LIQUID CRYSTALS. (U)

F/G 20/6

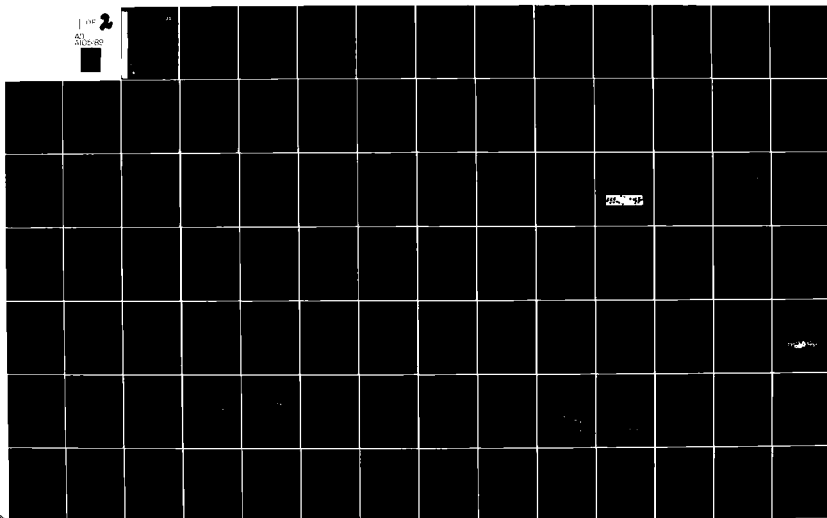
AUG 81 K D MARQUERUM

F49620-77-C-0017

UNCLASSIFIED

AFOSR-TR-81-0690

NL



AFOSR-TR- 81 -0690

18 AUG 1981

AD A105189

ANISOTROPIC AND ELECTRO--OPTICAL EFFECTS IN LIQUID CRYSTALS

J. David Margerum

Hughes Research Laboratories
3011 Malibu Canyon Road
Malibu, CA 90265

August 1981

Contract F49620-77-C-0017
Final Technical Report
For period 1 October 1976 to 30 November 1980

Prepared For
DIRECTORATE OF CHEMICAL SCIENCES
AIR FORCE OFFICE OF SCIENTIFIC RESEARCH
Bolling Air Force Base, Washington DC 20332

DTIC FILE COPY

DTIC
ELECTE
S OCT 7 1981 D

Approved for public release;
distribution unlimited.

81 10 5 000

UNCLASSIFIED

SECURITY CLASSIFICATION OF THIS PAGE (When Data Entered)

REPORT DOCUMENTATION PAGE		READ INSTRUCTIONS BEFORE COMPLETING FORM	
1. AFOSR/IR-81-0690		3. RECIPIENT'S CATALOG NUMBER	
2. TITLE (and Subtitle)		4. PERFORMING ORG. REPORT NUMBER	
ANISOTROPIC AND ELECTRO-OPTICAL EFFECTS IN LIQUID CRYSTALS		5. CONTRACT OR GRANT NUMBER(s)	
7. AUTHOR(s)		6. SECURITY CLASS. (of this report)	
J. David/Margerum		UNCLASSIFIED	
9. PERFORMING ORGANIZATION NAME AND ADDRESS		10. PROGRAM ELEMENT, PROJECT, TASK AREA & WORK UNIT NUMBERS	
Hughes Research Laboratories 3011 Malibu Canyon Road Malibu, CA 90265		2303/A1 6/10/2F	
11. CONTROLLING OFFICE NAME AND ADDRESS		12. REPORT DATE	
Air Force Office of Scientific Research/NC Building 410 Bolling AFB, DC 20332		August 1981	
14. MONITORING AGENCY NAME & ADDRESS (if different from Controlling Office)		13. NUMBER OF PAGES	
		193	
16. DISTRIBUTION STATEMENT (of this Report)		15. SECURITY CLASS. (of this report)	
Approved for public release; distribution unlimited.		UNCLASSIFIED	
17. DISTRIBUTION STATEMENT (of the abstract entered in Block 20, if different from Report)		15a. DECLASSIFICATION DOWNGRADING SCHEDULE	
18. SUPPLEMENTARY NOTES			
19. KEY WORDS (Continue on reverse side if necessary and identify by block number)			
Nematic liquid crystals Phenyl benzoate structures Conductivity dopants Viscosity of liquid crystal mixtures		Dynamic scattering mode Phenyl cyclohexanecarboxylates Conductivity anisotropy Cybotactic nematics	
20. ABSTRACT (Continue on reverse side if necessary and identify by block number)			
The effects of the average molecular length (\bar{L}) on the anisotropic properties of liquid crystal (LC) mixtures are studied systematically in three series of ester nematics: an RO-R' series of 4-alkoxyphenyl 4-alkylbenzoates, an RO-(C)R' series of 4-alkoxyphenyl 4-alkylcyclohexanecarboxylates, and an R-OR' series of 4-alkylphenyl 4-alkoxybenzoates. In each series, the flow viscosity increases substantially with the increasing \bar{L} : linearly for RO-R', exponentially for RO-(C)R',			

DD FORM 1473 EDITION OF 1 NOV 65 IS OBSOLETE

UNCLASSIFIED

SECURITY CLASSIFICATION OF THIS PAGE (When Data Entered)

1726

UNCLASSIFIED

SECURITY CLASSIFICATION OF THIS PAGE(When Data Entered)

and in between for R-OR'. In mixtures with shorter L's, the viscosities are in the sequence $R-OR' > RO-R, > RO-(C)R'$. The cybotactic-nematic character of the LCs increases with increasing L in each series, and is present at room temperature when the average number of R + R' carbons is 10 or more in the RO-R' series and 9 or more in the R-OR' and RO-(C)R' series. The conductivity anisotropy, birefringence, and density values in each series decrease with increasing L, while the dielectric anisotropy becomes relatively more negative in the RO-R' and R-OR' series and less negative in the RO-(C)R' series. The dynamic scattering (DS) threshold voltage increases markedly with L in the RO-R' and RO-(C)R' series, largely due to their decrease in conductivity anisotropy. The DS decay times in the RO-R' series increase linearly with increasing L in surface- \perp cells, while the decay times are nearly independent of L in surface- \parallel cells. The DS decay times are several times faster in the RO-(C)R' series than in the RO-R' series, although only the shorter L mixtures in the RO-(C)R' series show good DS due to the strongly cybotactic nematic character of the longer L cyclohexanecarboxylate mixtures.

The effects of \bar{L} and structure are studied on the flow viscosity of many different ester structures in RO-R' mixtures. The results include the assignment of class viscosities to 18 different types of ester LC structures. These class viscosities are used to calculate the viscosity (at 25°C) of new mixtures within about 10% of the actual values. The viscosity of new ester LCs can be estimated on the basis of structural correlations. The effect of \bar{L} of mixtures varies with the polarity of the LC structure, with the viscosity decreasing with increasing L for very polar structures.

Various factors affecting the anisotropic and DC of one ester LC mixture were investigated, including the effects of dopant structure, surface alignment, temperature, cell thickness, and type of electrical activating signal. These studies showed that the differences in the conductivity anisotropy of the dopant had the largest effect on the DS threshold voltage, however the change of threshold with temperature was more strongly affected by changes in the bend elastic constant. The optical density of scattering was found to increase linearly with the reciprocal of cell thickness. Thus, thin cells are advantageous not only because the LC response times are faster but also because the DS levels are higher and more multiplexing is possible.

UNCLASSIFIED

SECURITY CLASSIFICATION OF THIS PAGE(When Data Entered)

TABLE OF CONTENTS

SECTION		PAGE
1	INTRODUCTION AND SUMMARY	1
	A. Background and Applications	1
	B. Program Objective	2
	C. Program Summary	2
2	RESEARCH PROGRAM	5
3	RESEARCH PERSONNEL AND FACILITIES	11
	A. Personnel	11
	B. Facilities	11
4	CHRONOLOGICAL PUBLICATION BIBLIOGRAPHY	13
	REFERENCES	15
	APPENDIX I - Effects of Molecular Length of Nematic Mixtures. I. Ani- sotropic and Dynamic Scattering Properties of 4-Alkoxyphenyl 4-Alkylbenzoate Mixtures	17
	APPENDIX II - Effects of Molecular Length on Nematic Mixtures. II. Ani- sotropic and Dynamic Scattering Properties of 4-Alkoxyphenyl 4-Alkylcyclohexanecarboxylate Mixtures	47
	Appendix III - Variable Grating Mode Liquid Crystal Device for Optical Processing and Computing	79
	Appendix IV - Effects of Molecular Length on Nematic Mixtures. III. Ani- sotropic Properties of 4-Alkylphenyl 4-Alkoxybenzoate Mixtures	111

AIR FORCE OFFICE OF SCIENTIFIC RESEARCH (AFSC)
 NOTICE OF TRANSMITTAL TO DTIC
 This technical report has been reviewed and is
 approved for public release IAW AFR 190-12.
 Distribution is unlimited.
 MATTHEW J. KEEPER
 Chief, Technical Information Division

SECTION

PAGE

Appendix V — Effects of Molecular Length on Nematic Mixtures. IV. Structure Effects on Viscosity of Ester Mixtures	133
Appendix VI — Factors Affecting the Dynamic Scattering of a Nematic Ester Mixture	167

Accession For		
NTIS GRA&I	<input checked="checked" type="checkbox"/>	
DTIC TAB	<input type="checkbox"/>	
Unannounced	<input type="checkbox"/>	
Justification		
By		
Distribution/		
Availability Codes		
Dist	Avail and/or	
	Special	
A		

DTIC
SELECTE
OCT 7 1981
S D

SECTION 1

INTRODUCTION AND SUMMARY

A. BACKGROUND AND APPLICATIONS

The unique anisotropic properties of liquid crystal (LC) materials have stimulated research and development of many new electro-optical devices. In addition to the now well-known commercial uses of LC displays in watches, clocks, calculators, meters, etc., more sophisticated military applications have been developed and others are under study. For example, a LC light valve projector^{6,7} for large screen color symbology displays has been developed at Hughes for military command and control facilities. Many other LC devices are being studied for military application, and these include several devices which are based on electrohydrodynamic instabilities generated in the LC by applied fields. Two electro-optical effects based on such instabilities are the subject of the present study. One of these effects is known as the dynamic scattering (DS) mode,⁸ and the other is called the variable grating mode (VGM).^{9,10}

The DS mode involves both field alignment and ionic conduction effects and can be generated by either direct current (dc) or alternating current (ac) signals. Above the threshold voltage, the DS mode produces a turbulent motion of the LC molecules which result in a strong light scattering effect. The DS mode is being studied for several different military applications. One group of these applications is based on activating the DS in an LC display panel in which the LC is sandwiched between a substrate of semiconductor-controlled matrix electrodes and a transparent counter electrode.^{3,11-13} This MOSFET matrix display is being developed by the Hughes Aircraft Company for various possible military applications including: an integrated head-up airplane cockpit display, a helmet-mounted display, a color alphanumeric display, a flat panel status advisory board, and a missile image sighting display. An electronically-controlled reticle (cross-hair) is the basis for another group of DS applications.^{14,15} In this case the LC is sandwiched between two transparent windows, one with vertical lines of electrodes and one with horizontal electrode lines. The DS activation of the LC between selected lines results in an electronically controlled, movable reticle. This is being

developed¹⁶ as part of an improved fire-control system for tanks and armored vehicles. The VGM involves the formation of grating-like patterns in dc activated LCs of high resistivity, and the spatial frequency of these gratings varies with the magnitude of the applied voltage. Presently this is of greatest interest for new types of optical data processing techniques.^{17,18}

B. PROGRAM OBJECTIVE

The objective of this program was to study the effects of the chemical structure of liquid crystal components on the anisotropic properties of nematic mixtures, especially in regard to their electro-optical response characteristics. The program was particularly aimed at obtaining a better understanding of the effects of components on the DS mode. A similar, secondary goal was to study the effects of structure on the VGM in some of the same nematic mixtures. We chose to study ester LCs in this program because of our prior experience with phenyl benzoate LCs and dopants for DS effects.¹⁹⁻²⁴ The phenyl benzoate ester mixtures are of particular interest for DS because they are colorless and relatively stable to moisture, they can be formulated to have a negative dielectric anisotropy, they can be adequately purified for controlled doping,^{22,23} and they show good dc stability when used with redox dopants.¹⁹⁻²¹ In this program we have examined the properties and effects of many different types of ester LC components, including cyclohexanecarboxylates, biphenylcarboxylates, benzoyloxybenzoates, acyloxybenzoates, and thiobenzoates, as well as various benzoate structures.

C. PROGRAM SUMMARY

A key approach in this program was to study the effect of different ester mixtures by using the compounds in multi-component LC mixtures. This permitted us to study a wide range of structures as components in room temperature nematic mixtures with comparable clearpoint temperatures (nematic to isotropic transition). A major part of this study was centered on examining the effects of the average molecular length (\bar{L}) on the anisotropic properties of LC mixtures. This was done by using components with different length *n*-alkyl end groups and then using various combinations of these components to control the \bar{L} of the mixtures. Three different series of single class ester nematic

mixtures were studied in this manner. The central part of the structure was constant in each of the individual series, which consisted of 4-alkoxyphenyl 4-alkylbenzoates, 4-alkoxyphenyl 4-alkylcyclohexanecarboxylates, and 4-alkylphenyl 4-alkoxybenzoates. While some of the LC properties in these mixtures varied with increasing \bar{L} as might be expected by just the increased size of the aliphatic groups, other properties were more strongly affected. As the \bar{L} increased, the conductivity anisotropy decreased sharply, the viscosity increased greatly, and in one series the dielectric anisotropy completely changed sign. These changes were attributed partly to an increase in the short range smectic order, or cybotactic nematic character,²⁵⁻²⁸ of the mixtures with increasing \bar{L} . The decrease of conductivity anisotropy with \bar{L} greatly increased the threshold voltage for DS, and the increased viscosity slowed down the response time of DS in surface-perpendicular aligned cells. This showed that, in general, short \bar{L} ester mixtures are preferable for optimization of the DS effects.

Structural effects on viscosity were studied using eighteen different classes of esters as added components to standard mixtures of 4-alkoxyphenyl 4-alkylbenzoates. Short \bar{L} mixtures were used, and comparisons were made at the same \bar{L} to minimize molecular length effects. We used these data to calculate approximate viscosities for each of the eighteen classes at 25°C. These class viscosities clearly indicate many structural correlations which will be of value in predicting the effects of other related structures on viscosity. In addition, we found that the viscosity of new LC mixtures can usually be predicted within about 10% from combinations of LC esters from the 18 classes studied. The ability to predict the viscosity of mixtures is particularly valuable in the formulation of improved LC mixtures, e.g., with low viscosity as well as wide nematic temperature range, low DS threshold voltage, etc. Studies on the \bar{L} effects on viscosity were also made with several series of mixtures containing 25% of components added to standard mixtures. We found that when polar ester structures with high class viscosities are used as additives, then the viscosity can remain constant or even decrease as \bar{L} increases. This is attributed to a decrease in the association effects between the polar molecules as alkyl end groups are lengthened, which offsets the normal increase of viscosity with molecular length.

Various factors affecting the anisotropic and DS characteristics of a selected ester mixture were investigated in detail. The effects of dopant, surface alignment, signal, cell thickness, and temperature were studied. Variations in the conductivity anisotropy of the dopants had the largest effect on the DS threshold voltage at room temperature. However, cell thickness also changed the threshold slightly and had a large effect on the magnitude of the scattering obtained above threshold. Thinner cells gave higher DS levels and higher multiplexing capabilities. The optical density of scattering increased linearly with the reciprocal of cell thickness. When the temperature was increased the DS threshold voltage decreased, indicating that change in viscosity and elastic constants with temperature were more significant than the decrease in conductivity anisotropy.

The variable grating mode (VGM) electro-optical effect was also studied in various nematic LCs, primarily in regard to potential use in optical processing and computing techniques. We found that the VGM effects decreased as the \bar{L} of the ester mixtures increased, probably due to increased negative values of $\Delta\epsilon$. In studies with wedge-shaped cells, we found that the VGM effect can be obtained in much thicker cells than had previously been considered to be possible based on mechanisms that others have proposed for the effect.

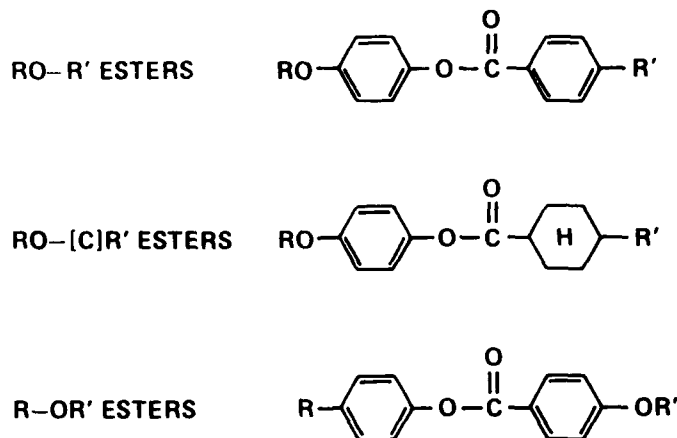
SECTION 2

RESEARCH PROGRAM

The results of this program are presented in the six papers which are included as appendices of this report. Three of these papers have been accepted for publication in Molecular Crystals and Liquid Crystals and will be published in 1981. The other three papers are drafted and will be submitted to the same journal for publication. Only some highlights of these papers are discussed here, and the appendices should be referred to for a more complete description of these studies.

There are large differences in the nematic temperature range of various individual ester LC compounds. Many have nematic ranges far above room temperature, some are monotropic, some have smectic phases, and others are isotropic at room temperature. Thus, we chose to study mixtures of ester LCs which were room-temperature nematics and had similar clearpoints. All of the LC compounds and all of the LC mixtures were prepared as part of the Hughes Research Laboratories contribution to this program. The LC mixtures were formulated either as eutectics compositions or as eutectics with limited amounts of other ester additives. Although the use of mixtures added complexity, it also enabled us to vary systematically parameters such as the average molecular length (\bar{L}) and the clearpoint. It also permitted us to study a much larger variety of ester structure than would have been feasible otherwise.

A major approach in this program was to investigate the anisotropic properties of ester LC mixtures as a function of their average molecular length (\bar{L}) and their structure. Three series of ester mixtures were studied, with each series containing only one class of LC components that differed only in the length of their R and R' n-alkyl end groups. The following RO-R', RO-[C]R', and R-OR' classes of esters were studied, using mixtures formulated to have similar nematic temperature ranges within each class.



These results are presented in Appendices I, II and IV.

The flow viscosity and the anisotropic values of refractive index, ionic conduction, and dielectric constant were studied in each series; the DS properties were studied in the RO-R' and RO-[C]R' series. In each series the viscosity increased as \bar{L} increased, as expected with these relatively low polarity structures. However, large viscosity increases in the longer \bar{L} mixtures are due to an increase in their cybotactic nematic characteristics (*i.e.*, short range smectic order). The cybotactic effect was identified by a relatively low value of conductivity anisotropy ($\sigma_{\parallel}/\sigma_{\perp}$) at 25°C along with a maximum value of $\sigma_{\parallel}/\sigma_{\perp}$ at a temperature between 25°C and the clearpoint temperature (where $\sigma_{\parallel}/\sigma_{\perp} = 1.0$). The cybotactic nematic effects were particularly strong in the longest RO-[C]R' and R-OR' mixtures, in which the $\sigma_{\parallel}/\sigma_{\perp}$ was less 1.0 at 25°C — clearly showing smectic-like properties in these nematic LCs. The effect of \bar{L} on $\sigma_{\parallel}/\sigma_{\perp}$ was most prominent in the cyclohexanecarboxylates, where the long \bar{L} RO-[C]R' mixtures had $\sigma_{\parallel}/\sigma_{\perp} = 0.5$ whereas the short \bar{L} mixtures had $\sigma_{\parallel}/\sigma_{\perp} = 1.6$. The effect of \bar{L} on dielectric anisotropy ($\Delta\epsilon = \epsilon_{\parallel} - \epsilon_{\perp}$) was different in each series; a surprisingly large effect was observed in the R-OR' series, in which $\Delta\epsilon$ was positive for short \bar{L} but negative for long \bar{L} mixtures, ostensibly due to enhanced anti-parallel molecular pairing in the long \bar{L} mixtures. In general, more favorable electro-optical DS

characteristics were found in the shorter \bar{L} mixtures of the RO-R' and RO-[C]R' series. This is because in the shorter length mixtures the conductivity dopants have greater solubility, the threshold voltages of DS are lower due to higher $\mu_{\parallel}/\mu_{\perp}$ values, and the response times are faster due to lower viscosities.

Another major area of study was the correlation of flow viscosity with the molecular structure of 18 different classes of ester LCs. (See Appendix V.) Comparative viscosity measurements were made at constant \bar{L} by adding components from a structural class to RO-R' mixtures in such a way that both the \bar{L} of the additives and the \bar{L} of the final mixture were constant. We used this data to calculate approximate class viscosities for each of the 18 structural categories, including the above RO-R', RO-[C]R' and R-OR' classes, as shown in Figure 1 (which is also in Appendix V). The class viscosities increased with structural contributions from aromatic, polar, and polarizable groups; the increases are especially large when multiple polar groups are present. These correlations are valuable in predicting the effects of structural variations on the viscosity of other classes of ester LCs. Also, we have found that our class viscosities can be used to calculate the approximate viscosity of LC ester mixtures within about 10% of their actual value. The pre-calculation of viscosity is very useful in choosing formulations for multi-component ester mixtures in which a low viscosity is desired as well as other properties such as a wide nematic temperature range. Another interesting result from our studies was the observation that the apparent viscosity of a polar ester additive decreased as the \bar{L} of the mixture (75% RO-R') increased. This effect, which is the opposite of that observed in the 100% RO-R', RO-[C]R' and R-OR' series, is attributed to a decrease in intermolecular association of the polar ester additive as longer alkyl groups are used in the mixture to increase \bar{L} . This was substantiated by observations of much higher viscosities in 100% mixture of the more polar ester than in their contributions as additives to RO-R' mixtures. A corresponding effect on molecular polarity was observed in the apparent activation energy of the ester mixtures, which were highest for those with the largest viscosity and lowest for those with the least viscosity.

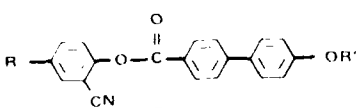
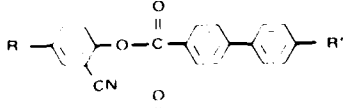
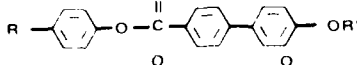
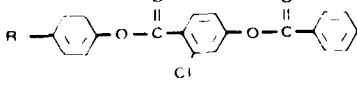
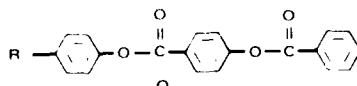
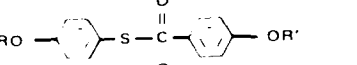
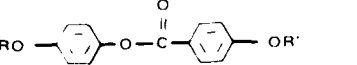
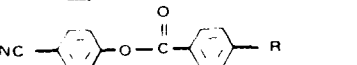
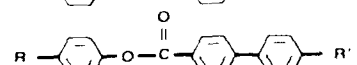
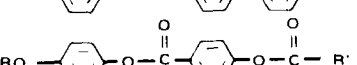
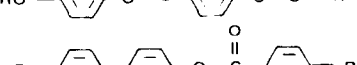
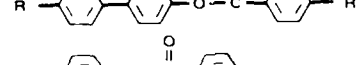
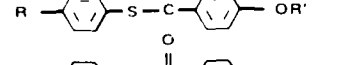
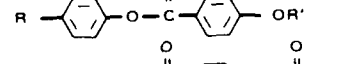
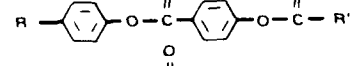
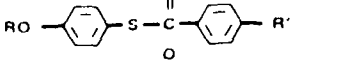
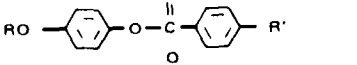
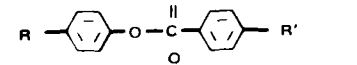
STRUCTURE CLASS	CLASS CODE	APPROX CLASS VISCOSITY (η_{CLASS})
	R(CN) ϕ OR'	310
	R(CN) ϕ R'	200
	R ϕ OR'	160
	R (Cl)OOC ϕ R'	153
	R OOC ϕ R'	130
	RO-S-OR'	92
	RO-OR'	82
	NC-R	82
	R ϕ R'	77
	RO-OOCR'	74
	R ϕ R'	65
	R-S-OR'	58
	R-OR'	55
	R-OOCR'	43
	RO-S-R'	37
	RO-R'	36
	R-R'	19
	RO-IC R'	16

Figure 1. Structure, Class Code, and Class Viscosities of LC Ester Components. (The η_{class} at 25°C Apply When 10 to 25% of these Components are used in RO-R' Mixtures with $\bar{L} \sim 22\text{\AA}$.)

Various factors affecting the anisotropic and DS characteristics of one particular eutectic mixture of LC esters were investigated, including studies on the effects of dopant structure, surface alignment, temperature, cell thickness, and type of electrical activating signal. (See Appendix VI.) These studies showed that the differences in the conductivity anisotropy of the dopant had the largest effect on the DS threshold voltage, however, the change of threshold with temperature was more strongly affected by changes in the bend elastic constant. The optical density of scattering was found to increase linearly with the reciprocal of cell thickness as did the maximum (theoretical) multiplexing capability. A minimum in the DS threshold voltage was observed in cells about 25 μm in thickness. However, thinner cells are advantageous not only because the LC response times are proportional to the square of the thickness, but also because thin cells provide higher scattering levels with DS activation. We began some systematic studies on the relationships between the structure of dopants and their conductivity anisotropy in LCs. Although some correlations were observed, more studies need to be carried out as a wider selection of organic salt structures become available.

The variable grating mode (VGM) electro-optical effect was also studied in various nematic LCs, primarily in regard to potential use in optical processing and computing techniques. We found that the VGM effects decreased as the \bar{L} of RO-R' ester mixtures increased, probably due to increased negative values of $\Delta\epsilon$. (See Appendix III.) Contrary to some literature reports, we observed VGM only with applied dc fields and not with ac activation. However, we could find no conductivity dopant which increased the VGM affect; instead they caused DS even when used in very low concentrations. In studies with wedge-shaped cells, we found that the VGM effect can be obtained in much thicker cells than had previously been considered to be possible based on mechanisms that others have proposed for the effect. The VGM appears to be propagated along the surface from the thinner to the thicker part of the wedge cell.

SECTION 3

RESEARCH PERSONNEL AND FACILITIES

A. PERSONNEL

The principal investigator for this contract was Dr. J. D. Margerum. The other major participants in these liquid crystal studies were Dr. J. E. Jensen, Mrs. A. M. Lackner, and Dr. S.-M. Wong.

The following personnel of the Exploratory Studies Department of the Hughes Research Laboratories participated in this project:

Dr. John E. Jensen (Member of the Technical Staff; PhD in Organic Chemistry).

Mrs. Anna M. Lackner (Member of the Technical Staff; BS in Chemistry).

Dr. Hong Sup Lim (Senior Member of the Technical Staff; PhD in Electrochemistry).

Dr. J. David Margerum (Senior Scientist and Head of Chemistry Section; PhD in Physical Chemistry).

Dr. Leroy J. Miller (Head of Device Materials Section; PhD in Organic Chemistry).

Gary P. Myer (Member of the Technical Staff; BS in Physics).

Dr. Michael Piliavin (Member of the Technical Staff; PhD in Physics).

Deborah S. Smythe (Member of the Technical Staff; BS in Biology).

Willis H. Smith (Research Assistant Senior).

Camille I. van Ast (Research Assistant Senior)

Scott A. Verzwylt (Member of the Technical Staff; BS in Biology).

B. FACILITIES

The facilities used in this contract were primarily those available in the Chemistry Section and the Device Materials Section of the Exploratory Studies Department, at the Hughes Research Laboratories in Malibu, California. Extensive capital equipment and all of the materials used in these studies were provided by the Hughes Aircraft Company without direct charge to the contract.

SECTION 4

CHRONOLOGICAL PUBLICATION BIBLIOGRAPHY

1. "Effects of Molecular Length on Nematic Mixtures. I. Anisotropic and Dynamic Scattering Properties of 4-Alkoxyphenyl 4-Alkylbenzoate Mixtures," J. D. Margerum, J. E. Jensen, and A. M. Lackner, Molecular Crystals and Liquid Crystals, in press (1981).
2. "Effects of Molecular Length on Nematic Mixtures. II. Anisotropic and Dynamic Scattering Properties of 4-Alkoxyphenyl 4-Alkylcyclohexanecarboxylate Mixtures," J. D. Margerum, S.-M. Wong, A. M. Lackner, and J. E. Jensen, Molecular Crystals and Liquid Crystals, in press (1981).
3. "Variable Grating Mode Liquid Crystal Device for Optical Processing and Computing," B. H. Soffer, J. D. Margerum, A. M. Lackner, D. Boswell, A. R. Tanguay, Jr., T. C. Strand, A. A. Sawchuk, and P. Chavel, Molecular Crystals and Liquid Crystals, in press (1981).
4. "Effects of Molecular Length on Nematic Mixtures. III. Anisotropic Properties of 4-Alkylphenyl 4-Alkoxybenzoate Mixtures," J. D. Margerum, S.-M. Wong, A. M. Lackner, J. E. Jensen, and S. A. Verzwylt, submitted for publication in Molecular Crystals and Liquid Crystals.
5. "Effects of Molecular Length on Nematic Mixtures. IV. Structure Effects on Viscosity of Ester Mixtures," J. D. Margerum, S.-M Wong, and J. E. Jensen, in preparation.
6. "Factors Affecting The Dynamic Scattering of a Nematic Ester Mixture," J. D. Margerum, A. M. Lackner, H. S. Lim, and J. E. Jensen, in preparation.

REFERENCES

1. G. Meier, E. Sackman, and J. G. Grabmaier, Applications of Liquid Crystals, (Springer Verlag, Berlin, 1975).
2. E. L. Williams, Liquid Crystals for Electronic Devices, (Noyes Data Corp., New Jersey, 1975).
3. J. D. Margerum, and L. J. Miller, J. Colloid and Interface Sci. 58, 559 (1977). (A review of the Electro-optical Applications of Liquid Crystals).
4. G. J. Sprokel, Editor, The Physics and Chemistry of Liquid Crystal Devices, (Plenum Press, New York, 1980).
5. T. Sasaki, Mol. Cryst. Liq. Cryst., 63, 281 (1981).
6. J. Grinberg, et al IEEE Trans. Electron Devices, ED-22, 775 (1975).
7. J. Grinberg, et al, Optical Engineering, 14, 217 (1975).
8. G. H. Heilmeyer, L. A. Zanoni and L. A. Barton, Appl. Phys. Lett., 13, 46 (1968); Proc. IEEE, 56, 1162 (1968).
9. W. Greubel and U. Wolff, Appl. Phys. Lett., 19, 213 (1971).
10. J. M. Pollack and J. B. Flannery, Liquid Crystals and Ordered Fluids, J. F. Johnson and R. S. Porter, Eds. (Plenum Press, 1974) 2, p. 557.
11. M. H. Ernstoff, A. M. Leupp, M. J. Little, and H. T. Peterson, IEEE Electron Device Conf. Digest, Washington, D. C. (Dec. 1973).
12. M. N. Ernstoff, 1975 AIAA Digital Avionics Systems Conf., Boston, Massachusetts, April 4, 1975.
13. C. P. Stephens, and L. T. Lipton, SID Internat. Sympos. Digest Techn. Papers, Beverly Hills, California, 44 (May 1976).
14. C. H. Gooch, R. Bottomley, J. J. Low, and H. A. Tarry, J. Phys, E 6, 485 (1973).
15. R. P. Farnsworth, L. W. Hill, and S. -Y. Wong, U.S. Patent 3,885,861 (May 27, 1975).
16. B. C. Gilbert, W. F. Stokes, and L. W. Hill, "Prototype Liquid Crystal Reticle", Contract DAAK70-78-C-0023, Final Technical Report, August 1979.
17. B. H. Soffer, et al, SPIE, 218, Devices and Systems for Optical Processing, p. 81.

18. P. Chavel, et al, Opt. Lett., 5, 398 (1980).
19. H. S. Lim and J. D. Margerum, Appl. Phys. Lett., 28, 478 (1976).
20. H. S. Lim and J. D. Margerum, J. Electrochem Soc., 123, 837 (1976).
21. H. S. Lim, J. D. Margerum, and A. Graube, J. Electrochem. Soc. 124, 1389 (1977).
22. M. J. Little, H. S. Lim, and J. D. Margerum, Mol. Cryst. Liq. Cryst. 38, 207 (1977).
23. J. D. Margerum, H. S. Lim, P. O. Braatz, and A. M. Lackner, Mol. Cryst. Liq. Cryst., 38, 219 (1977).
24. J. D. Margerum, "Molecular Basis for Liquid Crystal Field Effects", Contract F44620-72-C-0075, Final Technical Report, October 1976.
25. F. Rondelez, Solid State Comm. 11, 1675 (1972).
26. A. Mircea-Roussel, L. Legar, F. Rondelez, and W. H. DeJeu, J. de Physique, Colloq. C136, 93 (1975).
27. G. Heppke and F. Schnider, Z. Naturforsch 30a, 316 (1975).
28. A. DeVries, J. de Physique (Paris) Colloq. C136, 1 (1975).

APPENDIX I

EFFECTS OF MOLECULAR LENGTH ON NEMATIC MIXTURES. I. ANISOTROPIC AND DYNAMIC SCATTERING PROPERTIES OF 4-ALKOXYPHENYL 4-ALKYLBENZOATE MIXTURES*

J. David Margerum, John E. Jensen, and Anna M. Lackner

Hughes Research Laboratories
3011 Malibu Canyon Road
Malibu, California 90265

ABSTRACT

The properties of nematic mixtures of 4-alkoxyphenyl 4-alkylbenzoates are studied as a function of their average molecular length (\bar{L}). The \bar{L} 's of the mixtures vary between 20.46 and 27.14 Å, but they all have clearpoints in the 51 to 58°C range. The flow viscosity increases linearly with \bar{L} . The dielectric constant, refractive index, birefringence, and density decrease linearly with \bar{L} , and the dielectric anisotropy becomes more negative. With tetrabutylammonium tetraphenylboride added as a salt dopant, the conductivity anisotropy ($\sigma_{\parallel}/\sigma_{\perp}$) decreases with increasing \bar{L} , and the dynamic-scattering (DS) threshold voltage increases correspondingly. The effect of \bar{L} on the DS decay time (τ_D) is highly dependent on the surface alignment. In surface-1 cells, τ_D increases strongly with \bar{L} , while in surface-1 cells, τ_D decreases slightly with increasing \bar{L} . The temperature dependence of $\sigma_{\parallel}/\sigma_{\perp}$ indicates that the longer \bar{L} mixtures, with about ten or more total alkyl carbons from both end groups, have cybotactic nematic characteristics.

*Presented in part at the Symposium on the Physics and Chemistry
of Liquid Crystal Devices, San Jose, CA, February 7-8, 1979.

INTRODUCTION

Multicomponent liquid crystal (LC) mixtures are often used to widen the temperature range of nematics used in electrooptical device applications. Although there is an increasing amount of information being published on the properties of nematic mixtures of positive dielectric anisotropy for use in polarization switching displays, there is much less information on the properties of nematic mixtures of negative dielectric anisotropy for use in dynamic scattering (DS) displays.^{1,2} We are particularly interested in the use of para-substituted phenyl benzoate mixtures as relatively stable nematics for both dc- and ac-activated DS devices.³⁻⁶ Therefore, we have begun a series of studies to investigate systematically the relationships between the structure of ester LC components and the properties of their mixtures. The present study is designed specifically to examine the effect of the average molecular length of 4-alkoxyphenyl 4-alkylbenzoate mixtures on their viscosity, conductivity anisotropy, dielectric anisotropy, DS threshold voltage, and DS response time.

EXPERIMENTAL

The phenyl benzoate components of the LC mixtures are prepared by reacting the appropriate p-alkoxyphenols and p-alkylbenzoyl chlorides. Whenever possible, the reactants are obtained commercially (Eastman or Aldrich). The esters are purified by several recrystallizations and are checked for purity by thin-layer chromatography and by liquid chromatography (Waters Assoc. Model ALC-202/401, with a microporasil column). We estimate by these methods that the impurity content is less than 0.5% in all of the esters and is less than 0.1% in most of

them. In all cases, the materials have virtually no ionic impurities, and the resistivities of the undoped mixtures are greater than $10^{11} \Omega\text{-cm}$ at room temperature. The heat of fusion (ΔH_f), melting point (mp), and clearpoint (clpt) are obtained by differential scanning calorimetry (DSC) using a Mettler TA2000B thermal analysis system. The transition temperatures correspond to the lower part of any range obtained from the DSC slope extrapolated back to the baseline. A computer program is used to calculate the mole fraction of selected components for eutectic mixtures by applying the Schroeder Van Laar equation.^{7,8}

The flow viscosity is measured in calibrated (20 to 100 cS range) Cannon-Ubbelohde-type viscometer tubes (1.03-mm capillary bore size) held in a temperature-controlled water bath. Density measurements are made in calibrated pycnometer tubes. The refractive index and birefringence are measured with a Leitz-Jelly micro-refractometer. The dielectric anisotropy and conductivity anisotropy are measured using a previously described apparatus,⁵ modified by installation of a thermally controlled copper block in the cavity to achieve better temperature control over a wider range. This required a larger magnetic pole spacing than used previously, which resulted in a 7-kG magnetic field. An LC thickness of 229 or 503 μm is used. Samples are doped with tetrabutylammonium tetraphenylboride (TBATPB) by adding 0.1% of this salt, warming to dissolve, and then filtering the LC through a 0.2- μm filter after letting it cool overnight. The DS threshold measurements are taken in transmission with unpolarized green light and an acceptance angle of $\pm 0.5^\circ$ at the detector of the optical system.⁵ The cells are made with 3.2-mm-thick glass plates, with the LC contained by a

25.4- μm -thick polyester film perimeter spacer. These cells have indium tin oxide (ITO) conductive glass surfaces overcoated with SiO deposited at a 30° angle to produce surface- \parallel alignment of the LCs. The threshold voltages are obtained by extrapolating the initial steep decrease in transmission back to the baseline, using frequencies of 30 Hz. The decay times are taken from 10% to 90% T after activation at 30 V. To improve the reproducibility of decay times, measurements are made using thicker (12.7 mm) optical flats with an SiO_2 -overcoated ITO surface and deposited pads of SiO_x in the corners as spacers. One set of these flats is ion-beam etched at a shallow angle for surface- \parallel alignment,⁹ while a second set is spin-coated with an aqueous polyvinyl alcohol solution, baked in an oven, and rubbed gently for surface- \parallel alignment. The spacer thickness of the first cell is 15.86 μm and of the second is 15.43 μm . These cells are filled with doped LC, and the DS decay times are measured in a thermostated box. A third set of optical flats with a 15.90- μm spacing is used for surface- \perp alignment by first bonding a long chain alcohol ($n\text{-C}_{18}\text{H}_{37}\text{OH}$) on the SiO_2 coating.¹⁰ The LCs align perpendicular to the surface in this cell with very small off-normal tilt angles ($<0.5^\circ$). Undoped LCs are used in this third cell for measurements of the Fréedericks transition threshold voltage at 1 kHz, while doped LCs are used for DS decay time studies after activation with voltages at 30 Hz.

The k_{11} elastic constants are determined from capacitance versus voltage curves on LC cells using an apparatus similar to that described by Meyerhofer.¹¹ The cells are made using ITO-coated glass plates (3.2 mm thick) with a 25.4- μm -thick polyester film perimeter spacer

arranged to give an active area of 6.45 cm^2 . The ITO is overcoated with 2000 \AA of SiO_2 , and surface-1 alignment is obtained by treatment with $n\text{-C}_{22}\text{H}_{45}\text{OH}$. The tilt angles are less than 0.5° . The measuring signal is 25 mV at 10 kHz, and the alignment bias control is variable up to $30 \text{ V}_{\text{rms}}$ at 75 or 450 Hz. An empty cell is used to correct for the capacitance of the non-active area. The electronic components include a PAR Model 124A as a signal source and a lock-in amplifier, a Kiethley 427 current amplifier, and a Krohn-Hite 3322 variable filter (to help filter out the bias frequency).

RESULTS AND DISCUSSION

LC Components and Mixtures

The thermal properties of the phenylbenzoate compounds used in these mixtures are shown in Table I, where R and R' are n-alkyl groups as shown by the general structure in Figure 1a. The melting points and heats of fusion from Table I are used to calculate the eutectic mixtures shown in Table II. None of the components are known to have any smectic phases. In addition to the letter designations (A, B, etc.) used for the mixtures in this paper, the specific Hughes identifications (HRL-2N42, etc.) are also shown. The latter are cited in other publications.^{12,13} The molecular length (L) of each compound is measured from the end-to-end distance in CPK models, as indicated in Figure 1b. A fully extended configuration is used, with a twist angle of about 30° between the aromatic planes as described by Neubert et al.¹⁴ Table III shows the average molecular length (\bar{L}) of the mixtures, and both the calculated and the observed nematic ranges. Several features are worth noting regarding the composition of these different length eutectic mixtures. For one thing, the compound 10-1 is used as a pseudo-nematic

component even though it has not been observed to be an LC. Also, contrary to the guideline of making eutectic mixtures in which each component differs by more than 20% in overall molecular length,⁸ we mix some components of the same, or nearly the same, length. This is done when the R and R' end groups of one component are substantially different from those of another component (e.g., 20-3 with 40-1, 20-5 with 40-3, 40-6 with 60-5, and 60-5 with 80-3).

No systematic variation is made in the components with regard to the odd/even number of end group carbons, nor to the end of the molecule on which the longest alkyl groups are used. (However, longer alkyl groups and longer length components are not used in order to avoid smectic components.) Although the properties of the mixtures are probably affected by such end group effects in addition to being affected by the average length, we believe that the general trends of the \bar{L} effects that we report below are nevertheless valid.

Refractive Indices, Density, and Dielectric Constant

The refractive index and birefringence of the mixtures decrease linearly with increasing molecular length, as shown in Figure 2. The effect of the increasing length is to decrease the molecular polarizability of the molecules as the alkyl end groups are lengthened and to dilute the polarizability effect due to the rest of the molecule. The density of the mixtures also decreases with increasing average molecular length due to the increasing percentage of alkyl groups as compared with the aromatic ester group. A similar trend is also shown in Figure 2 for the dielectric constant (ϵ_1) variation with \bar{L} , as longer

alkyl groups dilute the effects of the more polar groups in the molecules. In these mixtures, the value of ϵ_1 at 25°C decreases by about 0.15 units per added methylene group.

Viscosity

The flow viscosity (η) of the ester mixtures is studied as a function of temperature between 20 and 50°C. These flow viscosities should correspond approximately to the viscosity along the LC director,¹⁵ corresponding to the Helfrich viscosity η_2 (or the Miesowicz viscosity η_B). Each mixture has as a linear relationship between $\log \eta$ and T^{-1} (in $^{\circ}\text{K}^{-1}$), as shown in Figure 3. These viscosities are the same with or without the addition of the TBATPB salt dopant. The viscosities at 25 and 45°C are plotted against the average molecular length in Figure 4. The viscosity increases linearly with the average length, and the viscosity changes substantially over the range of lengths studied. The clearpoints of all the mixtures are within a range of about 6°C, and there is no obvious effect of their clearpoint differences on the viscosities. The results at 25°C in Figure 4 correspond to about a 1.8 cP increase in viscosity per each additional methylene group in the average molecular length of these ester mixtures. At 45°C, the increase in viscosity is about 0.9 cP per added methylene group.

Conductivity Anisotropy

The conductivity anisotropy ($\sigma_{\parallel}/\sigma_{\perp}$) of TBATPB in each ester mixture is shown as a function of temperature in Figure 5. We found that at room temperature the $\sigma_{\parallel}/\sigma_{\perp}$ values of TBATPB in mixture A are constant with variations in the resistivity of the sample, and we have previously

observed this same type of consistency of $\sigma_{\parallel}/\sigma_{\perp}$ with the concentration of TBATPB in other liquid crystals.^{5,16} Thus, although the solubility of TBATPB decreases steadily from mixture A to F and thereby increases their resistivities, we believe that the $\sigma_{\parallel}/\sigma_{\perp}$ values of the different mixtures can be compared with one another. The general trend at room temperature is that the $\sigma_{\parallel}/\sigma_{\perp}$ value decreases as the molecular length of the mixture increases. As the temperature is increased, samples A-D show decreased $\sigma_{\parallel}/\sigma_{\perp}$ values, as expected in nematic LCs because of the decreasing order parameter. However, in mixtures E and F, the $\sigma_{\parallel}/\sigma_{\perp}$ values go through a maximum between 20 and 50°C. This general type of behavior in other nematics has been reported¹⁷⁻¹⁹ to be due to cybotactic nematic²⁰ characteristics (i.e., short range smectic order in a nematic LC). In our phenyl benzoate mixtures, this is observed when the average length is 25.9 Å and longer, corresponding to an average of about 10 or more carbons from the combination of both alkyl end groups in the molecules (see Table III). It is interesting that none of the pure components in these mixtures is reported to be a smectic and that our DSC analysis also does not show any smectic phase in the components or their mixtures.

Because $\sigma_{\parallel}/\sigma_{\perp}$ is an anisotropic ratio that depends on the order parameter, we show in Figure 6 comparisons of the mixtures at two values of reduced temperature. For these mixtures, the lower temperature of $T = 0.91 T_c$ is near 25°C, while the higher temperature of $T = 0.96 T_c$ is near 42°C. At both temperatures, the $\sigma_{\parallel}/\sigma_{\perp}$ values decrease approximately linearly as the \bar{L} 's of the mixtures increase. This may be due to several factors. At the lower temperature, the increasing cybotactic

nematic character with increasing \bar{L} appears to be important. However, since similar effects are observed at 42°C, where the cybotatic effects should be less significant, other factors are probably involved. Qualitatively, we ascribe these other factors to the increasing percentage of the relatively flexible alkyl end groups compared to the more rigid central phenyl benzoate structure. The percentage of alkyl group length goes from 31.5% in mixture A up to 48.6% in mixture F. The transverse nematic flow viscosities (η_1 and η_3) probably do not increase as rapidly with \bar{L} as η_2 does. Similarly, the σ_1 values probably do not decrease as rapidly with \bar{L} as does σ_3 , thus causing a decrease in σ_3/σ_1 .

Dielectric Anisotropy

The effects of temperature on the dielectric constants and dielectric anisotropy are shown for each mixture in Figures 7 and 8. The values of ϵ_1 decrease almost linearly with increasing temperature. On the expanded scale used in Figure 8, it can be seen that, although small in magnitude, the $-\Delta\epsilon$ values in each mixture go through a maximum in the 35 to 40°C range. This is most pronounced with the shorter mixtures. In addition, at a given reduced temperature, the $\Delta\epsilon$ values become more negative as the average molecular length increases, as shown by the approximately linear plots in Figure 9. Both the temperature effect and the molecular-length effect on $\Delta\epsilon$ are unexpected. We can only speculate that there is some type of weak intermolecular interaction that causes $\Delta\epsilon$ to be less negative in the shorter mixtures, and that this interaction decreases as the samples are heated. Such a molecular interaction might also decrease as the cybotatic nematic packing increases in the longer mixtures.

Field Effect Transition and Elastic Constants

The threshold voltage for the dielectric field-effect realignment (no conductive dopant) of the LC mixtures in surface-1 cells is shown in Figure 10, from optical birefringence measurements. This threshold voltage decreases with increasing \bar{L} of the mixtures. The effect of \bar{L} on the values of the bend elastic constant k_{33} are also shown in Figure 10, as calculated from the expression:

$$\left(V'_{th}\right)_{FE} = \pi \left(\frac{k_{33}}{\epsilon_o |\Delta\epsilon|} \right)^{1/2}$$

Dynamic Scattering

The threshold voltage (V_{th}) for DS for the TBATPB-doped mixtures increases sharply with increasing average molecular length, as shown in Figure 11. This effect appears to be due primarily to the $\sigma_{||}/\sigma_{\perp}$ values of these mixtures, as indicated by our observation that a Helfrich-type plot of V_{th}^{-2} versus $(\sigma_{||}/\sigma_{\perp})^{-1}$ is approximately linear, although such a linear relationship should actually be applicable only if all of the LC properties except $\sigma_{||}/\sigma_{\perp}$ are constant.⁵ Since we have found that k_{33} , ϵ , $\Delta\epsilon$, and η all vary with \bar{L} , this observation indicates that the $\sigma_{||}/\sigma_{\perp}$ values probably have a dominant effect on V_{th} when comparing these mixtures at room temperature in surface-1 cells.

The results of our DS decay time studies at 25°C are shown in Figure 12. For comparison, the decay times are all corrected to a nominal cell thickness of 16.0 μm , using a factor of $16^2/\ell^2$. (As indicated in the experimental section, the actual thicknesses, ℓ , of the surface-1 cells are 15.86 and 15.43 μm , while for the surface-1 cell

it is 15.90 μm .) The activated voltages used are high enough to give at least 90% scattering in our optical system without causing secondary scattering. The decay times are all compared from the same relative transmission changes of 10%T to 90%T. The effect of \bar{L} on the decay time is strikingly dependent on the initial LC surface alignment. The τ_D of the LC cells with surface- \parallel LC alignment decreases slightly with increasing \bar{L} (even though the flow viscosity increases appreciably), and it is independent of the alignment method. On the other hand, the τ_D of the surface- \perp cells increases with \bar{L} even more rapidly than the increase in the LC flow viscosity with \bar{L} . As shown in Figure 12, the ratio $(\tau_D)_\perp / (\tau_D)_\parallel$ goes from about 1.5 at short \bar{L} up to about 2.5 at long \bar{L} values.

The decay time of DS cells has been reported to be directly proportional to viscosity² and to fit the equation: $\tau_D = C\eta\ell^2/k$, where C is a constant characteristic of the LC, η is the viscosity, and k is an elastic constant.¹ Similarly, the decay time for Williams domains has been expressed²¹ by $\tau_D' = \ell^2\eta'/4\pi^2k$, where η' is a "viscosity parameter" and k is the appropriate elastic constant." In our series of mixtures at 25°C, $(\tau_D)_\parallel$ is nearly independent of η , while $(\tau_D)_\perp$ is directly proportional to η (where our $\eta \approx \eta_2$). On the other hand, the variation of the ratio η_2/k_{33} with \bar{L} is not directly proportional to the change of either $(\tau_D)_\parallel$ or $(\tau_D)_\perp$ with the \bar{L} of these mixtures.

CONCLUSIONS

Comparisons of *p*-alkoxyphenyl *p*-alkylbenzoate nematic mixtures with similar clearpoints show that several of their properties vary

linearly with the average molecular length of the mixtures: the flow viscosity increases with \bar{L} , while the refractive index, birefringence, density, conductivity anisotropy, dielectric constants, and dielectric anisotropy decrease as \bar{L} increases. The temperature dependence of $\sigma_{\parallel}/\sigma_{\perp}$ shows that mixtures with a total average of more than 10 carbon atoms from both aliphatic end groups have cybotactic nematic characteristics. The shorter length mixtures are advantageous for DS applications primarily because they have higher $\sigma_{\parallel}/\sigma_{\perp}$ values, lower threshold values for DS, and better solubility of conductive dopants than in the longer \bar{L} mixtures. In surface-I cells, \bar{L} has very little effect on the DS decay time at 25°C; however, in surface-I cells, the decay time increases steeply (linearly) with \bar{L} . Thus, in surface-I cells, the shorter \bar{L} mixtures are advantageous for faster decay times.

ACKNOWLEDGMENTS

We are indebted to the Directorate of Chemical Sciences, Air Force Office of Scientific Research, Contract F49620-77-C-0017, for partial financial support of this research; to S.-M. Wong and C.I. VanAst for assistance in synthesis; and to W.H. Smith, Jr., for assistance in the DSC measurements.

REFERENCES

1. L.T. Creagh, Proc. IEEE 61, 814 (1973).
2. U. Bonne and J.P. Cummings, IEEE Trans. Elec. Devices, ED-20, 962 (1973).
3. H.S. Lim and J.D. Margerum, Appl. Phys. Lett. 28, 478 (1976).
4. J.D. Margerum and L.J. Miller, J. Colloid and Interface Sci. 58, 559 (1977).
5. J.D. Margerum, H.S. Lim, P.O. Braatz, and A.M. Lackner, Mol. Cryst. Liq. Cryst. 38, 219 (1977).
6. H.S. Lim, J.D. Margerum, and A. Graube, J. Electrochem. Soc. 124, 1389 (1977).
7. E.C-H. Hsu and J.F. Johnson, Mol. Cryst. Liq. Cryst. 20, 177 (1973).
8. D. Demus, C. Fietkau, R. Schubert, and H. Kehlen, Mol. Cryst. Liq. Cryst. 25, 215 (1974).
9. M.J. Little, H.L. Garvin, and L.J. Miller, Liquid Crystal and Ordered Fluids, Vol. 3, p. 497, J.E. Johnson and R.S. Porter, eds (Plenum Pub. (1978).
10. L.J. Miller, J. Grinberg, G.D. Myer, D.S. Smythe, and W.H. Smith, ibid, p. 513 (1978).
11. D. Meyerhofer, J. Appl. Phys. 46, 5084 (1975).
12. B.H. Soffer et al., Proc. SPIE 81, 218 (1980).
13. B.H. Soffer et al., Paper I-17, 8th International Liquid Crystal Conference, Kyoto, Japan, July 1980.
14. M.E. Neubert, L.T. Carlino, R. D'Sidocky, and D.L. Fishel, Liq. Cryst. and Ordered Fluids, (Plenum Press, N.Y. 1974), Vol. 2, p. 293, J. Johnson and Porter, eds.

15. A.E. White, B.E. Cladis, and S. Torza, Mol. Cryst. Liq. Cryst. 43, 13 (1977).
16. J.D. Margerum, A.M. Lackner, and H.S. Lim, Paper DP28, 7th International Liq. Cryst. Conf., Bordeaux, France, 1978.
17. F. Rondelez, Solid State Comm. 11, 1675 (1972).
18. A. Mircea-Roussel, L. Legar, F. Rondelez, and W.H. DeJeu, J. de Physique, Colloq. C136, 93 (1975).
19. G. Heppke and F. Schenider, Z. Naturforsch 309, 316 (1975).
20. A. DeVries, J. de Physique (Paris) Colloq. C136, 1 (1975).
21. G. Meier, E. Sackman, and J.G. Grabmaier, Application of Liquid Crystals (Springer Verlag, Berlin, 1975), p. 16.

TABLE I
Thermal Properties of Components

Component			mp, °C		Clpt., °C		ΔH _f ,
RO	R'	Code	Obs.	Lit.	Obs.	Lit.	kcal/mole
CH ₃ O	CH ₃	10-1	96.2	97 ^a	(10) ^b	----	7.20
C ₂ H ₅ O	C ₃ H ₇	20-3	75.7	75.5 ^c	68	68.5 ^c	6.72
C ₂ H ₅ O	C ₅ H ₁₁	20-5	62.8	62.1 ^c	63	63.4 ^c	7.49
C ₄ H ₉ O	CH ₃	40-1	72.9	----	53	----	7.81
C ₄ H ₉ O	C ₃ H ₇	40-3	70.7	71.3 ^c	61	59.0 ^c	8.15
C ₄ H ₉ O	C ₆ H ₁₃	40-6	40.0	39 ^d	49	49 ^d	8.42
C ₆ H ₁₃ O	C ₃ H ₇	60-3	51.8	51.6 ^c	57.4	58.5 ^c	5.52
C ₆ H ₁₃ O	C ₄ H ₉	60-4	29	30.2 ^c	48	48.4 ^c	4.20
C ₆ H ₁₃ O	C ₅ H ₁₁	60-5	40.9	40 ^e	59.3	59 ^e	5.77
C ₈ H ₁₇ O	C ₃ H ₇	80-3	51.8	51.0 ^c	56.8	59.1 ^c	6.12
C ₈ H ₁₇ O	C ₆ H ₁₃	80-6	44.9	46 ^f	55.6	57 ^f	8.12

^aT.I. Gnilomedova et al., Zh. Prikladnoi Khimii, 49, 1337 (1976);

^bVirtual nematic clpt.; ^cM.E. Neubert et al., Liq. Cryst. and Ordered Fluids (Plenum Press, N.Y., 1974), Vol. 2, p. 293, J.F. Johnson and R.S. Porter, Eds.; ^dR. Steinstrasser, Z. Naturforsch 27b, 774 (1972);

^eJ.P. Van Meter and B.H. Klanderman, Mol. Cryst. Liq. Cryst. 22, 271 (1973); ^fGDR Patent 86269.

TABLE II
Composition of Liquid-Crystal Mixtures

Compound		Mole Fraction in Mixtures				
Code ^a	Length, Å	A	B	D	E	F
10-1	16.20	0.112	0.073	----	----	----
20-3	19.67	0.222	0.148	----	----	----
20-5	22.21	0.283	0.180	0.240	----	----
40-1	19.61	0.191	0.119	----	----	----
40-3	21.78	0.192	0.117	0.160	0.120	----
40-6	25.81	----	0.364	----	0.375	----
60-3	24.44	----	----	----	----	0.249
60-4	25.78	----	----	0.601	----	----
60-5	27.03	----	----	----	0.504	0.331
80-3	26.84	----	----	----	----	0.213
80-6	30.85	----	----	----	----	0.207
HRL Mixture Numbers		2N42	2N43	2N44	2N46	2N48
^a See TABLE I.						

TABLE III
Average Length and Nematic Range of RO-R' Mixtures^a

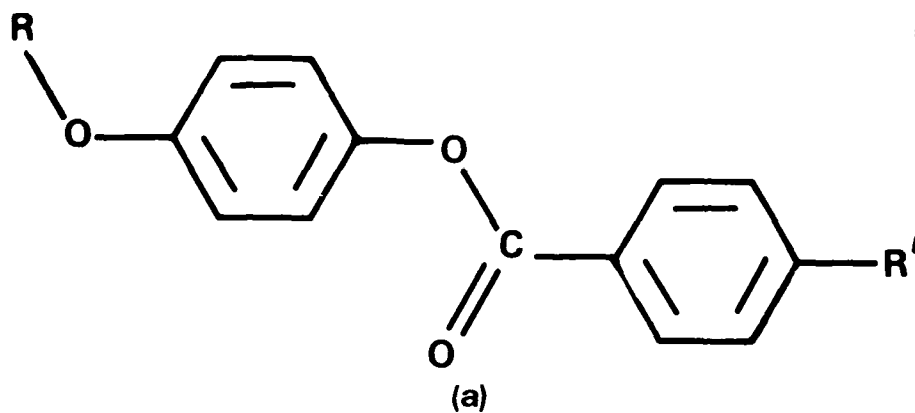
Mixture	Average Length (\bar{L}), Å	Average Number of R+R' Carbons	mp, °C		Clpt., °C	
			Calc.	Obs.	Calc.	Obs.
A	20.39	5.61	28.8	5.3	57.0	57.7
B	22.37	7.21	18.2	-5.8	54.4	52.4
C ^b	23.36	8.20	----	2.4	57.2	55.6
D	24.31	8.82	24.9	-7.8	54.0	51.4
E	25.92	10.12	18.8	16.1	54.6	55.0
F	27.14	11.50	6.1	18.0	57.4	56.3

^aCalculated as eutectic compositions, except Mixture C, with
 \bar{L} calc. from mole fractions of components of various L's.

^bEqual weight percent of A and F.

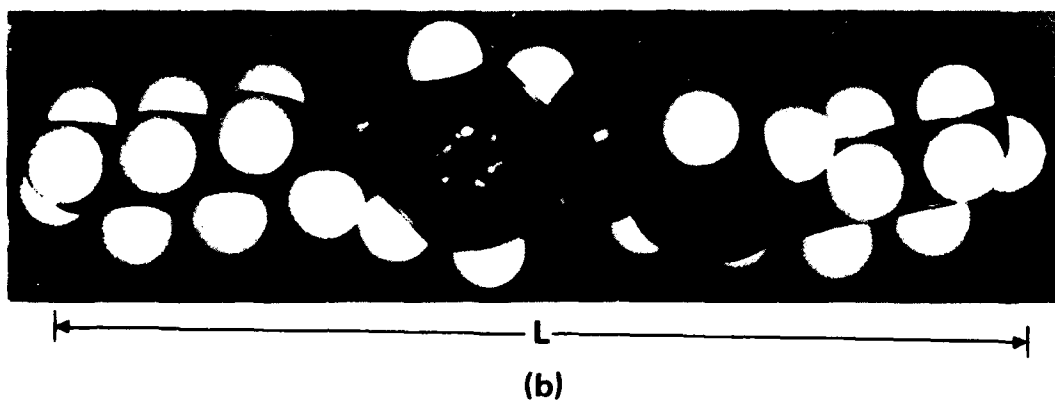
FIGURE CAPTIONS

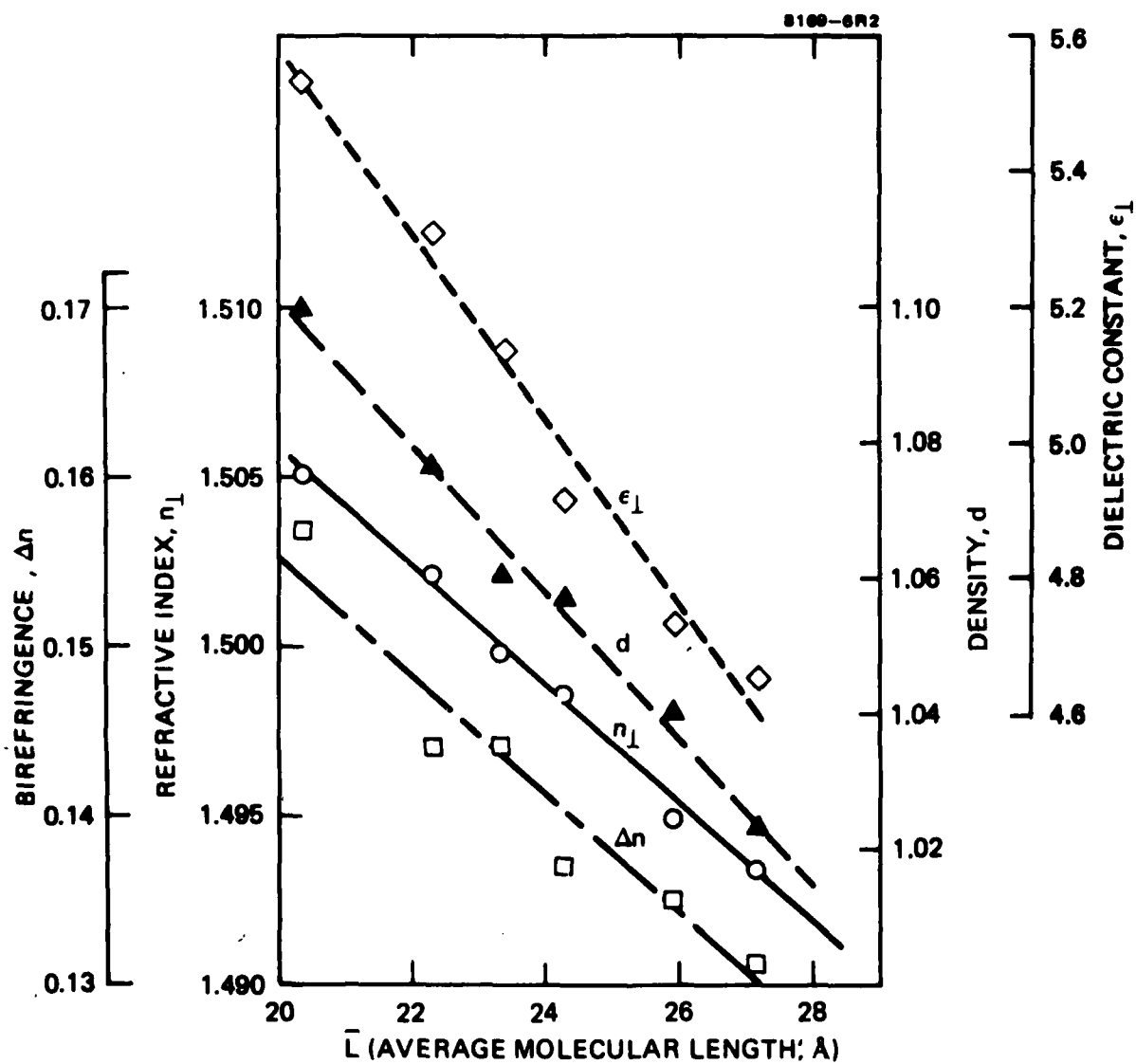
1. (a) General structure of LC mixture components.
(b) Model of 4-hexyloxyphenyl 4-butylbenzoate (60-4) showing the molecular length ($L = 25.78 \text{ \AA}$) used.
2. Effect of \bar{L} on refractive index (n_l at 23.5°C , 589 nm), birefringence (Δn at 22.0°C , 589 nm), density (d at 25.0°C), and dielectric constant (ϵ_l at 25.0°C).
3. Viscosity of RO-R' ester LC mixtures as a function of temperature.
4. Flow viscosity of RO-R' ester mixtures A-F as a function of their \bar{L} .
5. Conductivity anisotropy of TBATPB in RO-R' ester mixtures as a function of temperature.
6. Effect of \bar{L} of mixtures on their conductivity anisotropy at two reduced temperatures.
7. Dielectric constant (ϵ_l) of RO-R' mixtures as a function of temperature.
8. Dielectric anisotropy of RO-R' mixtures as a function of temperature.
9. Effect of \bar{L} of mixtures A-F on their dielectric anisotropy at two reduced temperatures.
10. Effect of \bar{L} of RO-R' mixture on the dielectric field effect transition and k_{33} at 25°C .
11. Variation of the threshold voltage for DS with \bar{L} of the mixtures. (Cells are $\sim 25 \text{ }\mu\text{m}$ thick and have surface- \parallel alignment.)
12. Effect of \bar{L} on DS decay times. Surface- \parallel cells: \circ - ion beam etched SiO_2 , \square - rubbed PVA; surface- \perp cells: Δ - C_{18} alcohol treated SiO_2 .

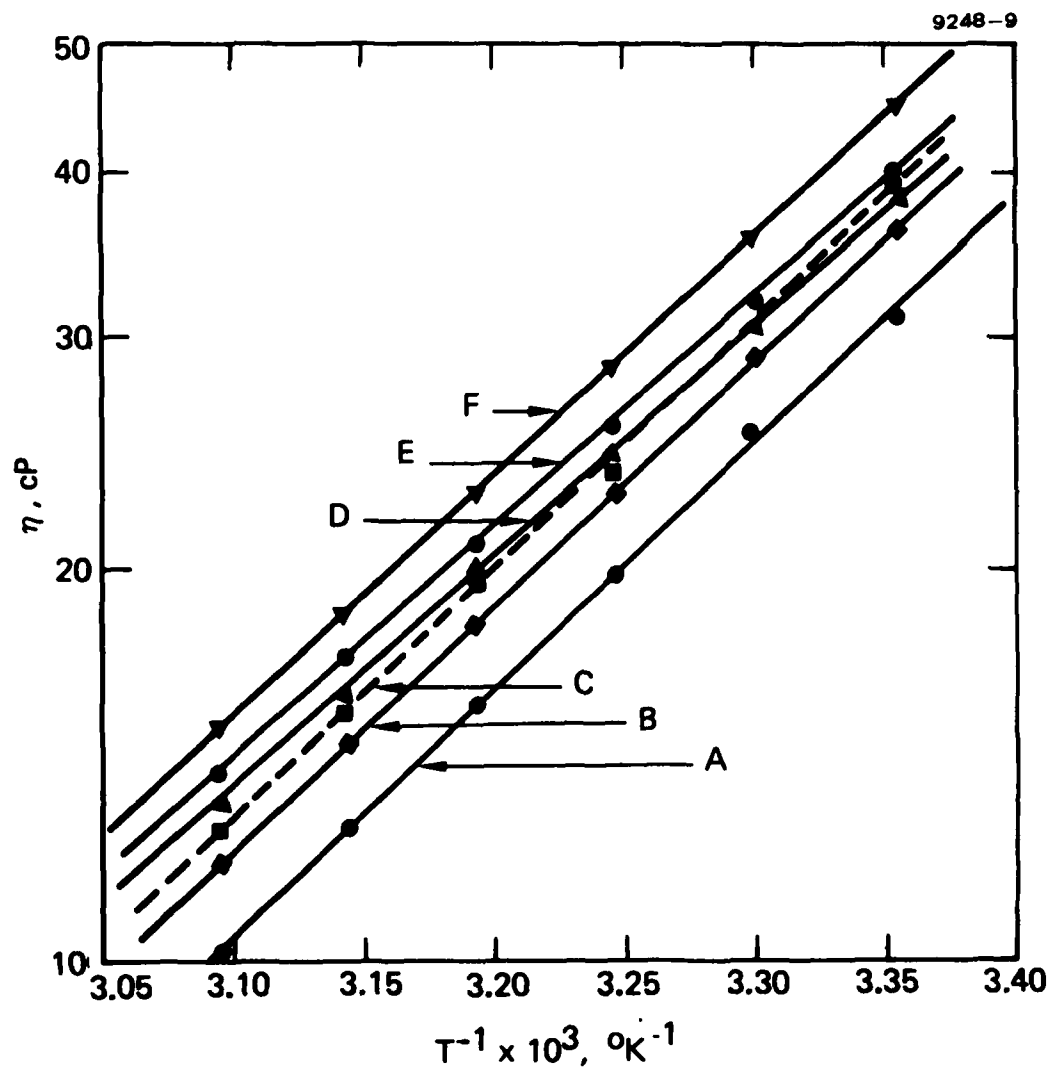


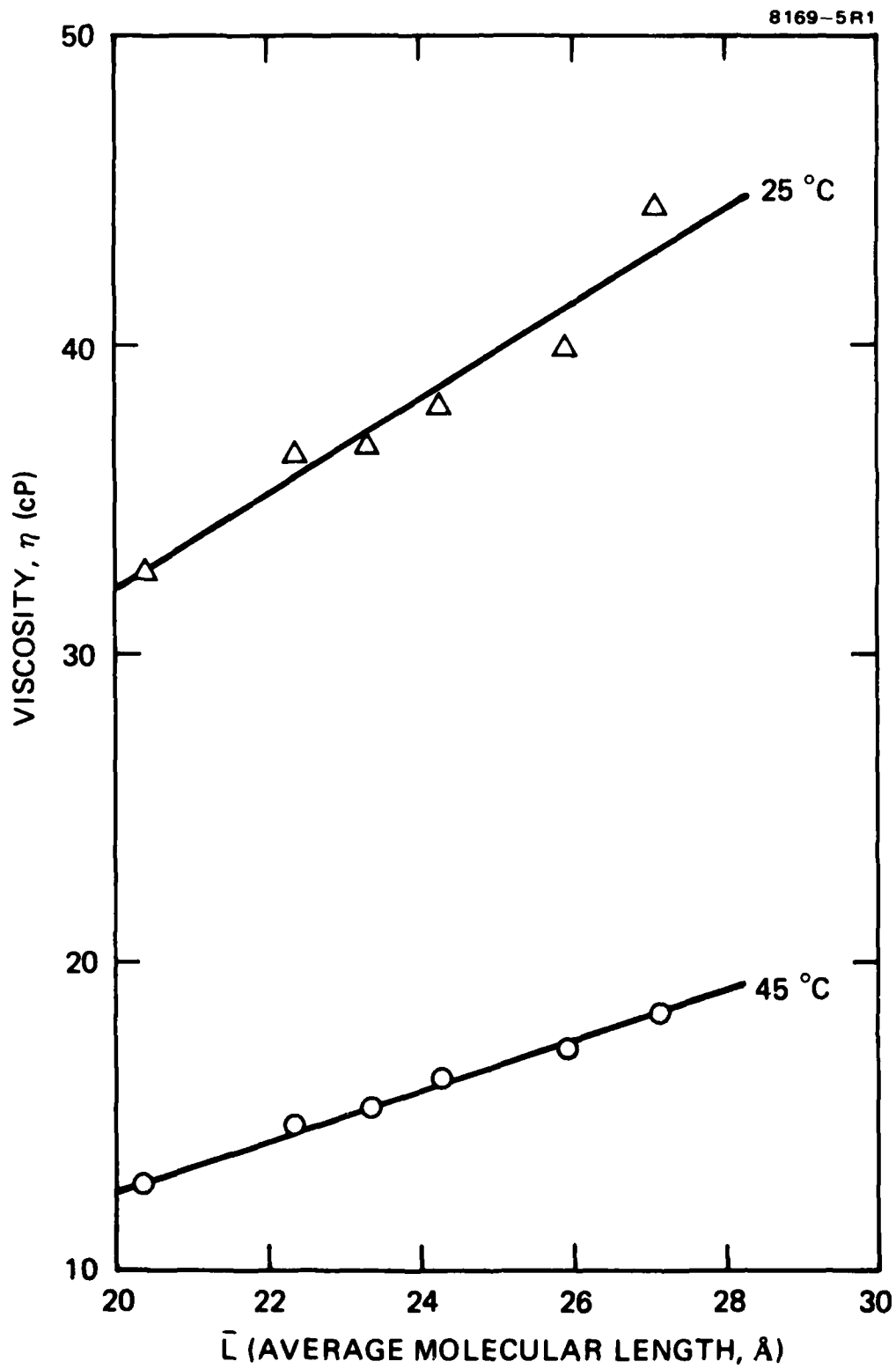
M13113

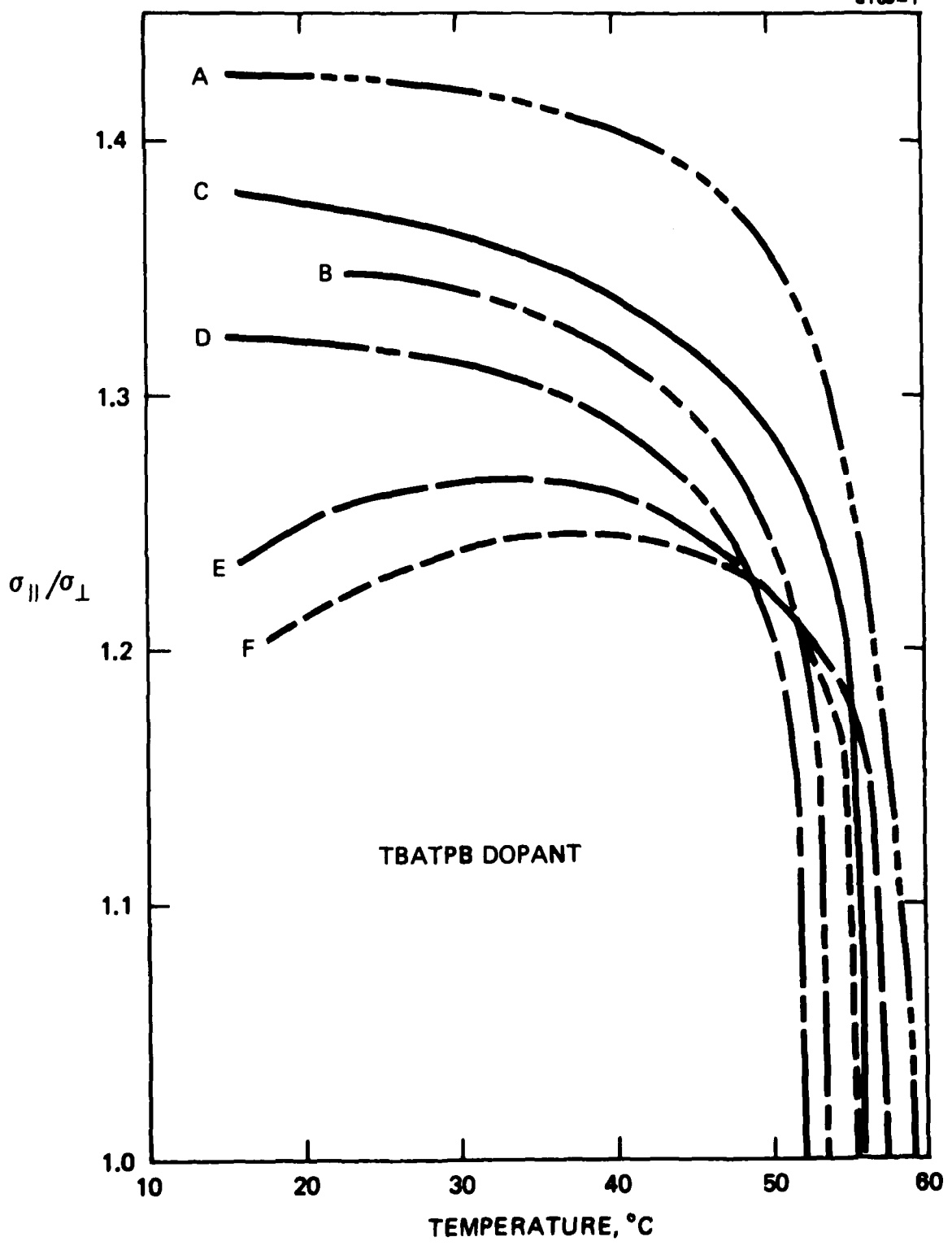
9248-1

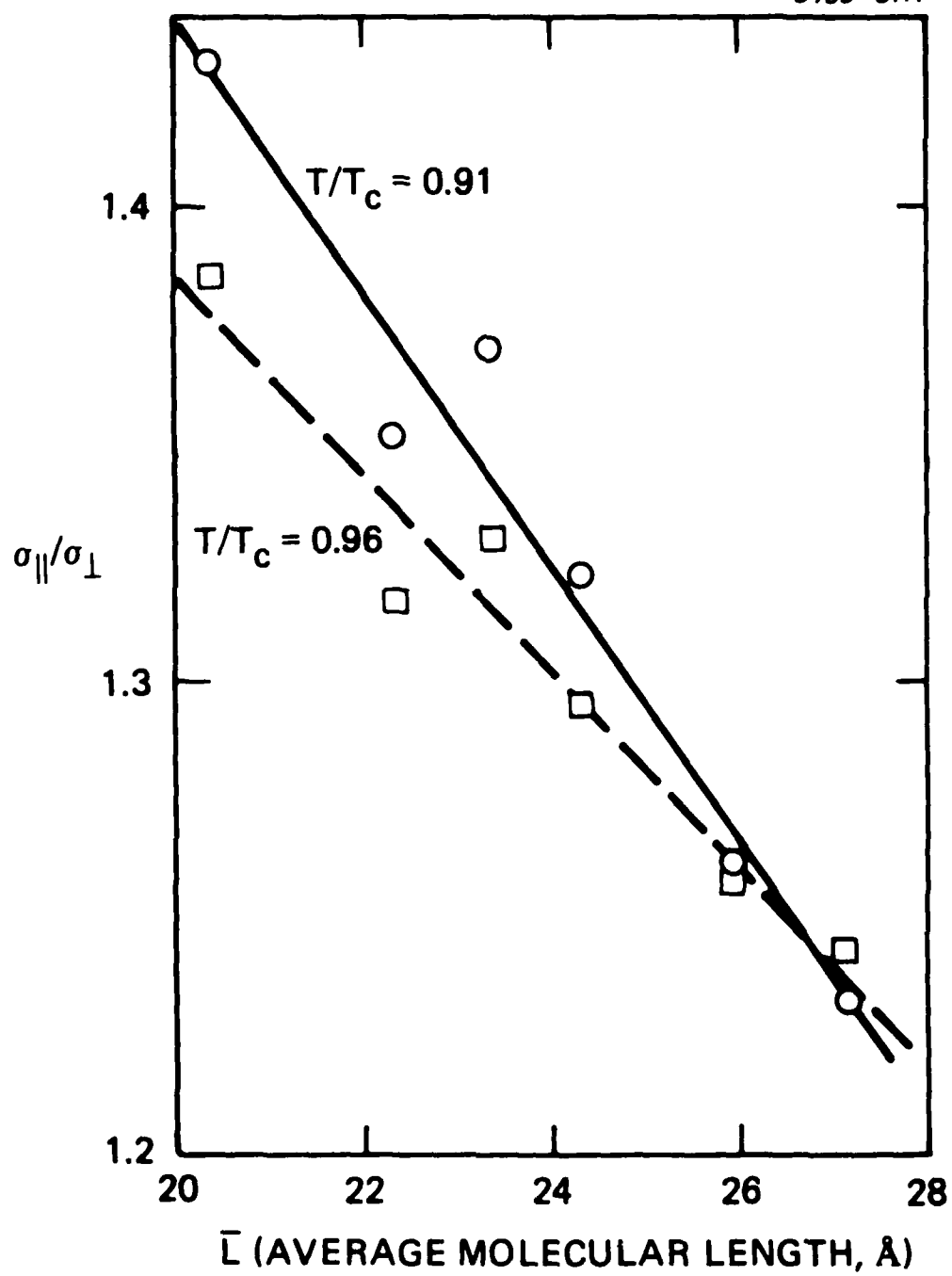


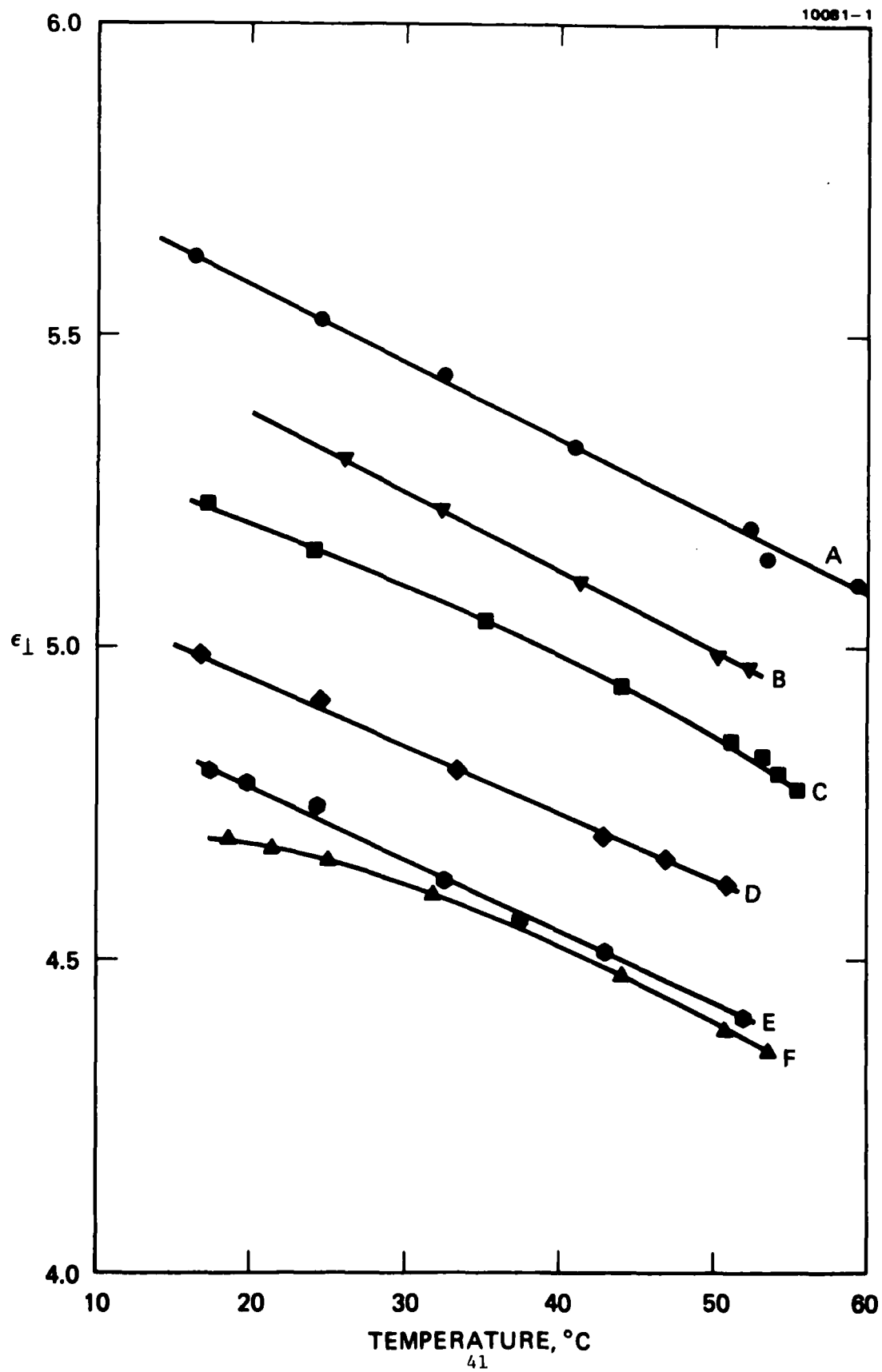


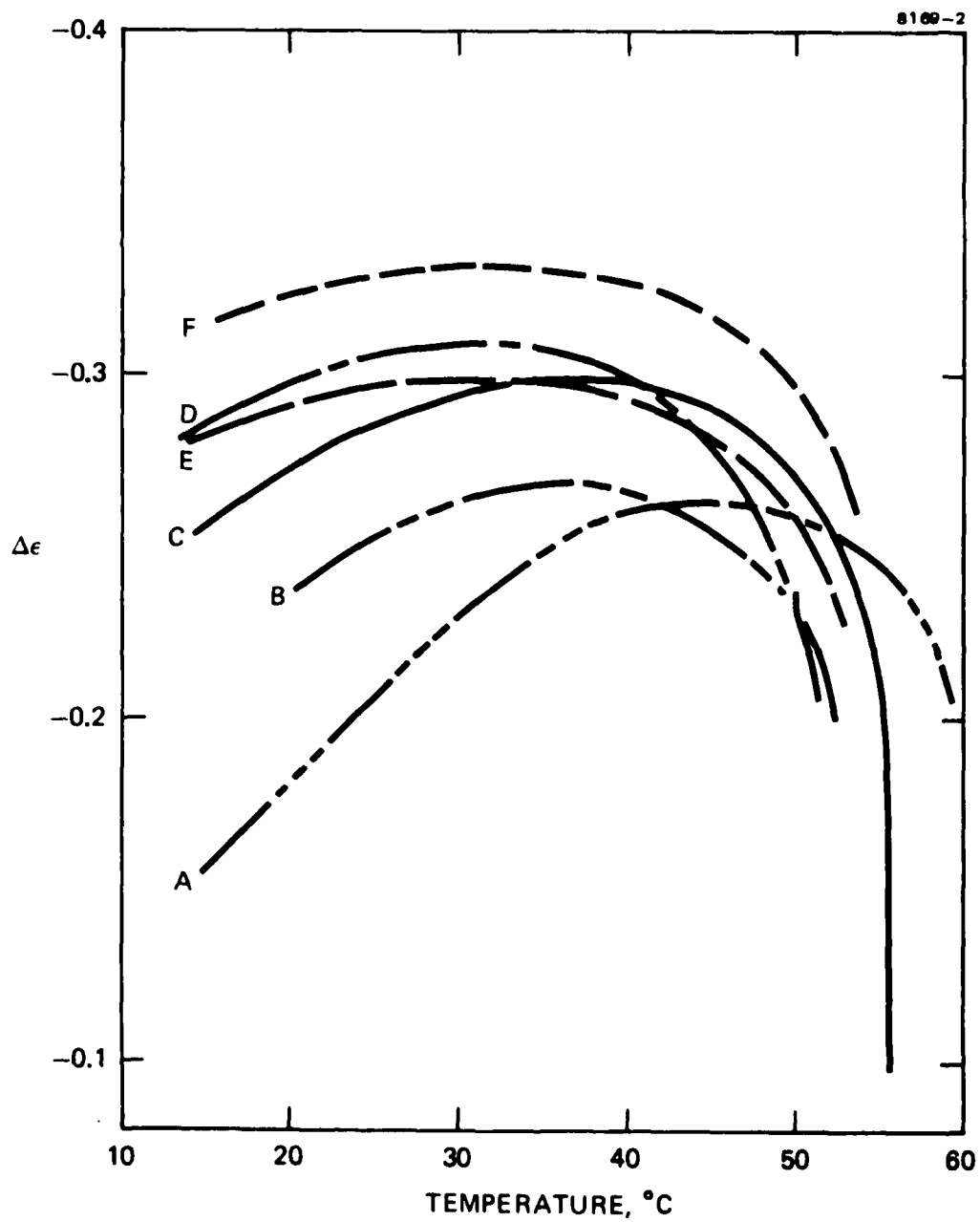


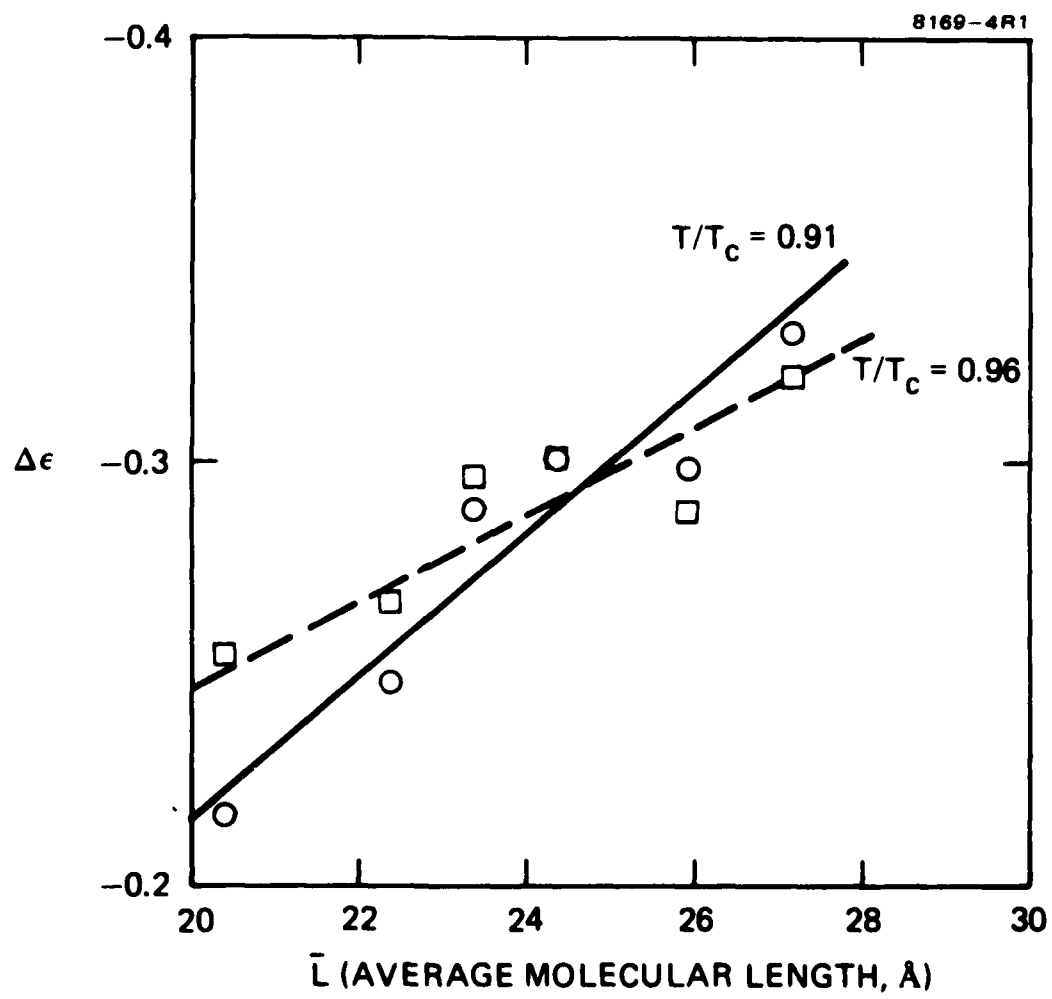


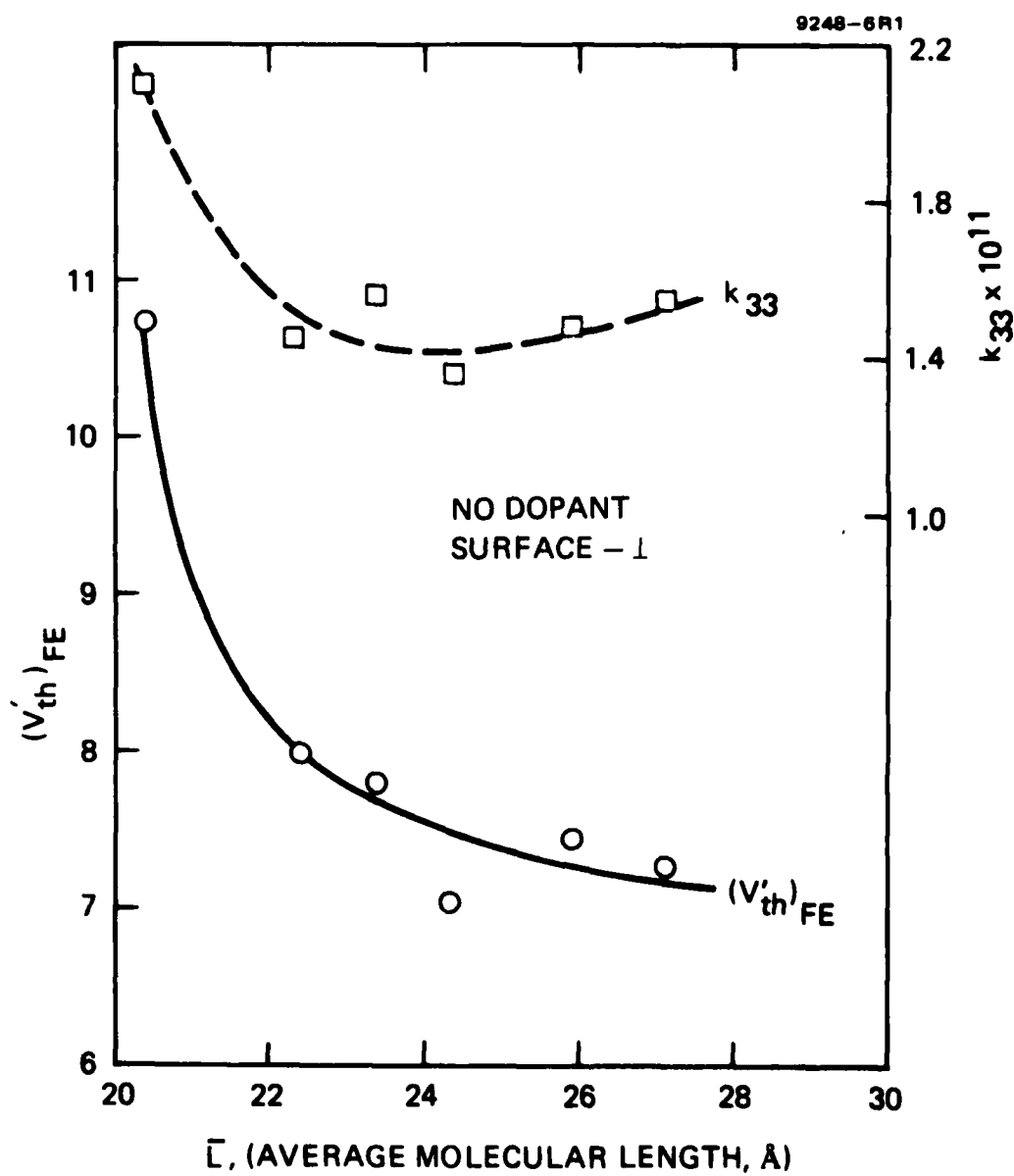


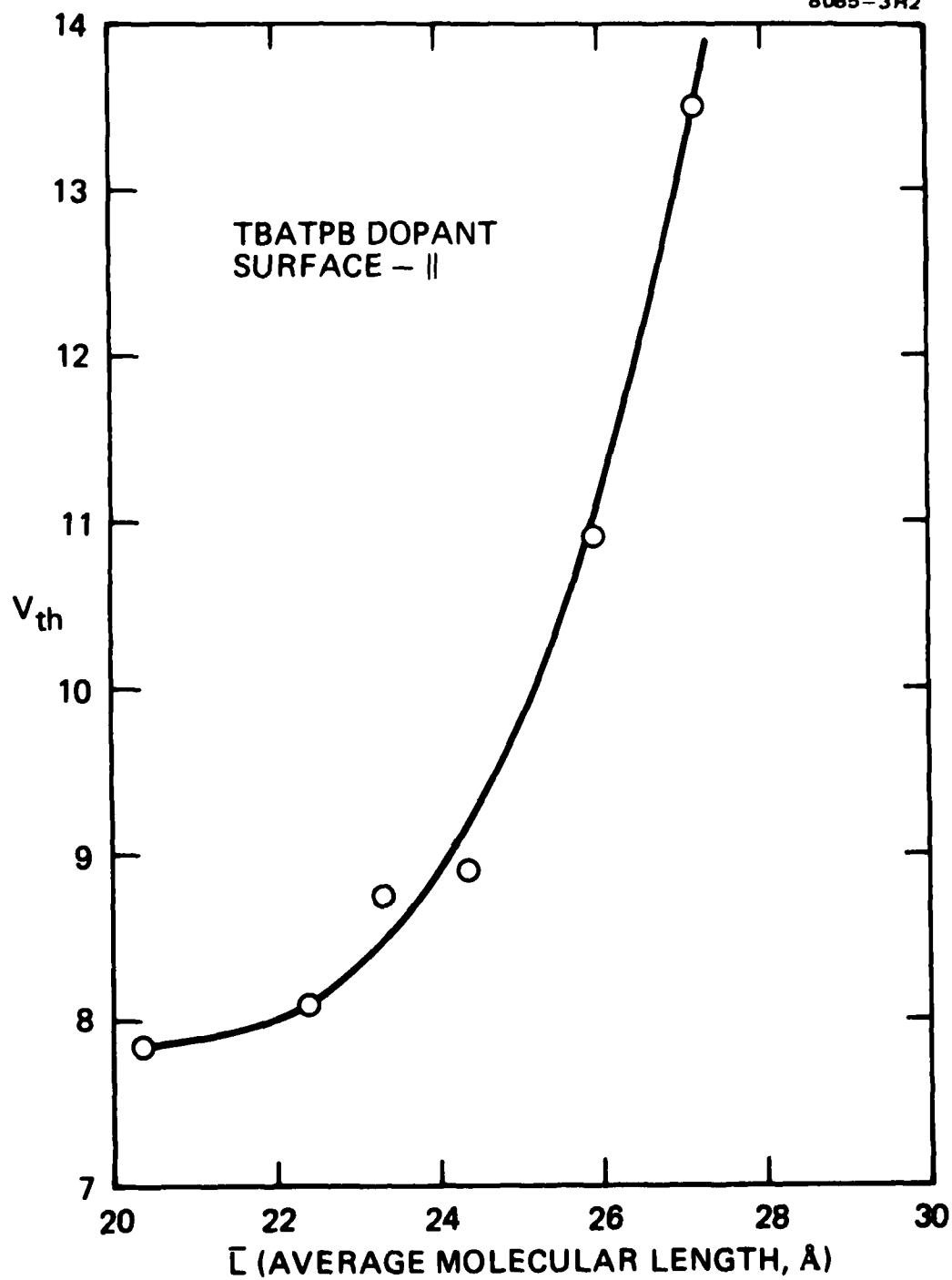


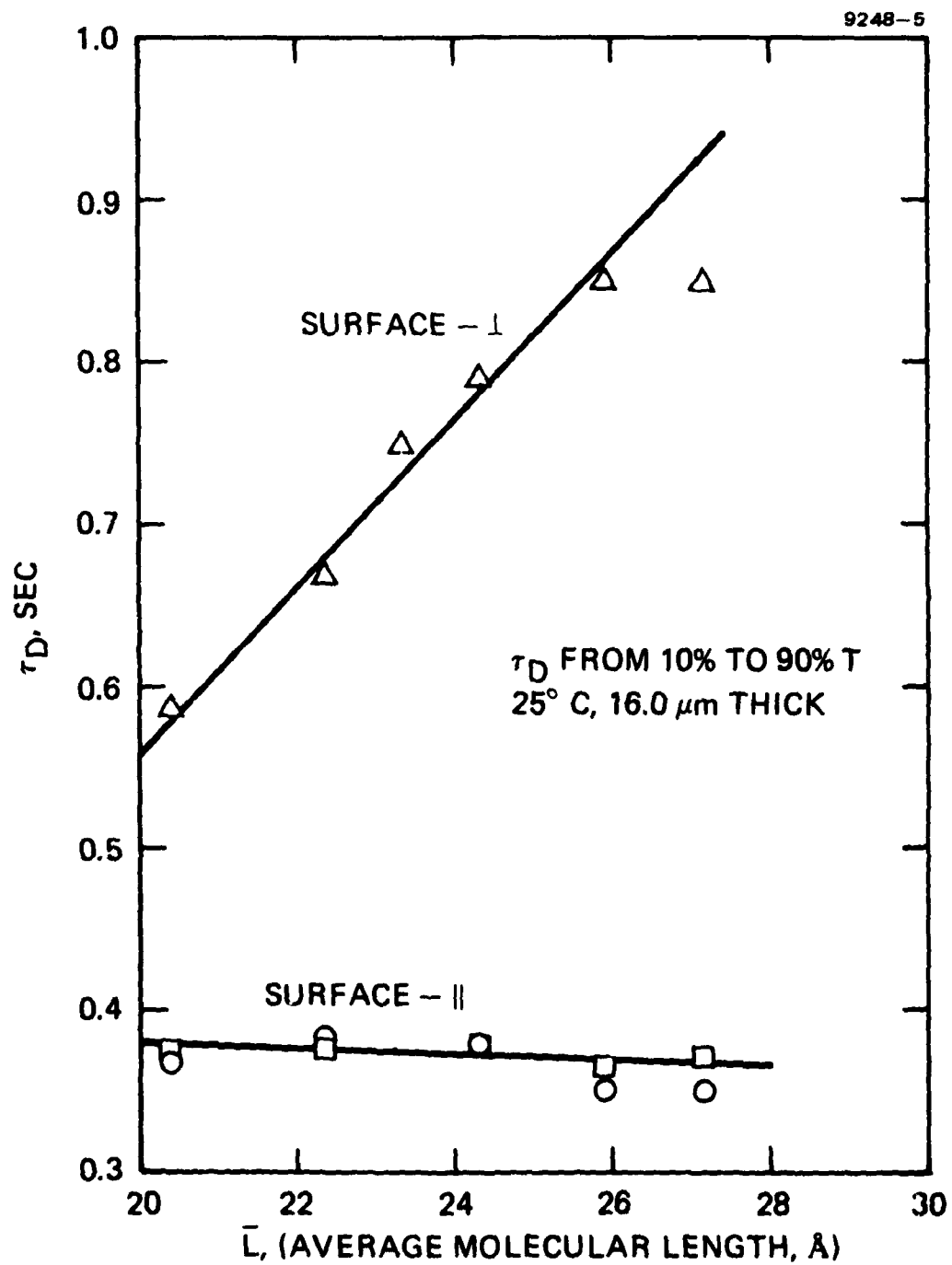












APPENDIX II

EFFECTS OF MOLECULAR LENGTH ON NEMATIC MIXTURES. II. ANISOTROPIC AND DYNAMIC SCATTERING PROPERTIES OF 4-ALKOXYPHENYL 4-ALKYLCYCLOHEXANECARBOXYLATE MIXTURES*

J. David Margerum, Siu-May Wong, Anna M. Lackner,
and John E. Jensen

Hughes Research Laboratories
3011 Malibu Canyon Road
Malibu, California 90265

ABSTRACT

The properties of nematic liquid-crystal mixtures of 4-alkoxyphenyl trans-4-alkylcyclohexanecarboxylates are studied as a function of temperature and their average molecular length (\bar{L}). Mixtures are prepared with clearpoints near 72°C ($\pm 3^\circ\text{C}$) and with \bar{L} varying between 21.20 and 26.15 Å. At 25°C, their flow viscosity increases exponentially (from 16.3 to 50.6 cP) as \bar{L} increases. The conductivity anisotropy ($\sigma_{\parallel}/\sigma_{\perp}$) also varies tremendously, decreasing from 1.62 to 0.49 as \bar{L} increases, when compared at 25°C with tetrabutylammonium tetraphenylboride as dopant. The low values of $\sigma_{\parallel}/\sigma_{\perp}$ and its temperature dependence indicate that cybotatic nematic characteristics occur when the average total number of alkyl carbons from both end groups is 8.5 or more. Short range smectic effects are dominant in the longer mixtures. All of the mixtures have a negative dielectric anisotropy, which linearly becomes less negative with increasing \bar{L} . At 25°C, dynamic scattering (DS) is observed only in the shorter \bar{L} mixtures (where $\sigma_{\parallel}/\sigma_{\perp} > 1$), and the

*Presented at the 8th International Liquid Crystal Conference, Kyoto, Japan, July 1980

DS decay times are relatively fast. Comparisons are made with similar studies on *p*-alkoxyphenyl *p*-alkylbenzoate mixtures.

INTRODUCTION

In recent years, there has been considerable interest regarding the incorporation of cyclohexane structures into liquid-crystal (LC) compounds and mixtures.¹⁻⁶ Most of the studies have been on materials with positive dielectric anisotropy, such as 4-cyanophenylcyclohexanes, for use in twisted nematic displays based on polarization switching.²⁻⁶ These cyanophenylcyclohexanes have a lower viscosity and birefringence than do the corresponding cyanobiphenyl nematic liquid crystals. Esters with phenyl cyclohexanecarboxylate structures have been reported to have wide nematic temperature ranges,¹ but relatively little has been reported on their anisotropic and electrooptical properties. We are interested in the use of cyclohexanecarboxylate esters as nematic mixtures for both dc- and ac-activated dynamic-scattering (DS) displays, particularly to obtain wide temperature range mixtures with fast response times. Since we have found that the average molecular length (\bar{L}) of *p*-alkoxyphenyl *p*-alkylbenzoate mixtures has a large effect on their nematic properties,⁷ the present study is directed particularly at the effects of molecular length on the properties of mixtures 4-alkoxyphenyl trans-4-alkylcyclohexanecarboxylates. We are especially interested in the effect of \bar{L} on the viscosity, dielectric anisotropy, conductivity anisotropy, and DS response of these mixtures, and in comparing these results with those from the similar phenyl benzoate mixtures.

EXPERIMENTAL

The cyclohexane liquid-crystal compounds were prepared by reacting the appropriate 4-alkoxyphenol with a 4-alkylcyclohexanecarbonyl chloride. The latter are obtained by first carrying out a catalytic reduction (H_2/Rh in a Paar apparatus) of the *p*-alkylbenzoic acid and then treating it with thionyl chloride. The catalytic reduction gives the cis-4-alkylcyclohexanecarboxylic acid, but heating the acid chloride converts it largely to the trans-4-alkylcyclohexanecarbonyl chloride. The mixture of these cis and trans acid chlorides are esterified, and the lower melting cis ester is removed from the 4-alkoxyphenyl trans-4-alkylcyclohexanecarboxylate by recrystallizations. Purity is checked by thin-layer chromatography and by high-pressure liquid chromatography (Waters Assoc. Model ALC-202/401, with a microporasil column). We estimate that there is less than 1% impurity in each ester. Thermal analysis data on the melting point (mp), clearpoint (clpt), and heat of fusion (ΔH_f) are obtained by differential scanning calorimetry (DSC) using a Mettler TA2000B thermal analysis system.

Our other experimental techniques are essentially the same as in paper I of this series.⁷ The density is measured in calibrated pycnometer tubes, as a function of temperature. The flow viscosity (η) is measured in calibrated Cannon-Manning-type viscometer tubes held in a temperature-controlled bath. The calibrated ranges were 3 to 15, 7 to 35, and 20 to 100 cS, respectively, in three different size tubes. Overlapping results from different tubes are in good agreement (i.e., there is no tube size effect on η). The refractive indices are measured with a Leitz-Jelly micro-refractometer at 589 nm. The dielectric

anisotropy and conductivity anisotropy are measured as described previously,^{7,8} using 503- μm -thick cells in a 7-kG magnetic field. The samples are doped with tetrabutylammonium tetraphenylboride (TBATPB) or tetrabutylammonium trifluoromethanesulfonate (TBATMS) by adding 0.1% of the salt, warming to dissolve, cooling at room temperature for 12 hr, and filtering through a 0.2- μm filter. The DS measurements are made in transmission with unpolarized green light using glass cells with indium tin oxide (ITO) transparent electrodes. Threshold voltages are made at 30, 20, and 10 Hz, in cells with nominal spacers of 25.4 μm , using baked polyvinyl alcohol (PVA) coatings rubbed for surface- \parallel alignment, and using an 800- \AA coating of sputter-deposited SiO_2 treated with $\text{C}_{22}\text{H}_{45}\text{OH}$ for surface- \perp alignment.⁹ The DS decay times are measured from 10% to 90%T at 25°C using SiO_2 -overcoated ITO electrodes on 12.7-mm-thick optical flats with SiO_x pad spacers. The surface- \parallel cell (15.43- μm -thick spacing) has a rubbed PVA coating, while the surface- \perp cell (15.86 μm) is treated with $\text{C}_{18}\text{H}_{37}\text{OH}$. Undoped samples are used for the dielectric field effect transition threshold voltage at 1 kHz in surface- \perp cells.

RESULTS AND DISCUSSION

LC Components and Mixtures

The thermal properties for the six nematic compounds used in these studies are shown in Table I, where R and R' are the n-alkyl groups in the general structure shown in Figure 1a. Our observed melting points and clearpoints are higher than the literature values, indicating that our compounds are of higher purity. We did not observe the low melting point of smectic-to-nematic transition reported for 60-(C)5. Mixtures

were prepared with the compositions shown in Table II. These were primarily mixtures from calculated eutectic compositions that were chosen to be room-temperature nematics, to have similar clearpoint temperatures, and to have as wide a range of \bar{L} as possible. The results in Table III show a close correlation between the calculated and the observed nematic ranges of these mixtures. The resistivities of the undoped mixtures are greater than $10^{12} \Omega\text{-cm}$. The molecular length (L) of each compound is measured from the end-to-end distance in CPK models, as indicated in Figure 1b. The average length, \bar{L} , of a mixture is obtained by summing the product of the mole fraction and the L of each component.

Refractive Index, Birefringence, Density, and Dielectric Constant

Plots of refractive indices (n_{\parallel} and n_{\perp}), birefringence (Δn), density (d), and dielectric constant (ϵ_1) of the mixtures are shown in Figure 2 as a function of their \bar{L} . Both n_{\parallel} and n_{\perp} decrease slightly as \bar{L} increases, as expected since longer \bar{L} increases just the aliphatic end group length of similar molecules already containing a cyclohexane ring in the central group. Their birefringence is small and is nearly independent of \bar{L} , with $\Delta n = 0.085 \pm 0.003$ at room temperature. This is substantially smaller than the birefringence of similar phenyl benzoate esters, in which Δn varied between 0.153 and 0.134 over the same \bar{L} range.⁷ The n_{\perp} of these cyclohexane ester mixtures is also lower than that of comparable length phenyl benzoate mixtures. The d and ϵ_1 values decrease approximately linearly as \bar{L} increase. Both the magnitudes of d and ϵ_1 and their rates of decrease with \bar{L} are smaller in these mixtures than in the phenyl benzoate series, as expected since the central group contains a cyclohexane ring in place of a phenyl group.

Flow Viscosity

The flow viscosities of these mixtures are shown as a function of temperature in Figure 3. Note that the plot for G includes a point above the clearpoint where η increases. In each mixture, the plots of $\log \eta$ versus T^{-1} deviate from the linear relationship often found for liquids and LCs. The effect of \bar{L} on the flow viscosity at a given temperature is quite large, as shown in Figure 4. At 25°C, the viscosity increases exponentially with increasing molecular length. This rapid increase of η with \bar{L} is probably related to the strong cybotactic nematic character observed (described below) for these mixtures as their \bar{L} increases. At 25°C, the short length RO-(C)R' mixtures have lower η 's than do the corresponding length RO-R' (phenylbenzoate) mixtures (e.g., 16 and 34 cP, respectively, at $\bar{L} = 21 \text{ \AA}$). However, the longer length RO-(C)R' mixtures have higher η 's than do the RO-R' mixtures (e.g., 48 and 41 cP, respectively, at $\bar{L} = 26 \text{ \AA}$). Thus, the substitution of cyclohexane rings for benzene rings in LC components does not always give a lower viscosity nematic mixture; it does so only for the short length ester mixtures in this series.

Conductivity Anisotropy

The conductivity anisotropy ($\sigma_{\parallel}/\sigma_{\perp}$) of five of the mixtures is shown in Figure 5 as a function of temperature. Although the solubility and conductivity of TBATPB in a mixture decrease as \bar{L} increases, our experience indicates that this should have no significant effect on the anisotropy measurements.^{7,8,10} The $\sigma_{\parallel}/\sigma_{\perp}$ values in A, the shortest \bar{L} mixture, are high (1.61 at 25°C) and decrease with increasing temperature, as is characteristic of a nematic liquid crystal. The values in

C, a slightly longer length mixture, are not quite as high as in mixture A and are nearly constant over a wide temperature range. The $\sigma_{\parallel}/\sigma_{\perp}$ values in D increase as the temperature increases, which is taken as evidence for some cybotactic character¹¹⁻¹⁴ (short range smectic order) at temperatures below about 50°C. Mixture E and compound G have the longest \bar{L} 's, and their $\sigma_{\parallel}/\sigma_{\perp}$ values are considerably below 1.0, which is characteristic of a smectic LC or very strongly cybotactic nematic LC. From the curves in Figure 5, we conclude that RO-(C)R' mixtures with an average of 8.5 or more R+R' alkyl carbons have cybotactic nematic characteristics. The corresponding number of R+R' carbons for cybotactic effects in the RO-R' mixtures is 10 carbons or more.⁷ Thus, the presence of a cyclohexanecarboxylate group in place of a benzoate group reduces the average length at which cybotactic effects are observed in their alkoxyphenyl ester LCs.

Because of the limited solubility of TBATPB in these cyclohexane esters, we also studied TBATMS, which is a smaller, more polar salt. It is more soluble and provides adequate conductivity for DS studies. Since we have previously found^{8,10} that the $\sigma_{\parallel}/\sigma_{\perp}$ values for TBATMS at a given temperature increase at low resistivity, we kept the ρ_{\perp} (25°) of these samples in the range of 8.4×10^8 to 5.8×10^9 Ω -cm. The results are shown in Figure 6. The cybotactic nematic criterion ($\sigma_{\parallel}/\sigma_{\perp}$ increasing with temperature) is less pronounced with TBATMS than with TBATPB, especially in mixture D. In other nematic LCs, we have found that at room temperature the $\sigma_{\parallel}/\sigma_{\perp}$ of TBATMS was less than that of TBATPB, as is the case in mixture A. However, they are about the same in mixture C, and TBATMS has higher $\sigma_{\parallel}/\sigma_{\perp}$ values than TBATPB in

mixtures D and G. This is seen more clearly in Figure 7, where the values are compared at two reduced temperatures. (In these mixtures, the reduced temperatures of 0.86 and 0.96 correspond to an average of about 26 and 60°C, respectively.) At $T/T_c = 0.86$, the curves for the two dopants cross because the values for TBATPB decrease more rapidly than those for TBATMS as \bar{L} increases. However, at the higher reduced temperature of 0.96, the $\sigma_{\parallel}/\sigma_{\perp}$ values for TBATMS are less than those of TBATPB throughout the \bar{L} range. The cybotactic nematic character of the RO-(C)R' mixtures clearly has a larger effect on the conductivity anisotropy of the TBATPB dopant than of the TBATMS dopant. In Figure 7, both plots of $\sigma_{\parallel}/\sigma_{\perp}$ versus \bar{L} at $T/T_c = 0.86$ show a large deviation from linearity due to the strong cybotactic nematic ordering in the longer \bar{L} mixtures.

Dielectric Anisotropy

The effects of temperature on the dielectric constants of these mixtures are shown in Figure 8. Because ϵ_{\perp} decreases appreciably while ϵ_{\parallel} changes only slightly with increasing temperature, the values of $-\Delta\epsilon$ decrease linearly as temperature increases in the 20 to 60°C range. This effect of temperature on $\Delta\epsilon$ is the one we would expect in the absence of molecular associations. Thus, while $\sigma_{\parallel}/\sigma_{\perp}$ and viscosity effects show strong evidence for cybotactic nematic molecular order, the $\Delta\epsilon$ effects do not indicate any molecular pairing of polar groups. (In contrast, the longer \bar{L} RO-R' mixtures⁷ showed less cybotactic nematic association than these RO-(C)R' mixtures, while the shorter \bar{L} RO-R' mixtures showed evidence of polar associations — as inferred by their $-\Delta\epsilon$ values going through a maximum as temperature increased.)

These mixtures have much more negative $\Delta\epsilon$ values (between -1.34 and -1.20 at 25°C) than do the corresponding RO-R' mixtures. As shown in Figure 9, $-\Delta\epsilon$ at a given reduced temperature decreases linearly with increasing \bar{L} . (In the RO-R' mixtures, $-\Delta\epsilon$ increased with \bar{L} .) The nearly parallel changes of $-\Delta\epsilon$ with temperature (Figure 8) and with \bar{L} (Figure 9) indicate that the dielectric effects in these RO-(C)R' mixtures are not significantly affected by the large differences in viscosity and cybotactic nematic character.

Field Effect Transition and Elastic Constant

The threshold voltage for the field-effect realignment, $(V'_{th})_{FE}$, of these undoped LC mixtures is shown by the lower line in Figure 10. It is nearly unchanged by the changes in \bar{L} . The corresponding k_{33} (bend elastic constant) values also do not vary much with \bar{L} , as shown in Table IV.

Dynamic Scattering

Typical DS curves (where $\%S = 100 - \%T$) for mixtures A, B, and C are shown in Figure 11. These are run at low frequency (10 Hz) to minimize effects from the cut-off frequencies of these samples, which have relatively high resistivities due to the low solubility of the TBATPB dopant. The $(V_{th})_{DS}$ values from these curves are shown in Figure 10. In the other mixtures, TBATPB does not provide adequate conductivity for DS studies, and mixtures E, F, and G are not expected to show DS at 25°C anyway because their $\sigma_{||}/\sigma_{\perp}$ ratios are less than 1.0. The TBATMS dopant is more soluble and gives better DS curves; the DS threshold voltage for mixtures A, C, and D are shown in Figure 10 for

both surface-|| and surface-⊥ alignment. (These samples have resistivities of $\rho_{\perp} = 1.6 \times 10^9$, 1.8×10^9 , and 4.9×10^9 Ω -cm, respectively.) The general trend is that $(V_{th})_{DS}$ increases with \bar{L} with either the TBATPB or the TBATMS dopant. These results are consistent with the conductivity anisotropy effects shown in Figures 5 through 7. Temperature effects on DS also correspond to the $\sigma_{||}/\sigma_{\perp}$ changes. TBATMS doped mixture F shows high-level scattering curves at higher temperatures (e.g., 60°C). Its $(V_{th})_{DS}$ value decreases sharply as temperature increases, going from an ill-defined 30 to 40 V value at room temperature, to ~20 V at 42°C, and down to 13.5 V at 53°C in surface-|| cells. Sample G does not show any DS below 35°C with either dopant, as expected since $\sigma_{||}/\sigma_{\perp}$ is less than 1.0 in this temperature range.

The DS decay time (τ_D) of TBATMS-doped samples of mixtures A, C, and D are shown in Figure 12. For comparison, the decay times are corrected to 16.0 μm thickness, using a $16^2/\ell^2$ correction factor. The actual thickness between the optical flats are 15.43 μm for the surface-|| and 15.86 μm for the surface-⊥ cells. Although high voltages (50 V_{rms}) are applied to mixture D to obtain high scattering levels (10% T), secondary scattering is not observed with our relatively short periods of DS activation. The effect of \bar{L} on τ_D is very similar to that observed in the RO-R' mixtures.⁷ As \bar{L} increases, τ_D for surface-|| cells decreases slightly, while τ_D for surface-⊥ cells increases substantially. However, all of these decay times are much faster than those of the corresponding phenyl benzoate mixtures. In the same \bar{L} range, the τ_D 's of the RO-R' mixture were about 375 msec for surface-|| and between 610 and 780 msec for surface-⊥ cells.

CONCLUSIONS

Studies of nematic mixtures of 4-alkoxyphenyl trans-4-alkylcyclohexanecarboxylates show that their viscosities, conductivity anisotropies, and DS threshold voltages are very strongly dependent on the average molecular length of the mixtures. As \bar{L} increases, their viscosities increase exponentially and their cybotactic nematic character increases greatly. At 25°C, the short \bar{L} cyclohexane ester mixtures have higher $\sigma_{\parallel}/\sigma_{\perp}$ values and much lower flow viscosities than do the comparable benzoate esters. The longer \bar{L} cyclohexane ester mixtures have stronger cybotactic nematic characteristics and much lower $\sigma_{\parallel}/\sigma_{\perp}$ values (less than 1.0) and are just as viscous as the same length benzoate mixtures. The dielectric anisotropies of the cyclohexane esters also vary with \bar{L} , linearly becoming less negative as \bar{L} increases. Their birefringences are nearly independent of \bar{L} . The solubility of organic salt dopants is low, and becomes worse as \bar{L} increases. Comparisons with similar length *p*-alkoxyphenyl *p*-alkylbenzoate mixtures show that the short length cyclohexane ester mixtures have much more negative $\Delta\epsilon$, higher $\sigma_{\parallel}/\sigma_{\perp}$, lower DS at a given V/V_{th} , and much faster DS decay times in both surface- \parallel and surface- \perp cells.

ACKNOWLEDGMENTS

We are indebted to the Directorate of Chemical Sciences, Air Force Office of Scientific Research, Contract F49620-77-C-0017 for partial financial support of this research; to C.I. VanAst for assistance in liquid chromatography analyses; and to W.H. Smith, Jr., for assistance in DSC measurements.

References

1. D. Demus, H.J. Deutscher, F. Kuschel, and H. Schubert, Bundes republic Deutschland Patentant 2429093 (1975).
2. R. Eidenschink, D. Erdmann, J. Krause, and L. Pohl, Angew. Chem. 89, 103 (1977).
3. L. Pohl, R. Eidenschink, J. Krause, and D. Erdmann, Phys. Lett. 60A, 421 (1977).
4. R. Eidenschink, D. Erdmann, J. Krause, and L. Pohl, 7th International Liq. Cryst. Conf., Bordeaux, France, 1978 (Paper No. A04).
5. G.W. Gray and D.G. McDonnell, Mol. Cryst. Liq. Cryst. 53 147 (1979).
6. Hp. Schad, G. Bauer, and G. Meier, J. Chem. Phys. 70, 2770 (1979).
7. J.D. Margerum, J.E. Jensen, and A.M. Lackner, Symposium on the Physics and Chemistry of Liquid Crystal Devices, San Jose, CA., Feb. 1979. (Paper I of this series; submitted for publication in Mol. Cryst. Liq. Cryst.)
8. J.D. Margerum, H.S. Lim, P.O. Braatz, and A.M. Lackner, Mol. Cryst. Liq. Cryst. 38, 219 (1977).
9. L.J. Miller, J. Grinberg, G.D. Myer, D.S. Smythe, and W.H. Smith, "Liquid Crystals and Ordered Fluids," Vol. 3, p. 513, J.E. Johnson and R.S. Porter, eds., Plenum Pub. (1978).
10. J.D. Margerum, A.M. Lackner, and H.S. Lim (Paper No. DP28), 7th International Liquid Crystal Conf., Bordeaux, France, July 1978.
11. F. Rondelez, Solid State Comm. 11, 1675 (1972).
12. A. Mircea-Roussel, L. Legar, F. Rondelez, and W.H. DeJeu, J. de Physique, Colloq. C136, 93 (1975).

13. G. Heppke and F. Schenider, Z. Naturforsch. 309, 316 (1975).
14. A. DeVries, J. de Physique (Paris) Colloq. C136, 1 (1975).

LIST OF FIGURES

1. (a) General structure of mixture components.
(b) Model of 4-hexyloxyphenyl 4-butylcyclohexanecarboxylate, or 6O-(C)4, showing the molecular length ($L = 26.15 \text{ \AA}$) used.
2. Refractive indices, birefringence, density, and dielectric constant of RO-(C)R' mixtures as a function of \bar{L} . (Δn at 22.8°C , d and ϵ_1 at 25.0°C).
3. Effect of temperature on flow viscosity of RO-(C)R' mixtures.
4. Effect of \bar{L} on viscosity of RO-(C)R' mixtures.
5. Conductivity anisotropy of TBATPB in RO-(C)R' mixtures as a function of temperature.
6. Conductivity anisotropy of TBATMS in RO-(C)R' mixtures as a function of temperature.
7. Effect of \bar{L} on conductivity anisotropy of RO-(C)R' mixtures at reduced temperatures. (T = measurement temperature and T_c = clearpoint, both in $^\circ\text{K}$).
8. Dielectric constants of RO-(C)R' mixtures as a function of temperature (5 kHz).
9. Effect of \bar{L} on dielectric anisotropy of RO-(C)R' mixtures at four reduced temperatures.
10. Threshold voltages at 25°C for field-effect transition (1 kHz) and dynamic scattering (10 Hz) as a function of \bar{L} in RO-(C)R' mixtures.
11. Dynamic scattering curves for mixtures A, B, and C containing TBATPB dopant. (22°C , 13- μm -thick cells surface- \parallel alignment).
A: $\rho_1 = 5.1 \times 10^9 \text{ } \Omega\text{-cm}$; B: $\rho_1 = 6.1 \times 10^9 \text{ } \Omega\text{-cm}$; C: $\rho_1 = 7.4 \times 10^9 \text{ } \Omega\text{-cm}$.

12. Effect of \bar{L} on DS decay time in RO-(C)R' mixtures.

TABLE I
Thermal Properties of Phenyl Cyclohexanecarboxylates

Compound			mp, °C		clpt, °C		ΔH_f kcal/mole
Code	RO	R'	Obs.	Lit. ^a	Obs.	Lit. ^a	
10-(C)5	CH ₃ O	<u>n</u> -C ₅ H ₁₁	40.9	36	71.3	63.5	5.01
20-(C)3	C ₂ H ₅ O	<u>n</u> -C ₃ H ₇	49.0	47	79.8	78.5	6.60
20-(C)5	C ₂ H ₅ O	<u>n</u> -C ₅ H ₁₁	56.9	55	85.9	85.5	7.69
40-(C)4	<u>n</u> -C ₄ H ₉ O	<u>n</u> -C ₄ H ₉	40.5	38	70.0	68.5	4.12
60-(C)4	<u>n</u> -C ₆ H ₁₃ O	<u>n</u> -C ₄ H ₉	26	25	70.0	69.0	5.36
60-(C)5	<u>n</u> -C ₆ H ₁₃ O	<u>n</u> -C ₅ H ₁₁	32.2 ^b	24(38.5) ^b	79.8	78.5	5.06

^aD. Demus, H.-J. Deutscher, F. Kuschel, H. Schubert, Offenlegungs-
schrift 2429093, Bundesrepublik Deutschland, Deutsches Patentamt,
(Jan. 23, 1975).

^bSmectic to nematic transition reported at 38.5°C, but not obs. here.

TABLE II

Composition of Liquid-Crystal Mixtures

Compound		Mole Fraction in Mixtures						
Code	Length, L, Å	A	B	C	D	E	F	G
10-(C)5	21.40	0.497	0.463	0.394	0.283	-	-	-
20-(C)3	20.06	0.311	-	-	-	-	-	-
20-(C)5	22.53	0.192	-	0.135	-	-	-	-
40-(C)4	23.84	-	0.537	0.470	0.358	0.507	0.483	-
60-(C)4	26.15	-	-	-	-	-	-	1.000
60-(C)5	27.41	-	-	-	0.359	0.493	0.517	-
HRL mixture No.		6N7	6N4	6N5	6N10	6N6	6N6R	60-(C)4

Table III. Average Length and Nematic Range of Mixtures

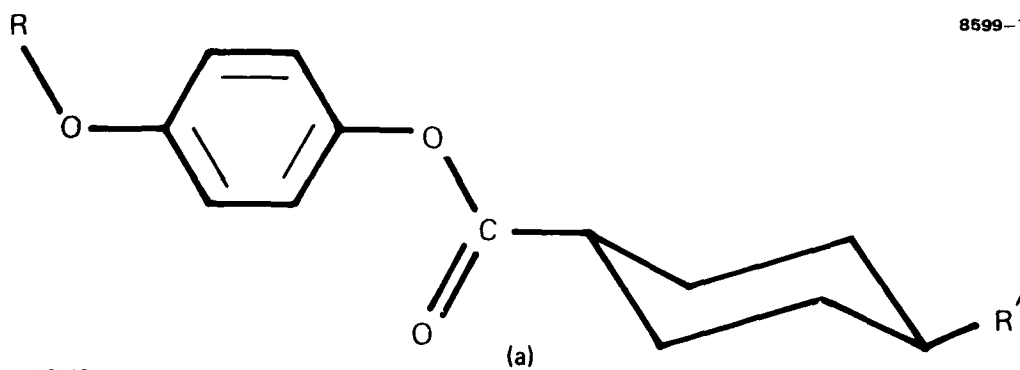
Mixture	\bar{L} , Average Length, Å	No. R + R' Carbons	mp °C		clpt, °C	
			Calc. ^a	Obs.	Calc. ^a	Obs.
A	21.20	5.88	16.2	14.4	76.7	76.1
B	22.71	7.07	13.9	14.2	70.6	69.3
C	22.70	7.07	8.8	4.8	72.6	71.6
D	24.43	8.51	-1.1	-10.0	73.8	73.2
E	25.60	9.48	—	13.4	—	75.4
F	25.68	9.55	9.9	—	75.0	74.8
G	26.15	10.00	—	26.0	—	70.0

^aCalculated eutectic mixture, using Schroeder-Van Laar equation.

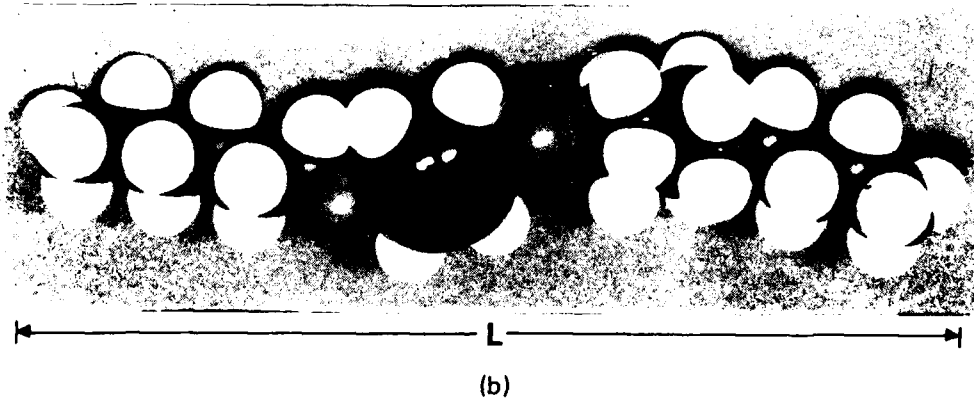
Table IV. Bend Elastic Constant at 25°C

Mixture	$(V'_{th})_{FE}$	$\Delta\epsilon$	$k_{33} \times 10^{11}$
A	3.50	-1.34	1.47
C	3.20	-1.26	1.16
D	3.56	-1.24	1.41
E	3.23	-1.25	1.17

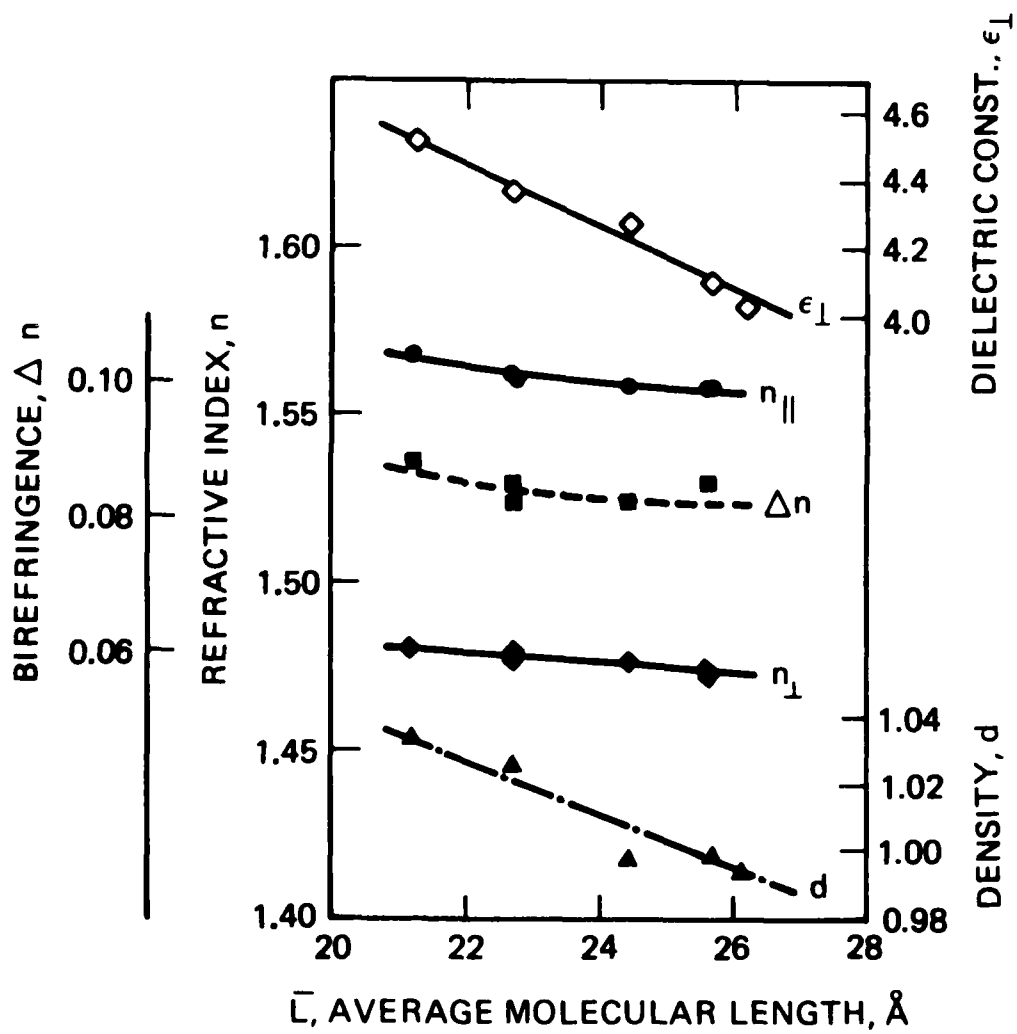
8599-7

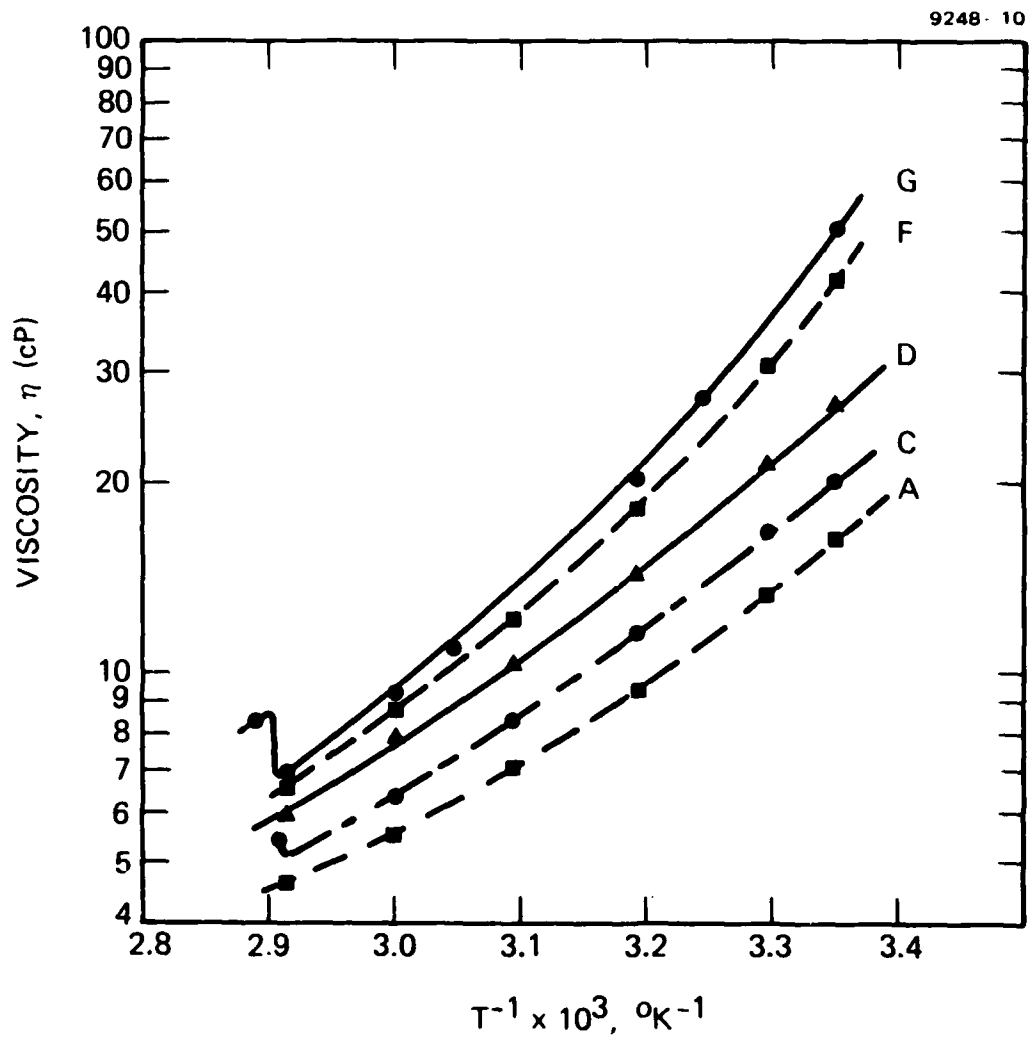


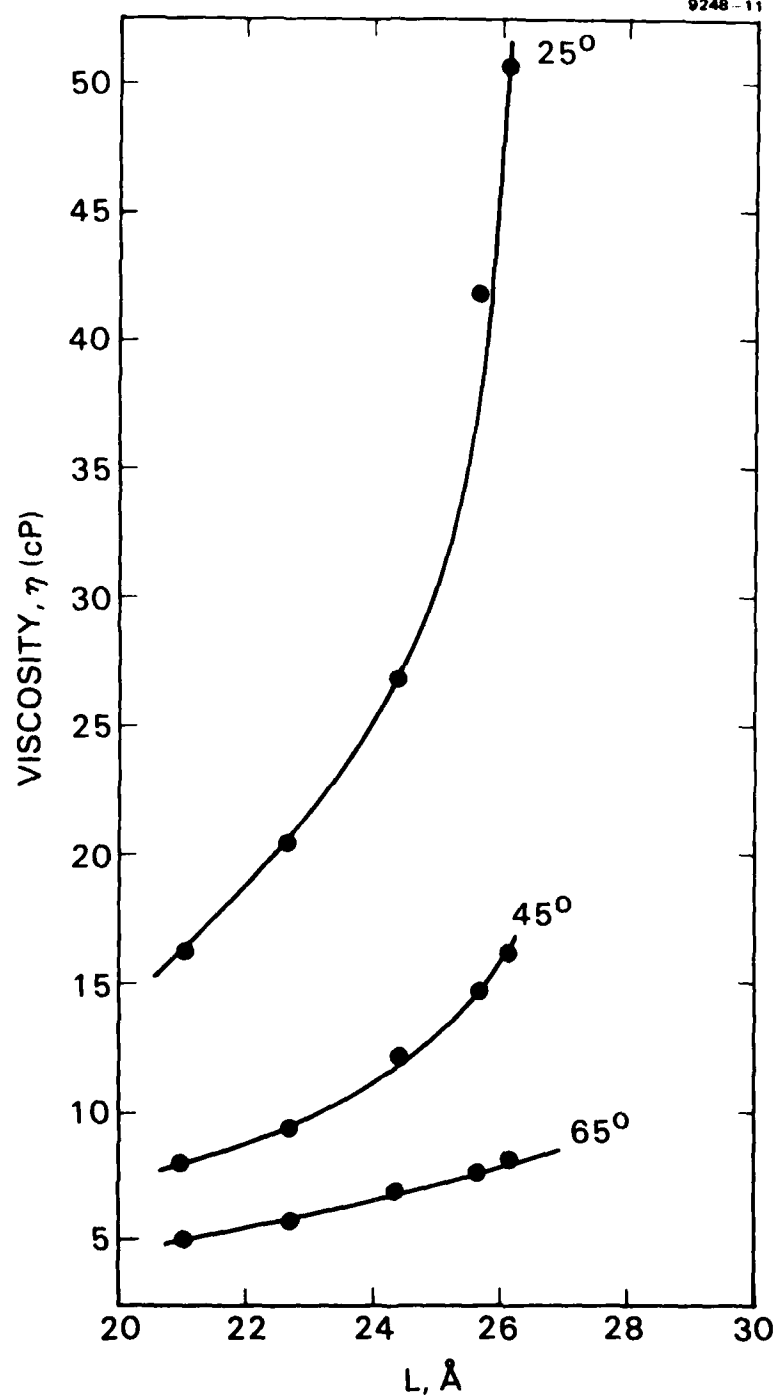
M13110

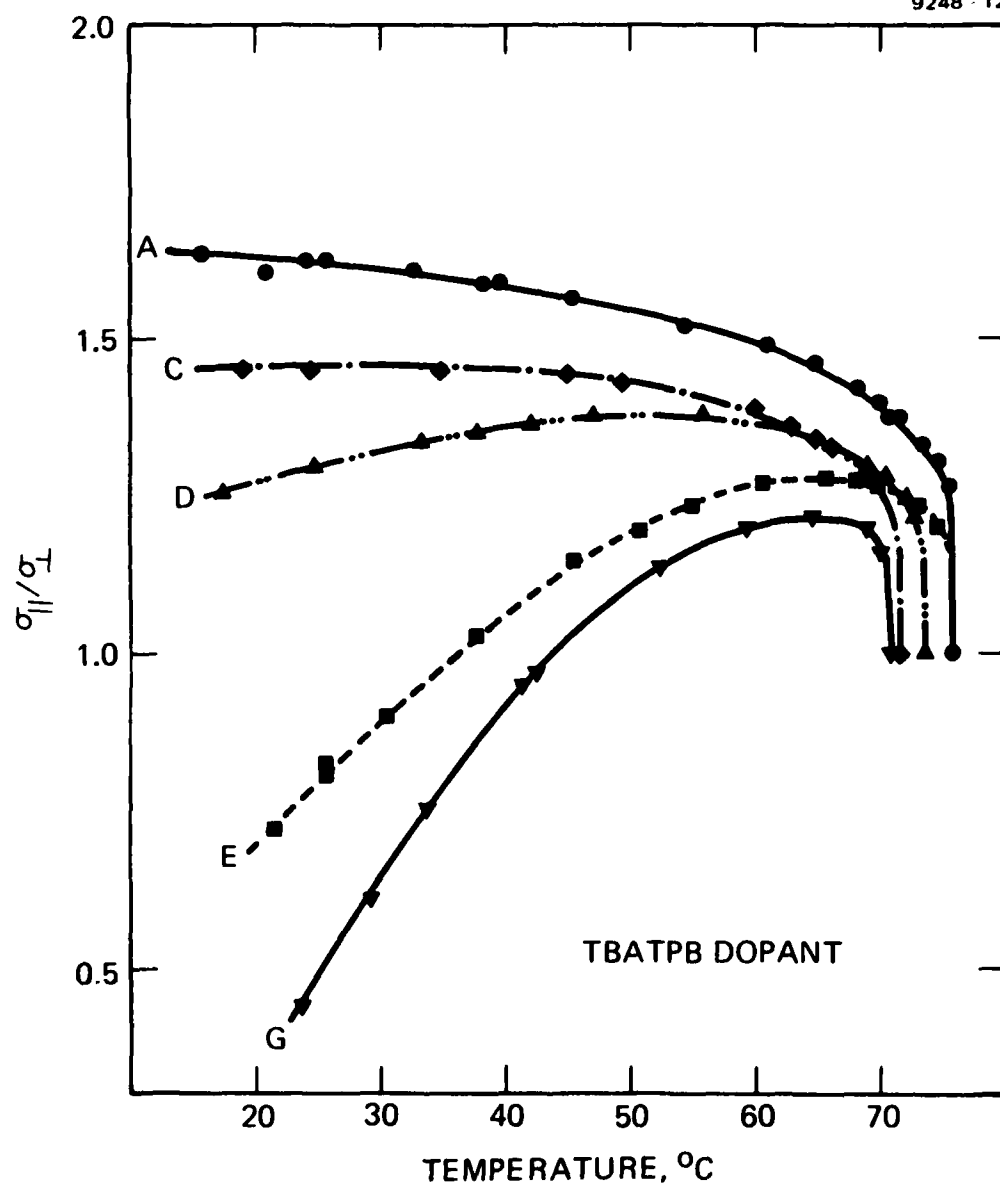


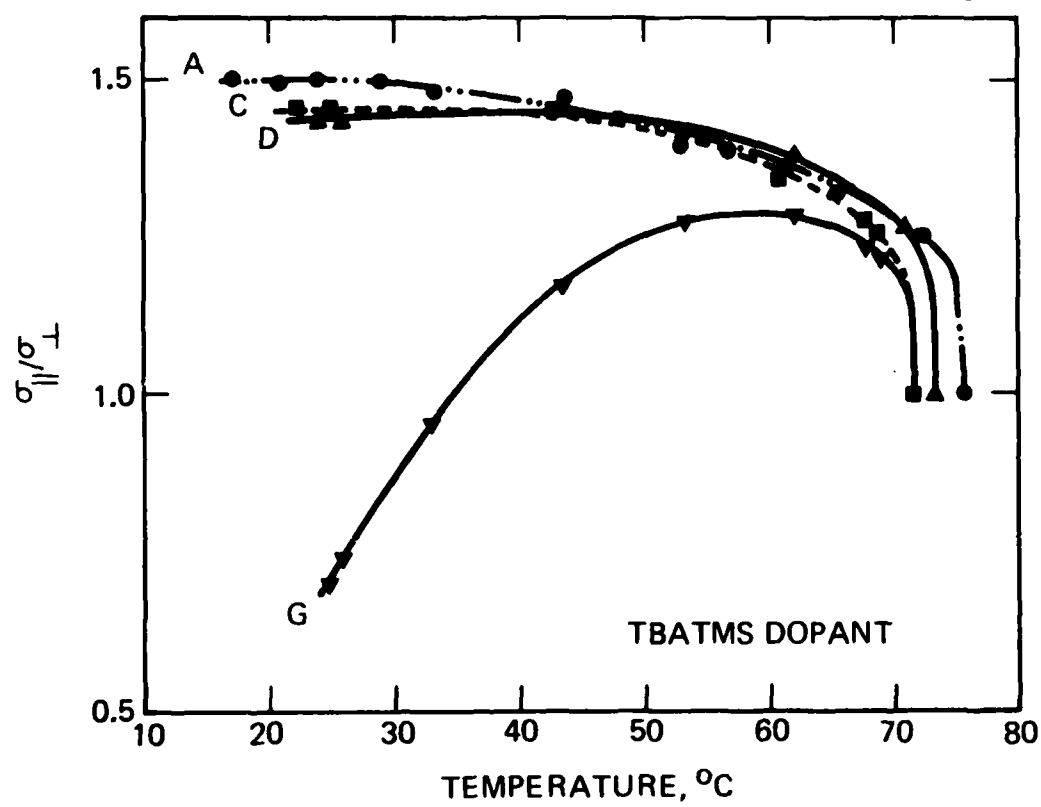
8599-1R2

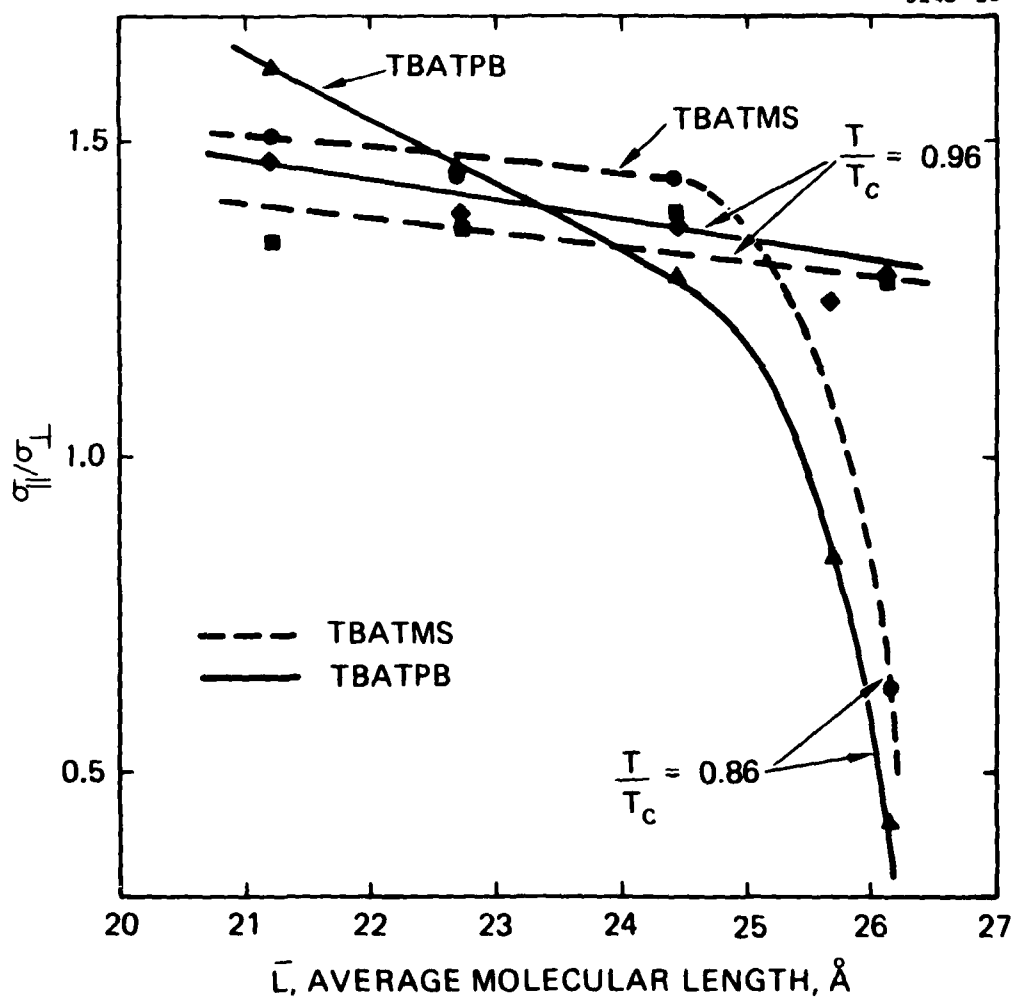


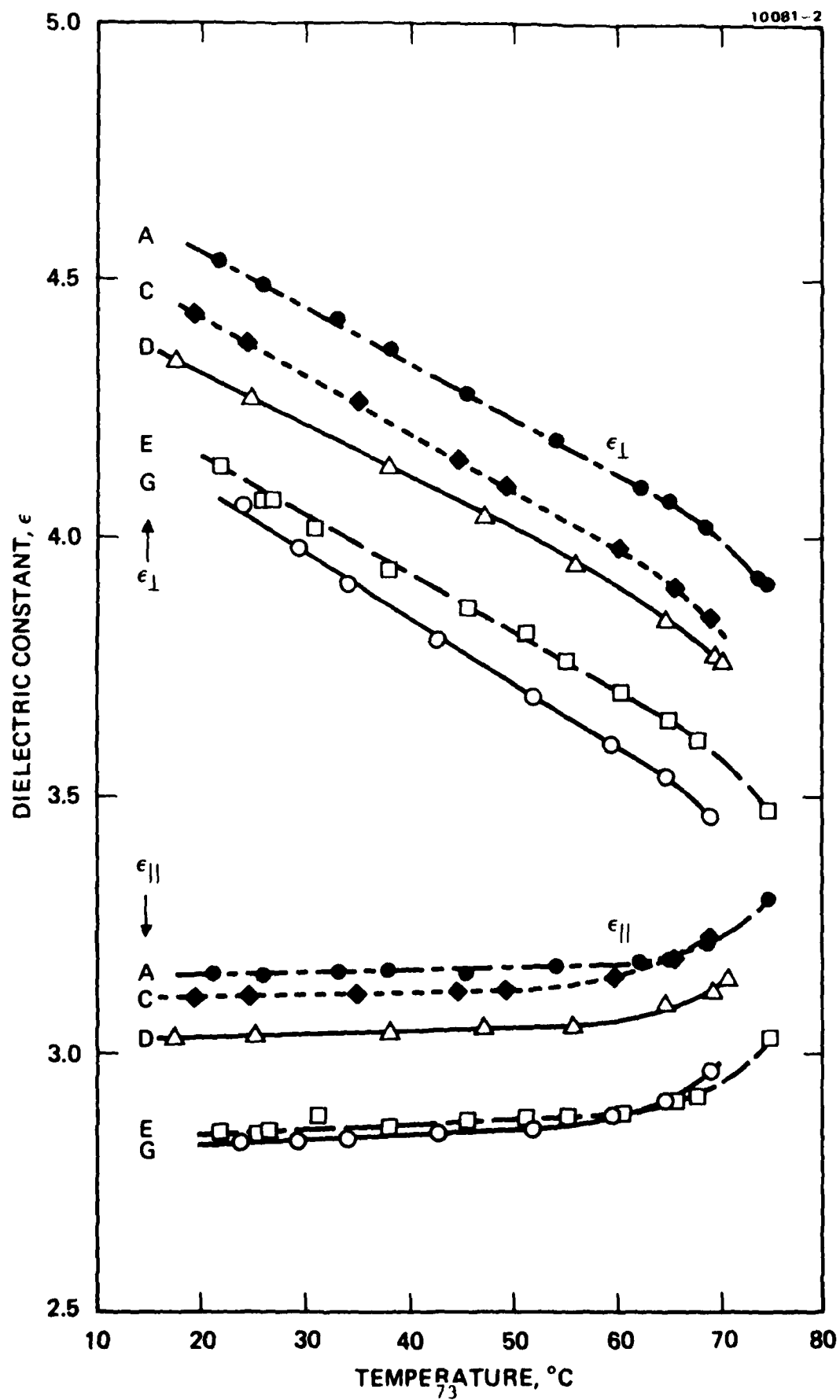


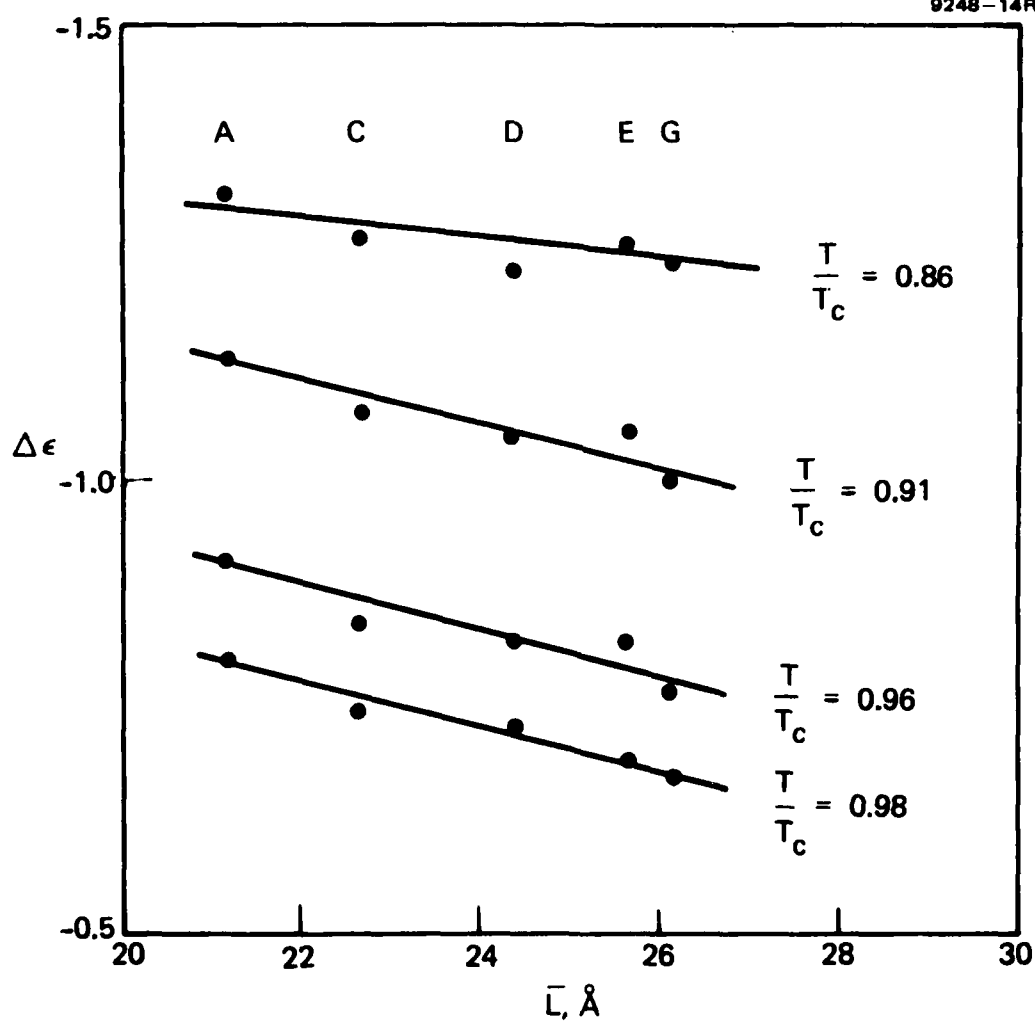


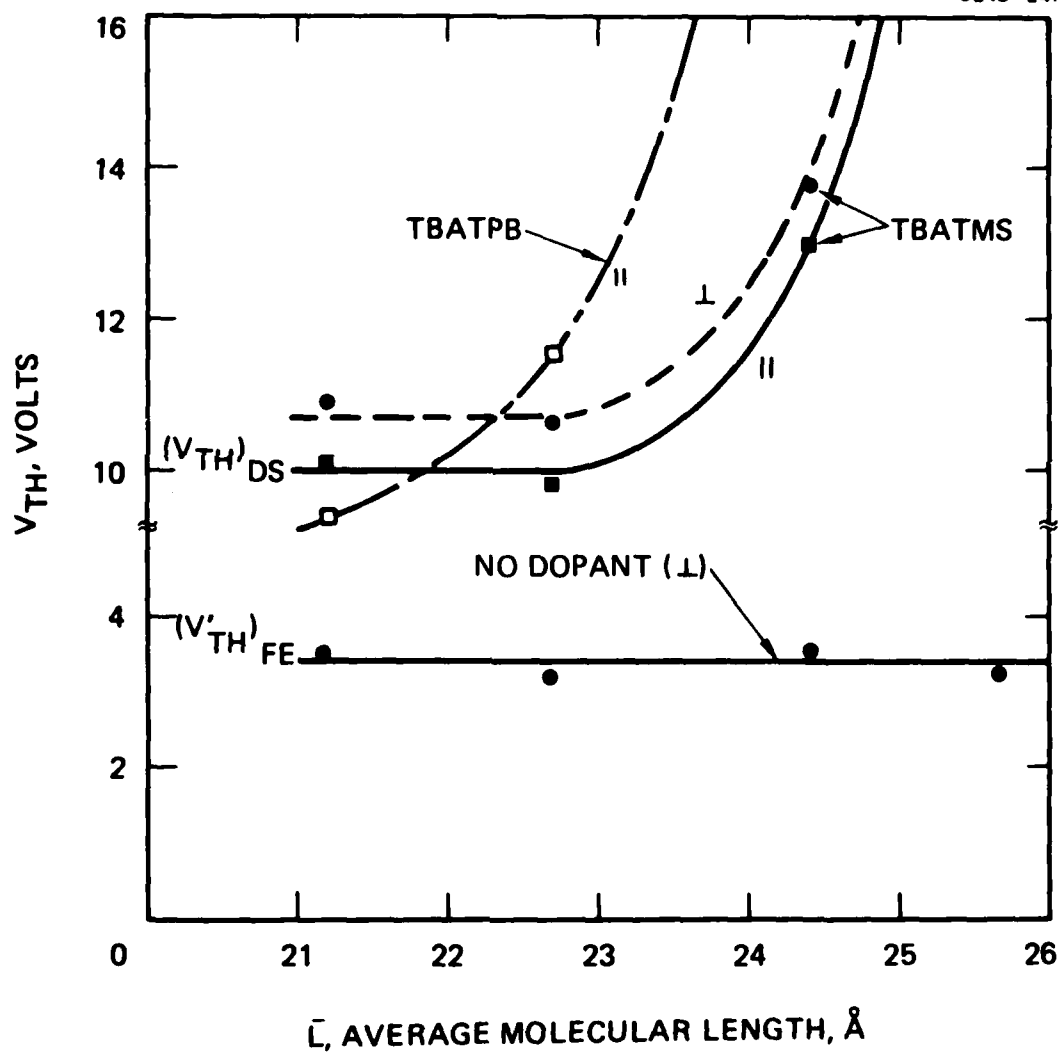


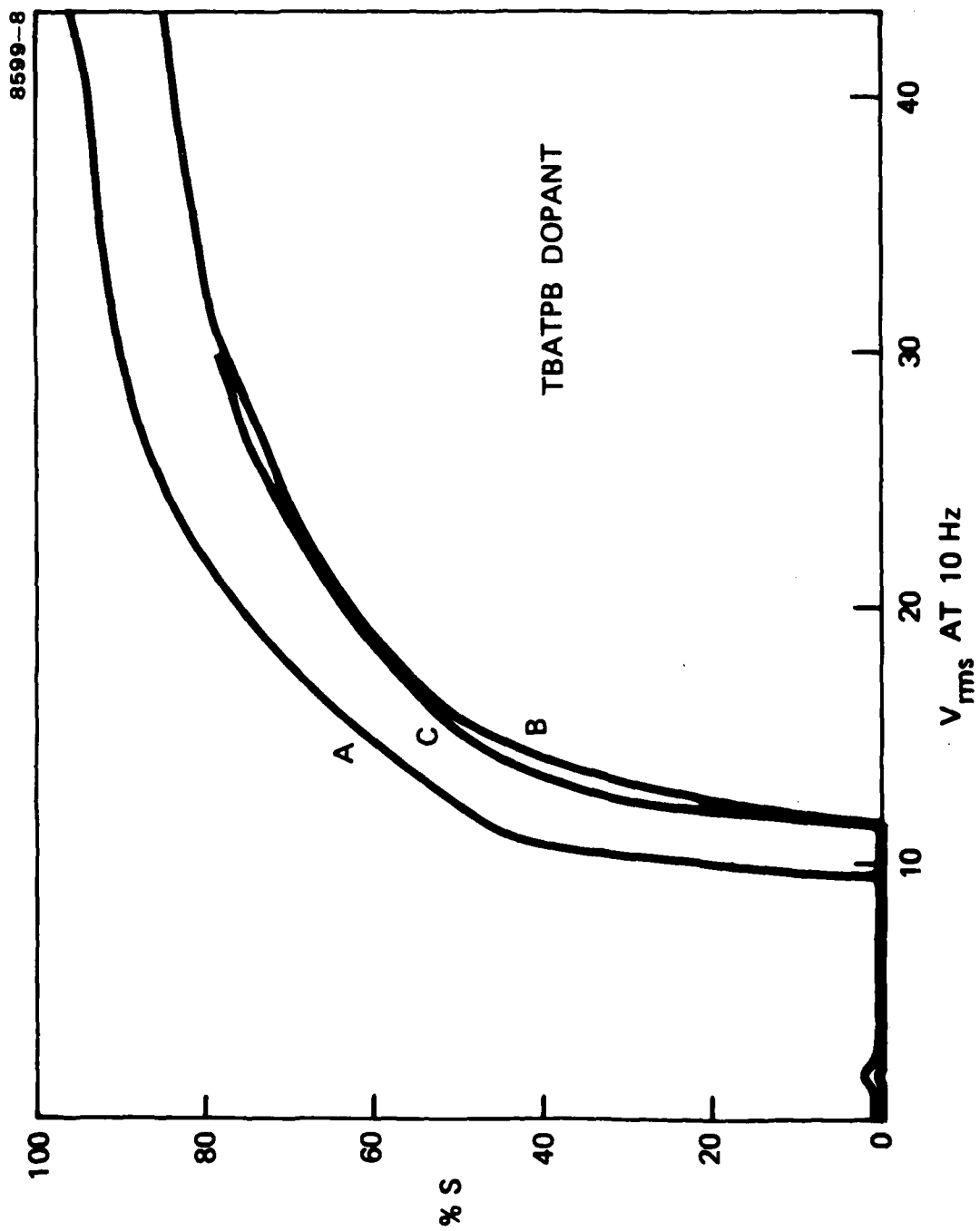


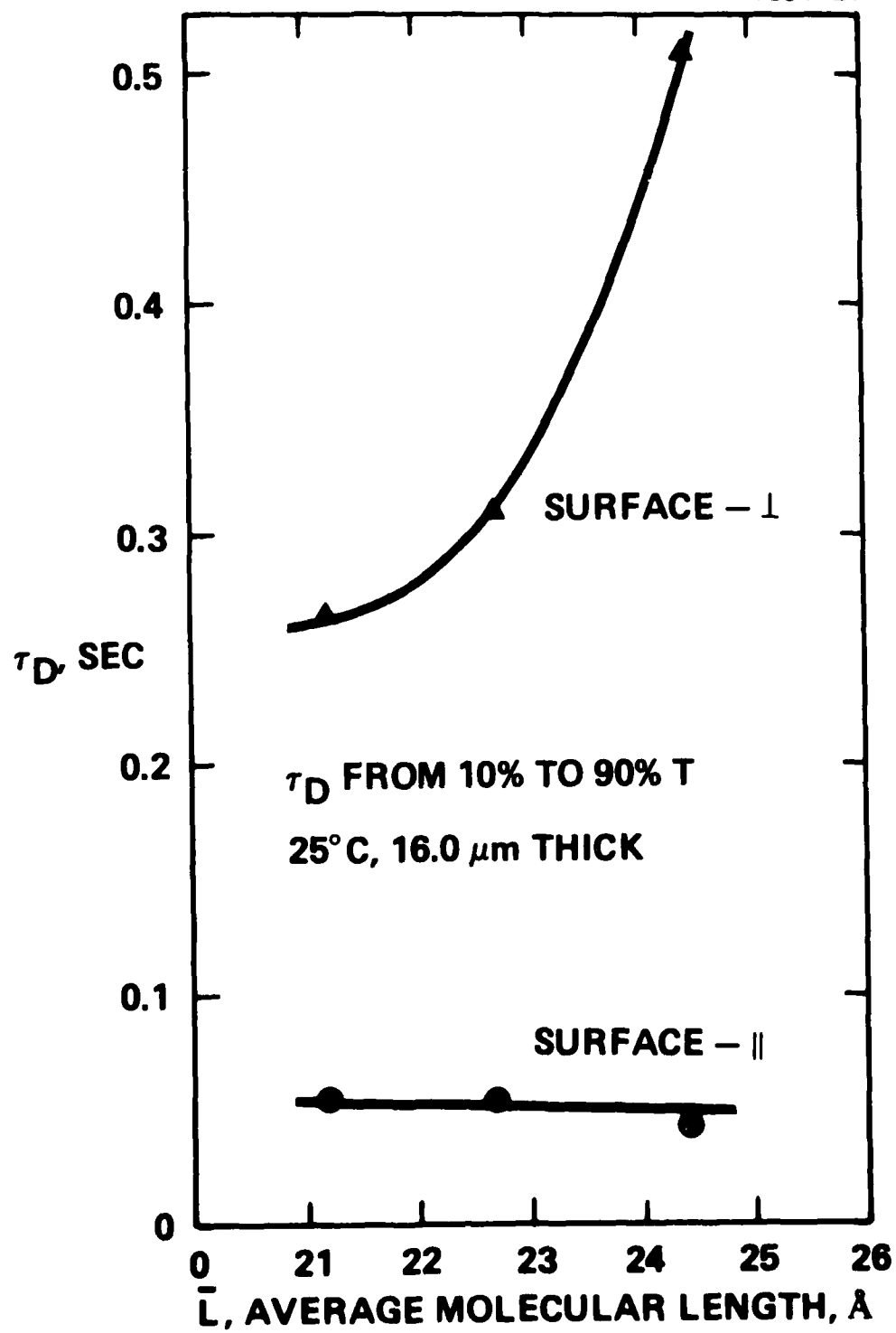












APPENDIX III

VARIABLE GRATING MODE LIQUID CRYSTAL DEVICE
FOR OPTICAL PROCESSING AND COMPUTING*

B.H. Soffer, J.D. Margerum, A.M. Lackner, D. Boswell
Hughes Research Laboratories
3011 Malibu Canyon Road
Malibu, California 90265

A.R. Tanguay, Jr., T.C. Strand, A.A. Sawchuk, P. Chavel**
Image Processing Institute
University of Southern California
Los Angeles, California 90007

Abstract

Certain nematic liquid crystal mixtures are observed to form a "variable grating mode" (VGM) for appropriate choices of cell design and applied voltage. In this mode of operation, a phase grating in the plane of the cell arises from a periodic variation in the orientation of the liquid crystal director. The grating spatial frequency is observed to vary linearly as a function of the applied voltage above the formation threshold. Liquid crystal and device parameters characteristic of the observed variable grating mode are presented. Utilization of the VGM effect in a photoconductively-addressed device is shown to provide an intensity-to-spatial frequency conversion. Applications of this unique type of optical transducer to arbitrary nonlinear optical processing problems are described. Results of level slicing experiments and implementation of optical logic functions are presented.

*Presented at the 8th International Liquid Crystal Conference, Kyoto, Japan, 1980.

**Permanent address: Institut d'Optique, Universite de Paris sud, Orsay, France.

I. Introduction

The variable grating mode (VGM) effect, in which some nematic liquid crystal layers exhibit a laterally periodic optical phase characterized by a voltage dependent spatial frequency, has been observed by several authors [1-6]. A VGM liquid crystal device can be constructed with the addition of a photoconductive layer in series with the liquid crystal layer [4]. When utilized as an optical-to-optical image transducer, this device has the rather unique property of converting in real time the intensity of an input image into a spatial frequency. Such an intensity-to-spatial frequency converter can be employed to implement arbitrary nonlinear point operations on input images.

In Section II of this paper, we describe our investigations on the VGM effect as a function of compositional differences in phenyl benzoate liquid crystal mixtures, from which we chose an ester mixture for use in our photo-activated device. The construction and operation of this VGM liquid crystal device is described in Section III. The unique approach to real time point nonlinear optical processing offered by this device is illustrated in Section IV. The principal advantages with respect to earlier point nonlinear optical processing schemes [7-12] including real time approaches [13-16] are discussed, especially for the implementation of optical binary logic operations [17-19].

II. VGM Effects and Materials Considerations

In the variable grating mode operation of liquid crystals, a phase grating is formed with a period that depends upon the voltage placed across the cell. This phase grating originates from a variation of the optical path length due to a periodic orientational perturbation of the liquid crystal uniaxial index

ellipsoid. The direction of periodicity is perpendicular to the quiescent state alignment of the liquid crystal molecules, i.e., the domains are parallel to the liquid crystal alignment in the off state. Typical spatial frequency variation is from 100 to 600 cycles/mm. Figure 1 shows typical voltage-induced behavior of a VGM cell as seen through a polarizing microscope. The period of the phase grating can be seen to decrease as the applied voltage increases. Some imperfections in the VGM device can also be observed in the photographs. Inconsistencies in the grating alignment within each picture and from picture to picture may be noted. The optical diffraction patterns resulting from the phase grating in a typical VGM cell are shown in Figure 2.

We have observed VGM domains in planar cells up to about 13 μm in thickness of the liquid crystal. These VGM domains for static fields are always parallel to the quiescent state alignment direction on the electrode surface and are observed only with applied dc fields. These effects are entirely consistent with the experimental results of Barnik et al. [6], but do not support other observations that the cells must be about 6 μm thick or less [2,4,5], that the domain can be either parallel or perpendicular to the alignment direction [2-5], and that ac activation can be used [2]. Our undoped liquid crystals were relatively high in resistivity ($>10^{10}$ ohm-cm) and showed little or no dynamic scattering even at dc voltages as high as five times the threshold voltage.

The VGM effect in nematic-phase liquid crystals of negative dielectric anisotropy has been previously studied primarily with azoxy mixtures, such as Merck NP-V. These yellow-colored eutectic mixtures absorb light strongly in the near ultraviolet and blue (below 430 nm) region of the spectrum, and can undergo photodecomposition during extended illumination. We studied

phenyl benzoate liquid crystal mixtures because they are colorless (strong absorption below 350 nm), are more stable to visible light exposures, and are more easily purified than the azoxy mixtures. Since we have been studying structural effects (particularly molecular length) on the anisotropic and dynamic scattering properties of a series of phenyl benzoate mixtures [21], we examined the VGM response of this series as well as several other mixtures. The purpose was two-fold: (1) to select phenyl benzoate mixtures suitable for VGM studies in photoactivated devices, and (2) to look for correlations of structures or physical properties with the VGM effect. The materials studied are shown in Table 1. Their VGM characteristics are compared with some of their anisotropic properties in Table 2. The voltage dependence of their VGM domain grating frequency is shown in Figure 3.

Typical cell used in the foregoing experiments were fabricated from indium tin oxide (ITO) - coated, 1.27 cm or 0.32 cm thick optical flats. The liquid crystal layer was confined by a 6 μ m Mylar perimeter spacer. The liquid crystal surface alignment was obtained by spin-coating an aqueous solution containing polyvinyl alcohol on the ITO-coated surfaces, drying at 100°C, and gently rubbing to give a uniform directionality. The effect of dc voltage was observed with a polarizing microscope at 258x magnification for each liquid crystal mixture. The width d of the domain period (line pair) is inversely proportional to applied voltage according to

$$d = \kappa/V \quad (1)$$

where κ is a constant that is dependent on the particular liquid crystal mixture. This relationship is illustrated in Figure 3, in which dc voltage as a function of grating frequency $1/d$ for each eutectic mixture is a straight line

with slope α . Values of α for various liquid crystal mixtures are given in Table 2. A smaller value of α is preferred, since a smaller slope gives a larger range of spatial frequency for the VGM effect per unit applied voltage. Thus, HRL-2N40 was chosen as the best of these ester liquid crystal mixtures for use in our studies of the photoactivated VGM device. The HRL-2N42 mixture is also of interest because its α value is almost as low as that of HRL-2N40 and its viscosity is considerably lower.

There is an interesting correlation between the VGM effect and the average molecular length of the mixtures in the RO-R' ester series in Tables 1 and 2. As their length increases (due to longer alkyl end groups), the V_{th} and α of the first three mixtures (2N42, 2N43, and 2N42/48) increase. The longer length mixtures (2N44, 2N46 and 2N48) do not show VGM effects. Since the dielectric anisotropy ($\Delta\epsilon$) is reported [6] to have a large effect on VGM, it may be the change of $\Delta\epsilon$ with average length that causes these results. In this series the V_{th} increases as $\Delta\epsilon$ becomes more negative (with increasing length), and no VGM is observed when $\Delta\epsilon$ is -0.3 and more negative. This is similar to the VGM effects reported by Barnik et al. [6] for a much wider range of $\Delta\epsilon$. In a more complex series of phenyl benzoate mixtures (containing four different classes of end groups) they found that V_{th} increased as $\Delta\epsilon$ became more negative, and they also reported a critical value of $\Delta\epsilon = -0.3$. However, the critical value of $\Delta\epsilon$ apparently varies with composition of the end group classes used since our 2N25 mixture of RO-R' and RO-OR' esters shows VGM and has $\Delta\epsilon = -0.40$. Our latter group of three mixtures (2N11, 2N40 and 2N25), also shows a general trend of increased V_{th} with more negative $\Delta\epsilon$. The effect of $\Delta\epsilon$ appears to be less

significant in these mixtures than in the RO-R' series, but it should be noted that the 2N11 mixture is quite different in composition from the other two mixtures.

The grating lines in the VGM lie parallel to the surface alignment of the liquid crystal director in the off state. Although rubbing has proven to be satisfactory for test cells, a much more uniform homogeneous alignment can be obtained by ion-beam etching certain types of surfaces [25]. Figure 4 shows the best quality of domains that we have thus far obtained.

With the application of alternating fields of about 10 Hz, some cells were conductive enough to exhibit Williams-type domains [26]. These domains are perpendicular to the quiescent state alignment and their periodicity is only slightly affected by the applied field. The Williams domains exist in a narrow range above the threshold voltage due to dynamic scattering resulting from increasing turbulent flow within the cell as the voltage is increased [27]. This effect in conjunction with the very small variation in the spacing of domains, limits the utility of this mode as a diffraction device. For frequencies below 10 Hz, a mixed-mode behavior is observed in the more conductive cells, with VGM and Williams-type domains appearing sequentially. The cells also exhibit severe scattering during the appearance of the Williams domains, especially as the frequency is raised. We have not been able to produce pure VGM behavior with alternating fields of zero average value even for cases of very asymmetric waveforms.

The diffraction efficiency of the VGM cells depends strongly on the applied voltage, and can be as large as 25% in the second order (utilizing HRL 2N40 in

a 6 μm thick cell). Interesting polarization effects of the odd and even diffraction orders as a function of the input light polarization are being investigated.

III. VGM Device Description

The structure of the present photoactivated VGM device is shown schematically in Figure 5. This configuration is similar to the dc photoactivated liquid crystal devices described previously [28,29]. The cell includes a vapor-deposited ZnS photoconductor and liquid-crystal layer placed between ITO transparent electrodes that have been deposited on glass substrates. In operation, the applied dc voltage is impressed across the electrodes.

The operating principle of the device is straightforward. The photoconductor is designed to accept most of the drive voltage when not illuminated; the portion of the voltage that drops across the liquid crystal layer is below the activation threshold of the liquid crystal VGM effect. Illumination incident upon a given area of the photoconductive layer reduces its resistance, thereby increasing the voltage drop across the liquid crystal layer and driving the liquid crystal into its activated state. Thus, because of the VGM effect, the photoconductor converts an input intensity distribution into a local variation of the phase-grating spatial frequency. The high lateral resistance of the thin photoconductive film prevents significant spreading of the photoconductivity and the associated liquid crystal electrooptic effect. As a result, the light-activation process exhibits high resolution, as will be discussed in more detail below.

Because the VGM phenomenon is a dc instability effect occurring in high-resistivity ($\rho > 10^{12}$ Ω -cm) pure liquid crystal compounds, the device requires a high resistance photoconductive layer. Zinc sulfide has been selected as the photoconductor material for the best resistance match with the liquid crystal layer. Because the liquid crystal molecules are sensitive to photodecomposition in the ultraviolet, the ZnS layer is preferably made thick enough to optimize photoactivation in the blue region of the spectrum.

The ZnS layer is deposited on transparent ITO electrodes by evaporation or ion-beam-sputtering methods. The sputtered films were 0.5 μ m thick, highly transparent smooth surface layers. With the evaporation technique, we produced photoconductors of 1.5 to 5 μ m thickness, characterized by a hazy, rough surface appearance that caused difficulties in liquid crystal alignment parallel to the electrodes. It has been reported that vaporized ZnS causes homeotropic or tilted homeotropic orientation of the liquid crystal material [30]. Mechanical polishing of the evaporated photoconductors increased their transparency and surface uniformity, while polymer (PVA) coating the top of these ZnS layers, supplemented by additional surface treatment, resulted in good parallel alignment. Photoconductors were evaluated and compared by measuring the dark current and switching ratios of the resulting VGM devices.

From the preliminary photosensitive devices fabricated using a ZnS photoconductive layer to achieve the necessary high resistance, one cell was selected that aligned well and did not suffer the usual rapid deterioration seen in dc operation. This deterioration is assumed to result from poisoning of the liquid crystal by the diffusion of ions from the photoconductor. This particular cell was constructed of a 5 μ m thick evaporated ZnS layer that had been polished

and then rubbed with surfactant polyvinyl alcohol. The counterelectrode was an ITO transparent layer treated with the same surfactant. The 6 μm thick liquid crystal layer was made of HRL 2N40 ester. The dark series resistance of the 2.5 cm square cell was measured to be $3 \times 10^8 \Omega$. With -160 V applied to the photoconductor electrode and with saturation illumination of 7.3 mW/cm^2 in the passband 410 to 550 nm, the spatial frequency of the VGM domains was calculated from the observed angles of diffracted orders to be 588 lines/mm. The device threshold at this illumination was 21 V, corresponding to a grating frequency of 103 lines/mm. The optical threshold at 160 V is of the order of $50 \text{ }\mu\text{W/cm}^2$.

Planar VGM test cells were studied with respect to edge effects on resolution and possible "spillover" of domains into adjacent unactivated areas. Electrodes were specially prepared by removing sections of the conductive coating by etching. A parallel plate cell was constructed such that there were conductive areas facing each other, either with conductive edges aligned or with a maximum overlap of 150 μm of a conductive electrode over the nonconducting area. Cell spacing was 6.3 μm and the material was Merck NP-V. For alignment parallel to the edge when operating close to the threshold voltage, domains were parallel to the edge and within the active area. For higher voltages, there was fringe spillover by not more than one fringe spacing. For alignment perpendicular to the edge, domains appear to either terminate at the edge or to join with an adjacent domain. The quality of the edge behavior is shown in Figure 6. These studies indicated that implementation of the VGM effect in an image processing device should ultimately produce a resolution not limited by degradation due to edge effects.

IV. Nonlinear Optical Processing Using VGM Devices

IV.A. Implementation of Point Nonlinear Functions

The VGM liquid crystal device can be considered to be an intensity-to-spatial frequency converter capable of operating on two-dimensional images. The intensity-to-spatial frequency conversion allows the implementation of arbitrary point nonlinearities with a simple Fourier plane filters. When an input image illuminates the photoconductor surface of this device the intensity variations of the input image change the local grating frequency. If coherent light is utilized to Fourier transform the processed image, different spatial frequency components of the encoded image, corresponding to different input intensities, appear at different locations in the Fourier plane as shown in Figure 7. Within the dynamic range of the device, intensities can thus be mapped monotonically into positions along a line in Fourier space. The input intensity distribution has thus been coded into Fourier (spatial frequency) space. If the spatial frequencies of the VGM domains are much larger than the largest spatial frequency component encountered in the images to be processed, we are in the tractable situation, familiar in communications theory, where the carrier frequency is much higher than the modulation frequencies. Thus, by placing appropriate spatial filters in the Fourier plane it is possible to obtain different transformations of the input intensity in the output plane as depicted in Figure 7b. This figure describes the variable grating mode nonlinear processing algorithm graphically. The input intensity variation is converted to a spatial frequency variation by the characteristic function of the VGM device (upper right-hand quadrant). These variations are Fourier transformed by the optical system and the spectrum is modified by a filter in the Fourier plane (upper left-hand quadrant). Finally, a

square-law detection produces the intensity observed in the output plane (lower left-hand quadrant). Considered together, these transformations yield the overall nonlinearity (lower right-hand quadrant). Design of a proper spatial filter for a desired transformation is a relatively easy task. For example, a level slice transformation requires only a simple slit that passes a certain frequency band or bands. A mathematical formulation of nonlinear processing utilizing the VGM device is presented elsewhere [31]. The principal result of this analysis is the relation

$$bv_0 \geq 2N \quad (2)$$

where b is the pixel width, v_0 is the lowest usable VGM spatial frequency, and N is the number of distinguishable grey levels. This relation requires that the pixel size contains $2N$ periods of the lowest grating frequency if N grey levels are to be processed. For example, a 100×100 pixel image could be processed with 50 distinguishable grey levels on a 50 mm square device with $v_0 = 200$ cycles/mm.

The ability to perform arbitrary point nonlinearities over two-dimensional images greatly increases the flexibility of optical processing system. In the past few years several different approaches to the problem of implementing generalized nonlinearities have been investigated. These have included half-tone screen techniques [7-10], nonlinear devices [13-16], feedback methods [11], and a variable level slice [16] among others. The main advantage of the VGM approach over previous methods is the ease of programming the functional nonlinearity desired for a given image transformation. This is done simply by changing the transmittance distribution of the spatial A filter in the optical processing system. The spatial filter is of relatively low resolution

and need only have a space-bandwidth product equal to the number of grey levels to be processed independent of the space-bandwidth product of the input image.

The same programmability advantage applies to the implementation of binary logic operations. One device can be used to implement any of the combinatorial logic operations (AND, OR, XOR, and their complements) by simple changing a Fourier plane filter. Previously described optical logic systems were "hard-wired" to perform specific operations [17-20], in most cases one or more logic functions proved difficult or cumbersome to implement. Use of the VGM liquid crystal device for the implementation of combinatorial logic operations is described below.

IV.B. Demonstration of a Level Slice Function with the VGM Device

In this experiment the ability of the VGM device to generate a level-slice nonlinearity is demonstrated. The experimental arrangement is shown in Figure 8. A continuous tone input picture is illuminated by an arc lamp source and imaged onto the photoconductor surface of a VGM device which initially exhibits a uniform phase grating structure due to a dc bias voltage. The grating period is locally modulated by the input picture intensity, and this modulation is mapped into a position along a line in the spatial filter plane. A red filter ensures that only the readout laser beam enters the coherent optical processor. Sectors of small circular annuli of varying radii are used to pass certain spatial frequency bands. This in effect allows only prescribed input intensity ranges to appear in the output. Circular rather than straight slits are used to capture the weak light which in small part is diffracted into circular arcs (see Figure 2) because of the grating imperfections (see Figure 1). Figure 9 shows both the input and level sliced output pictures.

Figure 9a shows a positive print of the original image as photographed on the imaging screen. A negative of the original was used in the experiments. Figure 9b shows a low intensity level slice corresponding to a VGM spatial frequency of 120 lines/mm with approximately 3% bandwidth. In Figure 9c another level, corresponding to 153 lines/mm, is shown. Figure 9d at 236 lines/mm illustrates the interference from second harmonics. Weak second harmonics of the low intensity image slice corresponding to 118 lines/mm can appear in the 236 lines/mm level slice. In Figure 9e, a broader slice of approximately 11% bandwidth was taken centered about the level corresponding to 140 lines/mm. This picture may be compared with the previous slices and particularly with the slice shown in Figure 9c. Finally, Figure 9f shows a very high input intensity slice at 440 lines/mm with 10% bandwidth. Three grey levels may be seen simultaneously; these correspond to the superposition of three broad intensity slices.

IV.C. VGM Implementation of Logic Functions

To see how the VGM device can be used to implement binary logic operations, one need only realize that the function of a logic circuit can be represented as a simple binary nonlinearity operating on the incoherent superposition of two binary images as input. As shown in Figure 10, NOT is simply a hard-clipping inverter, while AND and OR are hardclippers with different thresholds and XOR is a level slice function.

The VGM device is well suited to implementing this type of nonlinearity. Since the nonlinearities associated with logic operations are binary functions, they can be implemented with simple slit apertures, i.e., 0 or 1 transmittance

values. A noteworthy advantage of the VGM approach over previous optical logic methods [17-20] is the ease of programming the nonlinearity, by merely changing the aperture in the spatial frequency plane.

Another feature of the VGM technique that is especially suitable for logic processing is that the input and output are physically separate beams. The input beam modulates a photoconductor; concurrently the image is read out with a second beam. This separation of input and output provides for the possibility of restoring the output levels to the desired 0 and 1 values even if the input levels are not exactly correct. This feature is essential to the production of a reliable logic system that is immune to noise and systematic errors in the levels. Electronic logic elements possess such level restoring capability, but currently proposed optical logic schemes [17-20] lack this essential characteristic.

A series of experiments were conducted to demonstrate the fundamental logic functions. Two input fields were superimposed at the VGM plane along with a bias illumination. The total illumination intensity on the photoconductor of the VGM device was thus the sum of the two input intensities and the bias intensity. The input illumination was a filtered high-pressure mercury arc lamp. The bias illumination was provided by a collimated tungsten bulb source. The VGM device was read out in transmission using a HeNe laser. A filter was placed in the Fourier plane to select the desired spatial frequencies for each logic function.

For these experiments, the inputs consisted of one vertical rectangular aperture and one horizontal aperture. When these were superimposed along with

the bias, a square image was formed with the four quadrants having the intensity levels shown in Figure 11. This image corresponds to the logic truth table shown. Thus the output images have intensity levels determined by the truth table associated with the desired logic function. The logic functions AND, OR, XOR and their complements were implemented sequentially as shown in Figure 11 by altering only the Fourier plane filter. Imperfections visible in the output plane data arise from defects in the cell structure of the VGM device employed in these experiments.

A more complete discussion of VGM logic implementation can be found in Reference [32].

V. Conclusion

The variable grating mode effect can be incorporated in a photoconductively-addressed device structure which provides an overall intensity-to-spatial frequency conversion. The optical processing experiments using the VGM liquid crystal device described in this paper demonstrate the potential of this real time optical image transducer for numerous parallel nonlinear operations on images. The molecular origin of the VGM phenomenon is now being studied in connection with the behavior of the VGM phase grating as observed by polarization microscopy and polarization-dependent optical diffraction. Improvements in such characteristics of the device as response time, uniformity, dynamic range and density of defects are under continuing investigation.

Acknowledgements

We gratefully acknowledge the helpful contribution of M. Piliavin in the early phase of this work. This project was sponsored by the Air Force Office

of Scientific Research under Grant AFOSR-77-3285 at USC and Contract F49620-77-C-0080 at HRL. Liquid crystal work on the project was partially supported by the Air Force Office of Scientific Research on Contract F49620-77-C-0017 at HRL.

References

1. L. K. Vistin', Sov. Phys. Dokl., 15, 908 (1971).
2. W. Greubel and W. Wolf, Appl. Phys. Lett., 19, 213 (1971).
3. J. M. Pollack and J. B. Flannery, in Liquid Crystals and Ordered Fluids, J. R. Johnson and R. E. Porter, eds. (Plenum Press, New York, 1978), 2, 557.
4. J. M. Pollack and J. B. Flannery, Society for Information Display 1976 Intern. Symp. Digest, 143 (1976).
5. P. K. Watson, J. M. Pollack and J. B. Flannery, in Liquid Crystals and Ordered Fluids, J. F. Johnson and R. E. Porter, eds. (Plenum Press, New York, 1978), 3, 421.
6. M. I. Barnik, L. M. Blinov, A. N. Trufanov and B. A. Umanski, J. de Physique, 39, 26 (1978).
7. H. Kato and J. W. Goodman, Appl. Opt., 14, 1813 (1975).
8. T. C. Strand, Opt. Commun., 15, 60 (1975).
9. S. R. Dashiell and A. A. Sawchuk, Appl. Opt., 16, 1009 (1977).
10. S. R. Dashiell and A. A. Sawchuk, Appl. Opt., 16, 2279 and 2394 (1977).
11. B. J. Bartholomew and S. H. Lee, Appl. Opt., 19, 201 (1980).
12. A. Tai, T. Cheng, and F. T. S. Yu, Appl. Opt., 16, 2559 (1977).
13. D. Casasent, Opt. Eng., 19, 228 (1974).
14. S. Iwasa and J. Feinleib, Opt. Eng., 13, 235 (1974).
15. A. Armand, A. A. Sawchuk, T. C. Strand, D. Boswell, and B. H. Soffer, Opt. Lett., 5, 129 (1980).
16. J. D. Michaelson and A. A. Sawchuk, Proc. Soc. Photo Opt. Instrum. Engin., 218, 107 (1980).

17. R. A. Athale and S. H. Lee, Opt. Eng., 18, 513 (1979).
18. S. A. Collins, Jr., U. H. Gerlach, and Z. M. Zakman, Proc. Soc. Phot. Opt. Instrum. Eng., 185, 36 (1979).
19. D. H. Schaefer and J. P. Strong, III, Proc. IEEE, 65, 129 (1977).
20. L. Goldberg and S. H. Lee, Appl. Opt., 18, 2045 (1979).
21. J. B. Margerum, J. E. Jensen, and A. M. Lackner, Mol. Cryst. Liq. Cryst. (in press).
22. A. D. Jacobson, "Development of a Reflective Mode Liquid Crystal Light Valve," NAVSEA Contract N0024-73-C-1185 Final Report (May, 1975).
23. H. S. Lim and M. J. Little, U.S. Pat. 4,128,312 (Dec. 5, 1978).
24. J. D. Margerum, "Anisotropic and Electro-Optical Effects in Liquid Crystals," AFOSR Contract N49620-77-C-0017 Final Report (Nov. 1980).
25. M. J. Little, H. L. Garvin and L. J. Miller, in Liquid Crystals and Ordered Fluids, J. F. Johnson and R. E. Porter, Eds. (Plenum Press, New York, 1978) 3, 497.
26. R. Williams, J. Chem. Phys., 39, 384 (1963).
27. G. H. Heilmeyer, L. A. Zanon and L. A. Barton, Proc. IEEE, 56, 1162 (1968).
28. J. D. Margerum, J. Nimoy and S. Y. Wong, Appl. Phys. Lett., 17, 51 (1970).
29. J. D. Margerum, T. D. Beard, W. P. Bleha and S. Y. Wong, Appl. Phys. Lett., 19, 216 (1971).
30. H. Kruger, H. F. Mahlim and W. Rauscher, U.S. Pat. 4, 112, 157, September 1978.
31. B. H. Soffer, D. Boswell, A. M. Lackner, P. Chavel, A. A. Sawchuk, T. C. Strand, and A. R. Tanguay, Jr. Proc. Soc. Photo-Opt. Instrum. Eng., 232, (1980) (in press).
32. P. Chavel, A. A. Sawchuk, T. C. Strand, A. R. Tanguay, Jr., and B. H. Soffer, Opt. Lett., 5, 398 (1980).

AD-A105 189

HUGHES RESEARCH LABS MALIBU CA F/G 20/6
ANISOTROPIC AND ELECTRO-OPTICAL EFFECTS IN LIQUID CRYSTALS (U)
AUG 81 K D MARGERUM F49620-77-C-0017

UNCLASSIFIED

AFOSR-TR-81-0690

NL

2 OF 2
ALL INFORMATION
CONTAINED
HEREIN IS UNCLASSIFIED

10-81

END
DATE
FILMED
10-81
DTIC

List of Tables

Table I. Liquid Crystal Mixtures Used for VGM Studies

Table II. Liquid Crystal Anisotropic Properties and VGM Response

List of Figures

Figure 1 VGM viewed through polarizing microscope.

Figure 2 Diffraction patterns of a VGM cell.

Figure 3 VGM voltage dependence for various liquid crystals.

Figure 4 The phase grating structure of the VGM device at a fixed voltage viewed through a phase contrast microscope.

Figure 5 Schematic diagram of the VGM device construction. Current devices are read out in transmission at a wavelength at which the photo-conductor is insensitive.

Figure 6 Behavior of domains near an edge.

Figure 7 VGM nonlinear processing. a) Experimental setup indicating the mapping of intensity to spatial frequency. b) The overall input-output characteristic can be found by stepping through the successive nonlinear transformations including 1) the intensity to spatial frequency conversion, 2) spatial filtering, and 3) intensity detection.

Figure 8 Experimental setup used to perform the level slice experiments. The spatial filter was a variable annular aperture.

Figure 9 Level slice results. a) Original image b-f) Level slice results for various apertures as discussed in the text.

Figure 10 Logic functions as simple nonlinearities. Given an input consisting of the sum of two binary inputs, different logical operations can be effected on those inputs by means of the depicted nonlinear characteristics. a) NOT, b) AND, c) OR, d) XOR.

Figure 11 VGM logic results. The right-hand column indicates ideal output levels for an image consisting of four quadrants corresponding to truth table values. The left-hand column shows the corresponding experimental results. The first row shows the input for all experiments which consisted of a superposition of two binary images. Succeeding rows show results for the logic operations OR, NOR, AND, NAND, XOR, and NXOR, respectively.

Table I. Liquid Crystal Mixtures Used for VGM Studies

Class and Number	End Group Composition			Nematic Range		Average Length, Å
	Mole Fraction			mp, °C	clpt, °C	
	Alkoxy/Alkyl	Dialkoxy	Dialkyl			
<u>Azoxy</u>						
Merck NP-V	1.000	-	-	-5	73	18.69
<u>RO-R' Esters^a</u>						
HRL-2N42	1.000	-	-	5	58	20.39
HRL-2N43	1.000	-	-	-6	52	22.37
HRL-2N42/48	1.000	-	-	2	57	23.36
HRL-2N44	1.000	-	-	-8	51	24.31
HRL-2N46	1.000	-	-	16	55	25.92
HRL-2N48	1.000	-	-	18	56	27.14
<u>RO-OR' Components^b</u>						
HRL-2N11	-	.428	.572	13	47	22.26
HRL-2N40	.755	.245	-	0	58	22.68
HRL-2N25	.772	.228	-	0	56	24.48

^a RO-R' refers to 4-alkoxyphenyl 4-alkylbenzoate esters. See Reference 21 for the exact composition of these multicomponent mixtures.

^b RO-OR' refers to 4-alkoxyphenyl 4-alkoxybenzoate esters. See References 22, 23, and 24 for the exact composition of 2N11, 2N40, and 2N25, respectively. The 2N11 mixture has a R-R' component, 4-butylphenyl 4-toluate, and no RO-R' components.

Table II. Liquid Crystal Anisotropic Properties and VGM Response

LC Number	Viscosity at 25°C, (cP)	Δn at 22°C & 589 nm	AC-Resistivity $\rho_{AC} \times 10^{-10}$ (ohm-cm)	$\Delta \epsilon$ at 25°C & 5 KHz	VGM Characteristics ^a		
					V_{th} (volts)	Width, d_{th} (μm)	Slope, α (Vmm/lp)
NP-V	24.9	0.290	2.0	-0.2	10	8.5	0.082
2N42	32.6	0.162	6.1	-0.22	10	5.4	0.099
2N43	36.5	0.148	7.2	-0.25	25	8.1	0.287
2N42/48	36.9	0.140	33.0	-0.29	35	5.6	0.340
2N44	38.1	0.136	10.0	-0.03	— ^b	—	—
2N46	39.8	0.135	21.0	-0.30	— ^b	—	—
2N48	44.5	0.134	23.1	-0.33	— ^b	—	—
2N11	43.8	0.133	2.8	-0.05	15	5.1	0.122
2N40	46.9	0.151	8.5	-0.28	16	4.3	0.089
2N25	48.5	0.139	11.0	-0.38	21	7.1	0.203

^a The threshold voltage, V_{th} , is the lowest voltage at which the width of the domain period, d_{th} , was easily measured in cells with 6 μm spacers.

^b No VGM observed up to 100 V dc.

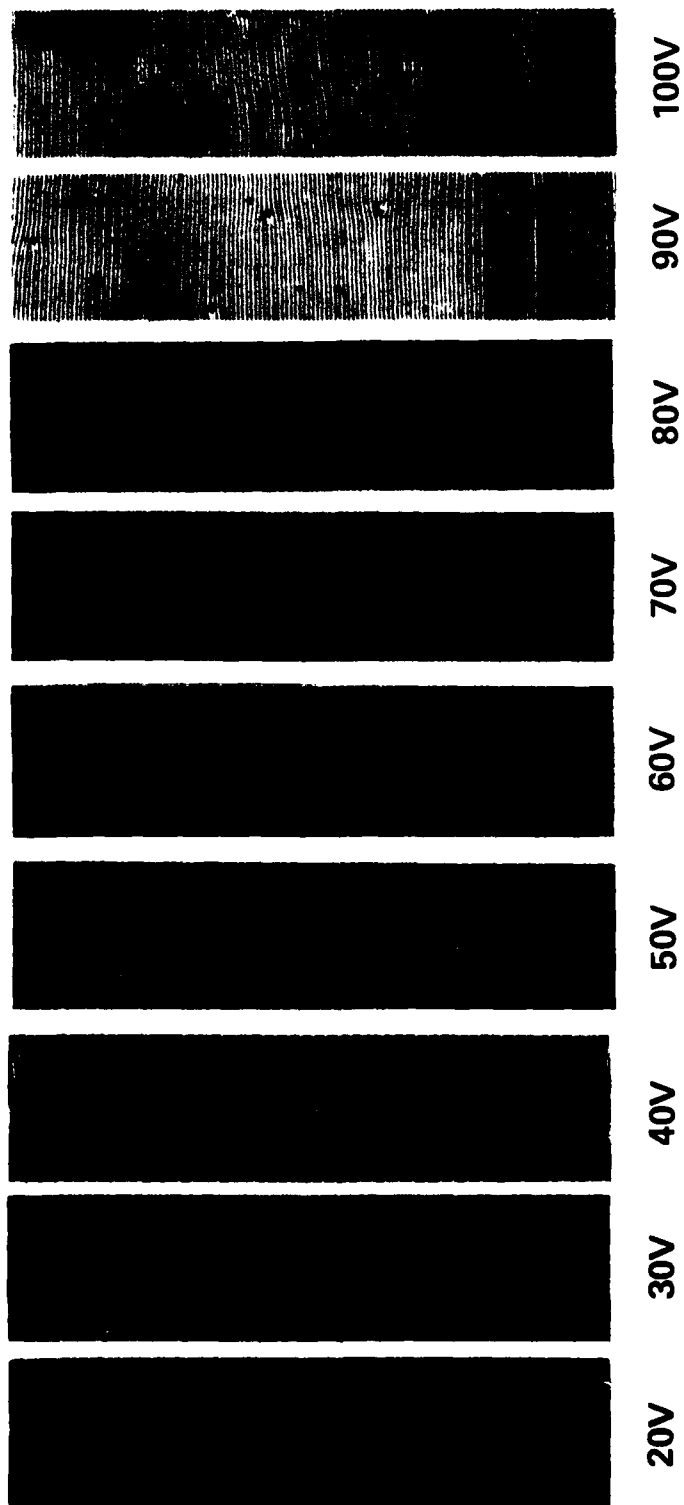
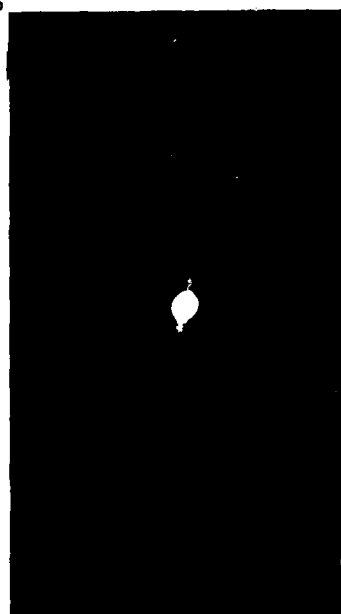
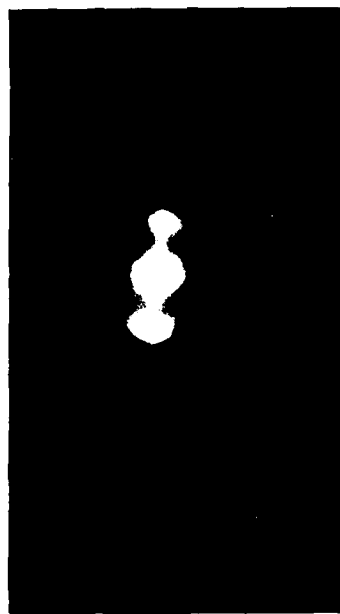


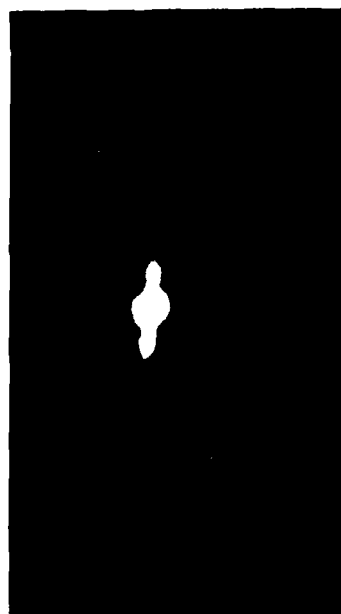
Figure 1. VCM viewed through polarizing microscope.



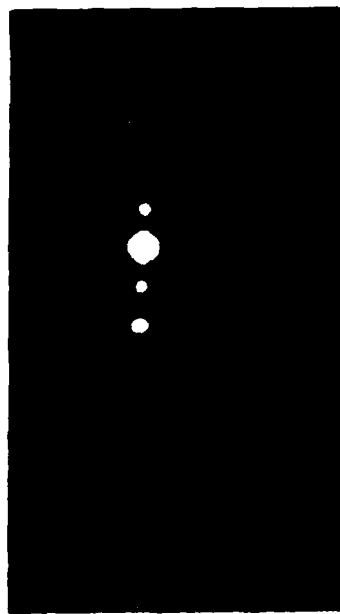
20V



40V



10V



30V

Figure 2. Diffraction pattern of well aligned VCM cell.

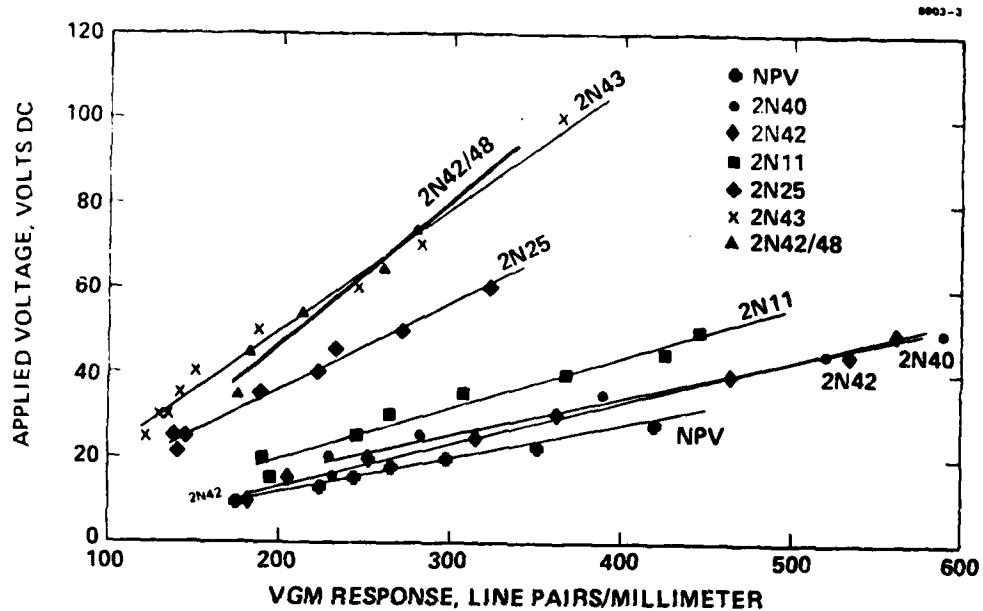


Figure 3 VGM voltage dependence for various liquid crystals.

7007-2

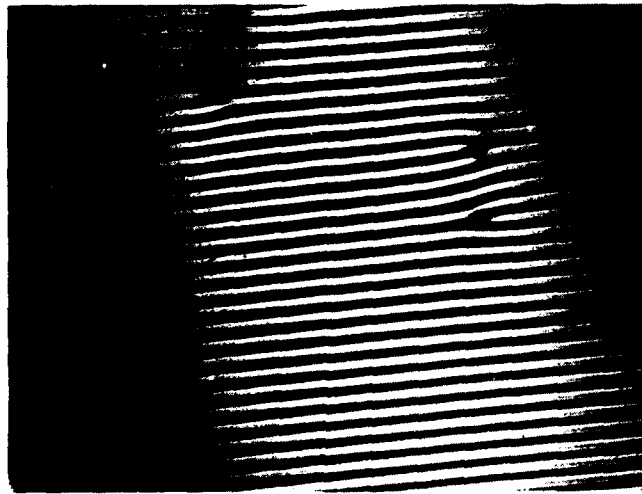


Figure 4. Domains in an etched cell. Magnification 133 times.

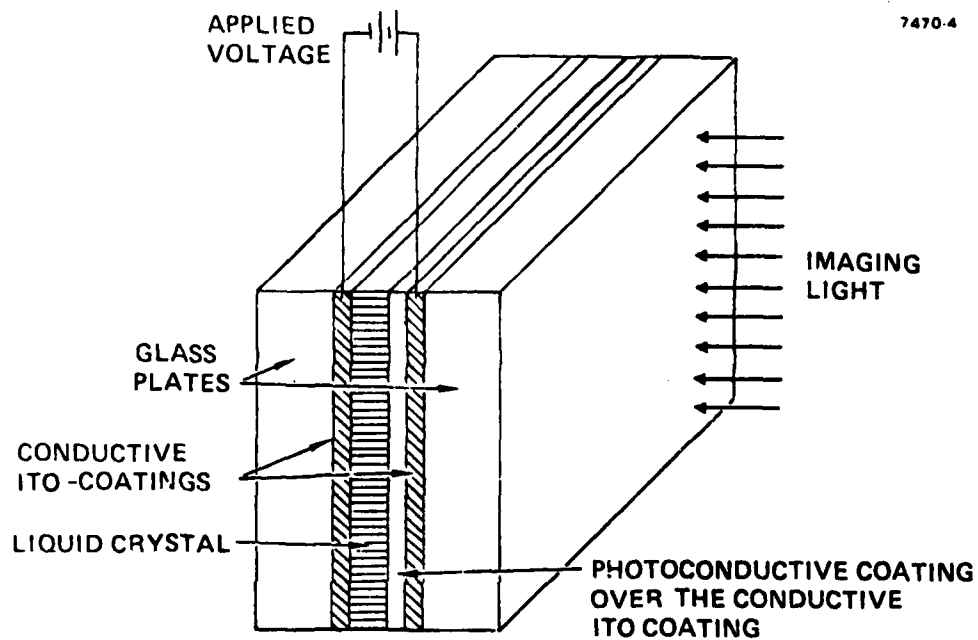
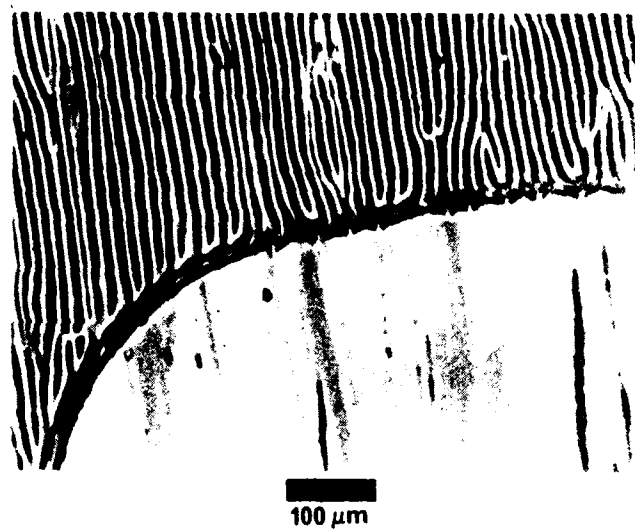


Figure 5. Schematic diagram of the VGM device construction. Current devices are read out in transmission at a wavelength at which the photoconductor is insensitive.



7007-3R1

Figure 6. Behavior of domains near an edge.

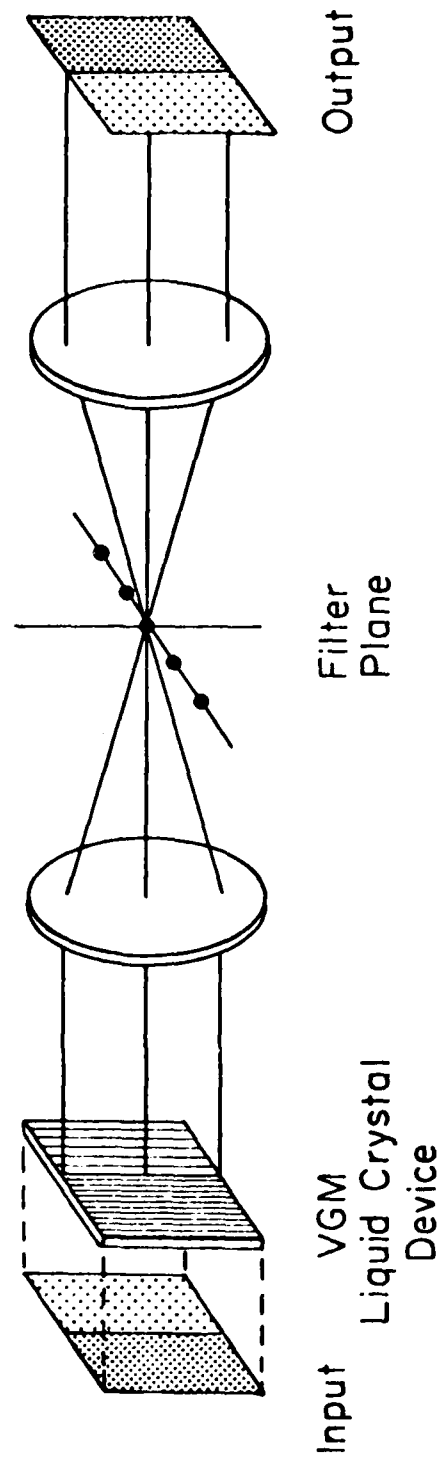


Figure 7. VGM nonlinear processing. (a) Experimental setup indicating the mapping of intensity to spatial frequency. (b) The overall input-output characteristic can be found by stepping through the successive nonlinear transformations including (a) the intensity to spatial frequency conversion, (2) spatial filtering, and (3) intensity detection.

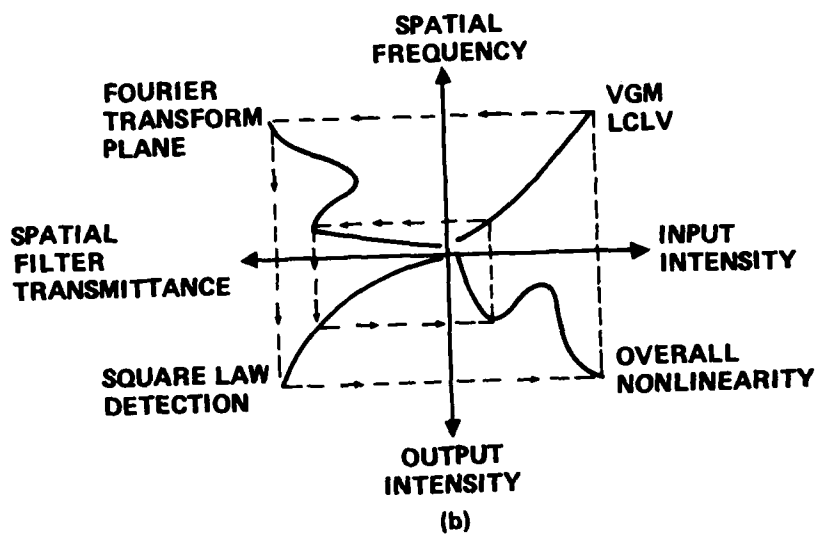


Figure 7(b).

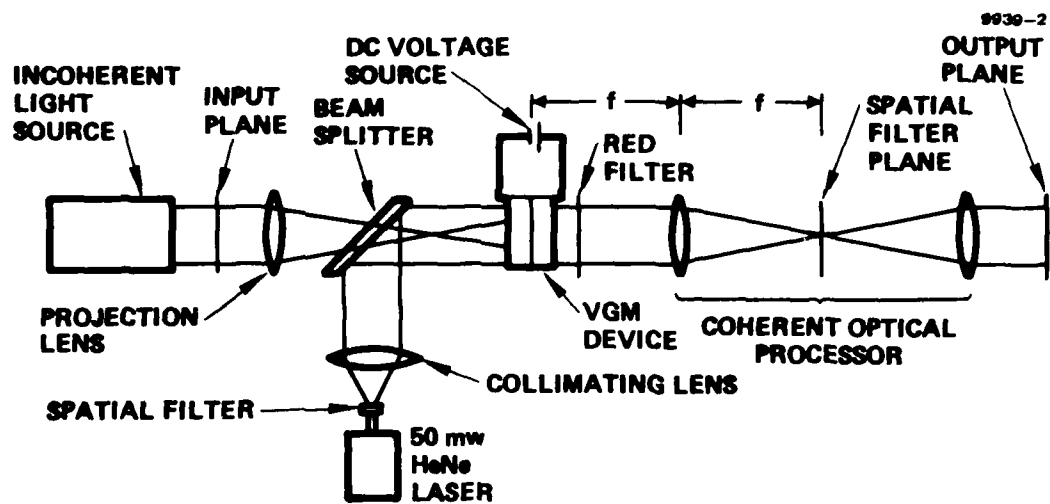
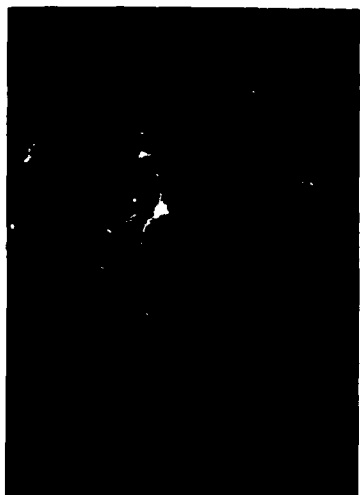


Figure 8. Experimental setup used to perform the level slice experiments. The spatial filter was a variable annular aperture.



C



B



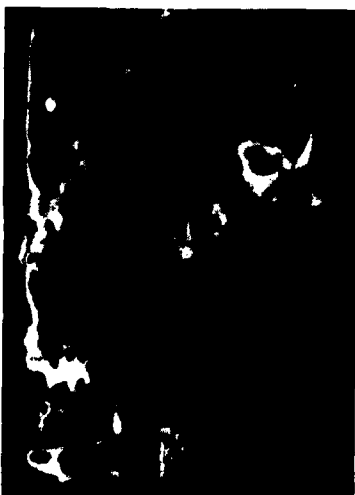
A ORIGINAL IMAGE



F



E



D

Figure 9. Level slicing with the VGM LCLV.

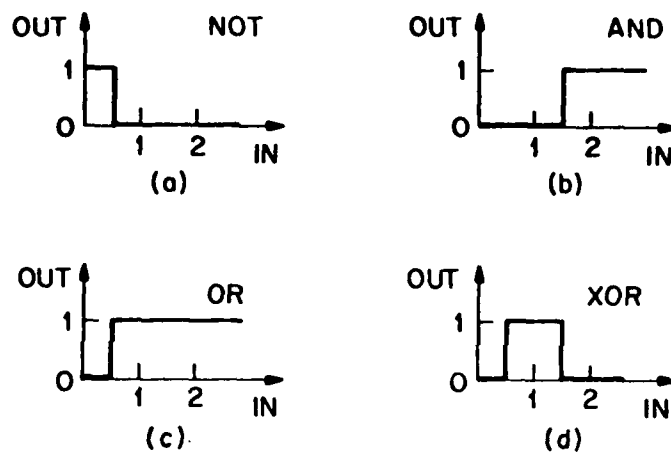


Figure 10. Logic functions as simple nonlinearities. Given an input consisting of the sum of two binary inputs, different logical operations can be effected on those inputs by means of the depicted non-linear characteristics. (a) NOT, (b) AND, (c) OR, (d) XOR.

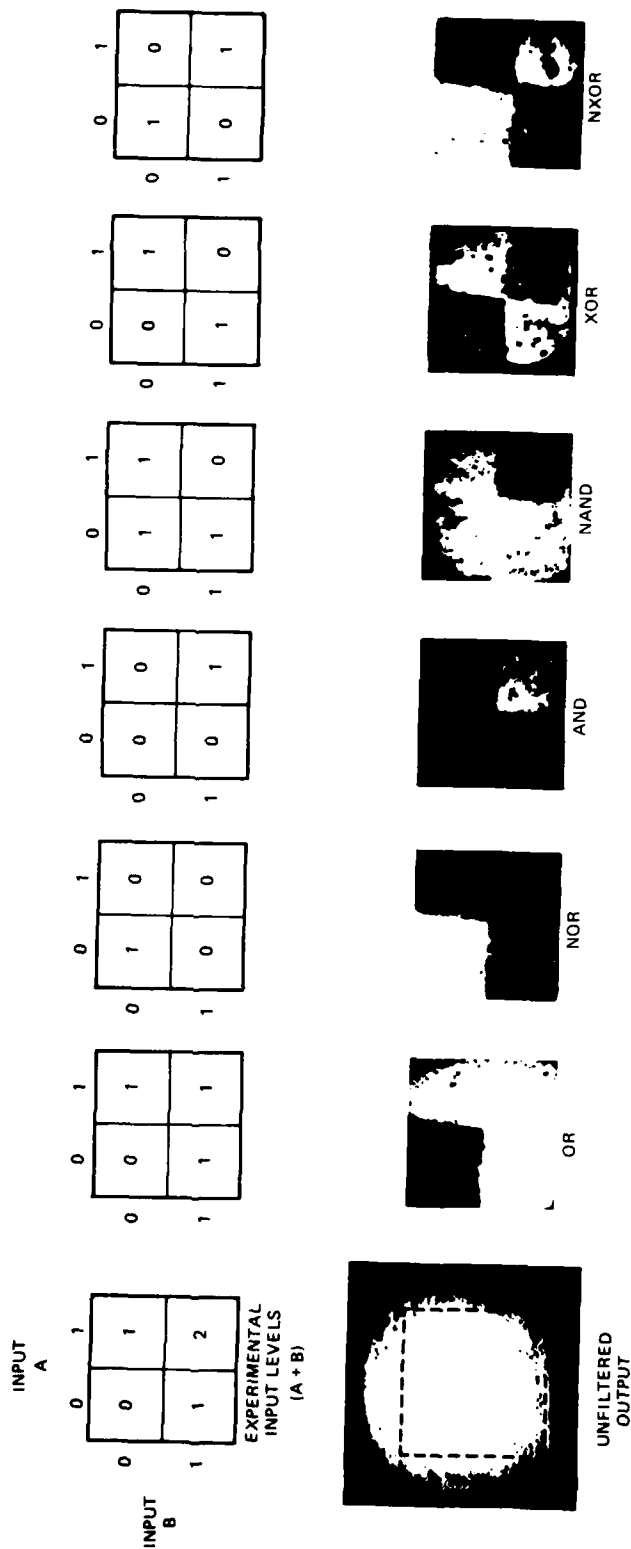


Figure 11. VGM logic results. The right-hand column indicates ideal output levels for an image consisting of four quadrants corresponding to truth table values. The left-hand column shows the corresponding experimental results. The first row shows the input for all experiments which consisted of a superposition of two binary images. Succeeding rows show results for the logic operations OR, NOR, AND, NAND, XOR, and NXOR, respectively.

APPENDIX IV

EFFECTS OF MOLECULAR LENGTH ON NEMATIC MIXTURES. III. ANISOTROPIC PROPERTIES OF 4-ALKYLPHENYL 4-ALKOXYBENZOATE MIXTURES.

J. David Margerum, Siu-May Wong, Anna M. Lackner,
John E. Jensen, and Scott A. Verzwylt

Hughes Research Laboratories
3011 Malibu Canyon Road
Malibu, California 90265

Abstract

Properties of multicomponent nematic mixtures of 4-alkylphenyl 4-alkoxybenzoates are studied as a function of temperature and their average molecular length (\bar{L}). The \bar{L} 's vary between 21.47 and 27.67 Å for mixtures with clearpoints in the 43 to 60°C range. The refractive indices, density, and the ϵ_{\perp} component of dielectric permittivity all decrease approximately linearly as \bar{L} increases. There are much larger changes in flow viscosity (η), conductivity anisotropy ($\sigma_{\parallel}/\sigma_{\perp}$), and dielectric anisotropy ($\Delta\epsilon$). At 25°C as \bar{L} increases: The η is relatively high and increases sharply (from 47 to 78 cP), the $\sigma_{\parallel}/\sigma_{\perp}$ decreases and drops below unity (from 1.35 to 0.58), and the $\Delta\epsilon$ changes from positive to negative (from +0.27 to -0.26). The temperature dependence of $\sigma_{\parallel}/\sigma_{\perp}$, with tetrabutylammonium tetraphenylboride as a dopant, indicates cybotactic nematic characteristics are present for the longer \bar{L} mixtures in which there are an average of about nine or more alkyl carbons from both end groups. The large decrease in $\Delta\epsilon$ at higher \bar{L} is attributed to increased molecular association effects in the cybotactic nematic mixtures.

I. Introduction

We have found that the anisotropic properties of nematic liquid crystals (LCs) in two series of ester mixtures depend strongly on their average molecular length (\bar{L}), which was varied by using mixtures of components with different length alkyl end groups.^{1,2} The present study is designed to determine if similar correlations also pertain to mixtures of 4-alkylphenyl 4-alkoxybenzoates (R-OR' mixtures), and particularly to find out how \bar{L} affects their cybotactic nematic characteristics and the related anisotropic properties of flow viscosity (η), conductivity anisotropy ($\sigma_{\parallel}/\sigma_{\perp}$), and dielectric anisotropy ($\Delta\epsilon$). Comparisons are made with the other two series of esters already studied, namely 4-alkoxyphenyl 4-alkylbenzoate (RO-R') mixtures¹ and 4-alkoxyphenyl 4-alkylcyclohexanecarboxylate (RO-[C]R') mixtures².

II. Experimental

The components in the LC mixtures are phenylbenzoate esters made by reacting the appropriate p-alkylphenols and p-alkoxybenzoyl chlorides. Most of the reactants are obtained commercially from either Aldrich Chemical, Frinton, or Eastman Organic. The hexyloxy-, pentyloxy-, and octyloxy-benzoyl chlorides are prepared from the corresponding benzoic acids. The esters are purified by several recrystallizations and are checked for impurities by thin-layer chromatography and by high-performance liquid chromatography (Waters Assoc. Model ALC-202/401 with a microporasil column). The esters all show less than 0.5% impurities, and their undoped LC mixtures all have resistivities greater than $10^{11} \Omega\text{-cm}$ at 25°C. The equipment used for studies on thermal analysis, flow viscosity, density, refractive index, dielectric anisotropy, and conductivity anisotropy were described previously.^{1,2}

III. Results and Discussion

III.A. LC Components and Mixtures

The thermal properties of the phenylbenzoate compounds used in our mixtures are shown in Table I, where R and R' are n-alkyl groups indicated by the general structure in Figure 1a. The melting points and heats of fusion from Table I are used to calculate the eutectic mixtures shown in Table II. The molecular length (L) of each compound is measured from the end-to-end distance in CPK models as indicated in Figure 1, using a fully extended conformation. Table III shows the average molecular length of each mixture and the observed nematic range compared to the calculated nematic range. In several mixtures, components with only small differences in L are used together. This can be done when the R and R' end groups of one component differ substantially from those of another component (e.g., 3-05 with 7-01, and 1-06 with 5-01). All of the mixtures are nematic in the temperature ranges of this study, but mixture M (HRL-2P36) has a smectic to nematic transition just below room temperature, at 20°C.

III.B. Refractive Index, Birefringence, Density, and Dielectric Constant

The effect of \bar{L} on the refractive indices ($n_{||}$ and n_{\perp}) and birefringence (Δn) are shown in Figure 2. Changes in the density (d), and dielectric constant (ϵ_1) as a function of \bar{L} are shown in Figure 3. Both $n_{||}$ and n_{\perp} decrease as \bar{L} increases, as expected since longer \bar{L} increases just the aliphatic end group length of the molecules, while the more polarizable central part of the structure is the same. There is an overall trend in which Δn decreases with \bar{L} , although the results are somewhat variable from mixture to mixture. The d and ϵ_1 values decrease linearly as \bar{L} increases, due to the increasing

contribution of alkyl groups to the molecular volume of these aromatic esters. The value of ϵ_1 at 25°C decreases by about 0.12 units per added methylene group, which is similar to the changes observed in the RO-R' series.

IV. Viscosity

The effect of temperature on the flow viscosity is shown for four of the mixtures in Figure 4. The plots of $\log \eta$ versus T^{-1} are not quite linear; similar curves are found for all of the other mixtures, whose plots are all within the range of those shown in Figure 4. The sharp rise in each viscosity curve at higher temperatures corresponds to the clearpoint transition to the isotropic liquid, which has a higher η than that of the nematic mixture. This rise of η at the clearpoint is expected because LC flow viscosities are often approximately equal to the Helfrich viscosity η_2 , which has been shown to increase near the clearpoint.^{3,4a} The effect of \bar{L} on viscosity is shown in Figure 5. Although there is considerable scatter in the η values at 25°C, both the 25 and 40°C curves indicate that, in general, η increases rapidly with increasing \bar{L} . These values of η at 25°C range from about 47 to 78 cP, which are considerably higher than the 33 to 44 cP values observed for RO-R' mixtures over the same \bar{L} variation. Presumably, the higher η of the R-OR' mixtures is partly due to the increased polarity of its molecules, in which the electron-donating alkoxy group is in a para-position to the electron-accepting carbonyl group of the aromatic ester. The exponential increase of η_{25° as \bar{L} increase from 25 to 28Å is attributed to the presence of cybotactic nematic characteristics (short range smectic ordering) as described below.

V. Conductivity Anisotropy

The conductivity anisotropy ($\sigma_{\parallel}/\sigma_{\perp}$) of tetrabutylammonium tetraphenylboride (TBATPB) in six different R-OR' LC mixtures is shown as a function of temperature in Figure 6. Included are mixtures with the shortest as well as the longest average molecular length in this series. The temperature dependence of $\sigma_{\parallel}/\sigma_{\perp}$ in mixtures K and M, in which $\sigma_{\parallel}/\sigma_{\perp}$ increases substantially as the temperature increases, is indicative of cybotactic nematic characteristics.^{5,6,7,8} Mixture M shows smectic-like $\sigma_{\parallel}/\sigma_{\perp}$ values (less than 1.0) below 41°C, with a value of only 0.58 at 25°C, although we observe its smectic nematic transition to be at 20°C. Cybotactic nematic effects are just discernible in mixtures H and I, where the total average number of carbon atoms in the R+R' end groups are 7.8 and 9.5 respectively. Thus, in the R-OR' mixtures, short range smectic ordering appears when the sum of the end group n-alkyl carbons is about nine or more. Similar cybotactic nematic effects were observed in the RO-R' series when the sum of the alkyl end group carbons reached an average of ten or more. The cybotactic nematic effects are stronger and occur at shorter \bar{L} s in these R-OR' mixtures than in the RO-R' mixtures.¹ The effect of \bar{L} is shown more clearly in Figure 7, where the $\sigma_{\parallel}/\sigma_{\perp}$ values are all compared at the same reduced temperature of $T = 0.93T_c$. At the shorter \bar{L} s the $\sigma_{\parallel}/\sigma_{\perp}$ values of TBATPB in these R-OR' mixtures are just a little lower than those in the RO-R' mixtures at the same reduced temperature. However, the steep decrease of $\sigma_{\parallel}/\sigma_{\perp}$ above 26Å which is shown in Figure 7 for these R-OR' mixtures was not observed in the RO-R' series. Because the viscosity of these R-OR' mixtures also increases sharply above 26Å (Figure 5), we attribute the η_{25° changes to the corresponding increase in cybotactic nematic character.

VI. Dielectric Anisotropy

The temperature effects on $\Delta\epsilon$ are shown for six of the mixtures in Figure 8. In the shorter length mixtures (A and C) the $\Delta\epsilon$ decreases steadily with temperature and drops to zero, as expected for positive nematic mixtures. The medium length mixtures (H and I) and the longer length mixtures (K and M) all show an increase of $\Delta\epsilon$ with increasing temperature, with maximum values not far below their clearpoints. At 25°C mixture K is nearly zero and M has a negative $\Delta\epsilon$ value rather than the positive $\Delta\epsilon$ usually associated with R-OR' LCs; the $\Delta\epsilon$ mixture of M is as negative as that of mixture A is positive. The effect of \bar{L} on $\Delta\epsilon$ is shown in Figure 7 at the reduced temperature of $T = 0.93T_c$, where there is a linear decrease of $\Delta\epsilon$ with increasing \bar{L} . The effects of temperature on the ϵ_{\perp} is similar in all of these mixtures, as shown in Figure 9. Thus, the maxima seen for the $\Delta\epsilon$ of H, I, K and M in Figure 8 are caused mainly by the changes in the ϵ_{\parallel} of these mixtures. This is probably due to increased polar associations of the central part of the molecules in the cybotactic nematic phase. Such an increase in the anti-parallel correlation of the dipoles along the director has been described in general by deJeu^{4b} for pre-transitional smectic order in the nematic phase. He cited 4,4'-diheptylazoxybenzene as an example in which $\Delta\epsilon$ decreased as the nematic phase approached the smectic transition. We observe here a much larger $\Delta\epsilon$ effect in mixture M in the 25 to 50°C range. However, we note from prior studies^{2,3} that cybotactic nematic ordering alone is not sufficient to cause decreases in ϵ_{\parallel} and $\Delta\epsilon$. This can be seen in Figure 10, where the temperature effects on $\Delta\epsilon$ are shown for both short and long \bar{L} mixtures in the three series R-OR', RO-R', and RO-[C]R'. The $\Delta\epsilon$ of each of these structural

classes is affected differently by \bar{L} , although cybotactic nematic effects are observed in each class at long \bar{L} . There are strong cybotactic nematic characteristics in the long RO-[C]R' mixtures but the $\Delta\epsilon$ is less negative in the long \bar{L} mixtures than in the short \bar{L} mixtures where no cybotactic effects are observed. The intermolecular association effects appear to be much larger in the R-OR' mixture, probably due to the dipolar character of the p-alkoxybenzoate structure.

VII. Conclusions

The flow viscosity of R-OR' mixtures increases strongly with increasing \bar{L} , and the η values are substantially higher than in RO-R' LC mixtures of comparable length. Cybotactic nematic effects are observed when the total average number of R + R' alkyl end group carbons is 9 or more. The $\sigma_{\parallel}/\sigma_{\perp}$ and $\Delta\epsilon$ values decrease with increasing \bar{L} . The R-OR' nematic mixtures with long \bar{L} have smectic-like characteristics of $\sigma_{\parallel}/\sigma_{\perp} < 1$, $\Delta\epsilon < 0$, and high η instead of the usual (nearly opposite) characteristics found at short \bar{L} . The behavior in long \bar{L} mixtures appears to be related to increased anti-parallel association of central molecular dipoles along the director as the cybotactic nematic character is increased by the longer alkyl end groups.

Acknowledgements

We are indebted to the Directorate of Chemical Sciences, Air Force Office of Scientific Research, Contract F49620-77-C0017 for partial financial support of this research; to C. I. van Ast for assistance in synthesis; and to W. H. Smith, Jr., for assistance in the DSC measurements.

References

1. J. D. Margerum, J. E. Jensen, and A. M. Lackner, Mol. Cryst. Liq. Cryst., in press, 1981. (Paper I of this series).
2. J. D. Margerum, S. -M. Wong, A. M. Lackner, and J. E. Jensen, Mol. Cryst. Liq. Cryst., in press, 1981. (Paper II of this series).
3. A. E. White, P. E. Cladis and S. Torza, Mol. Cryst. Liq. Cryst., 43, 13 (1977).
4. W. H. deJeu, Physical Properties of Liquid Crystalline Materials, (Gordon & Breach, New York, 1980): (a) p. 121, (b) p. 61.
5. F. Rondelez, Solid State Comm., 11, 1675 (1972).
6. A. Mircea-Roussel, L. Legar, F. Rondelez, and W. H. deJeu, J. de Physique, Colloq., C136, 93 (1975).
7. G. Heppke and F. Schneider, Z. Naturforsch., 309, 316 (1975).
8. A. DeVries, J. de Physique (Paris) Colloq., C136, 1 (1975).

List of Tables

- Table I. Thermal Properties of Components
- Table II. Composition of Liquid Crystal Mixtures
- Table III. Average Length and Nematic Range of R-OR' Mixtures^a

List of Figures

- Figure 1 (a) General structure of R-OR' LC mixture components.
(b) Model of 4-n-propylphenyl 4-n-heptyloxybenzoate (3-07) showing the molecular length used ($L = 25.87\text{\AA}$).
- Figure 2 Refractive index and birefringence of R-OR' LC mixtures as a function of \bar{L} . (589 nm, 21°C).
- Figure 3 Effect of \bar{L} on density and dielectric constant of R-OR' LC mixtures.
- Figure 4 Temperature dependence of viscosity of R-OR' mixtures.
- Figure 5 Effect of \bar{L} on flow viscosity of R-OR' LC mixtures.
- Figure 6 Effect of temperature on conductivity anisotropy of R-OR' mixtures with TBATPB dopant.
- Figure 7 Effect of \bar{L} on conductivity anisotropy and dielectric anisotropy of R-OR' mixtures (T = temperature, °K and T_c = clearpoint, °K).
- Figure 8 Effect of temperature on dielectric anisotropy in R-OR' mixtures.
- Figure 9 Effect of temperature on the ϵ_1 dielectric constant of R-OR' mixtures.
- Figure 10 Comparison of \bar{L} and temperature effects on $\Delta\epsilon$ in three series of mixtures. The \bar{L} s for R-OR' are 21.47 and 27.67 \AA , for RO-R' are 20.39 and 27.14 \AA , and for RO-[C]R' are 21.20 and 26.15 \AA .

Table I. Thermal Properties of Components

R	Compound OR ^a	Code	mp, °C		Clpt, °C		ΔH_f Kcal/Mole
			Obs.	Lit.	Obs.	Lit.	
CH ₃	OC ₄ H ₉	1-04	77.4	-	^a	-	6.96
CH ₃	OC ₆ H ₁₃	1-06	62.5	-	50.7	-	5.86
C ₃ H ₇	OC ₅ H ₁₁	3-05	42.5	41 ^b	51.7	47 ^b	6.76
C ₃ H ₇	OC ₇ H ₁₅	3-07	65.0	65 ^b	56.5	58 ^b	6.63
C ₅ H ₁₁	OCH ₃	5-01	28.6	29.5 ^b	42.1	43.5 ^b	3.56
C ₅ H ₁₁	OC ₆ H ₁₃	5-06	49.8	48 ^b	62.2	62 ^b	5.23
C ₇ H ₁₅	OCH ₃	7-01	32.6	34 ^c	42.8	42.5 ^c	5.56
C ₇ H ₁₅	OC ₆ H ₁₃	7-06	46.0	45.5 ^c	63.5	63 ^c	5.77
C ₇ H ₁₅	OC ₈ H ₁₇	7-08	47.7	-	67.3	-	6.92

^aNo clpt observed, but 30°C is used as an approximate virtual
neumatic clpt.

^bJ. P. Van Meter and B. H. Klanderman, Mol. Cryst. Liq. Cryst., **22**,
271 (1973).

^cR. Steinstrasser, 4th International Liq. Cryst. Conf., Kent, Ohio
(1972).

Table II. Composition of Liquid Crystal Mixtures

Compound		Mole Fraction in Mixtures												
Code ^a	L, Å	A	B	C	D	E	F	G	H	I	J	K	M	
1-04	19.81	-	0.067	-	-	-	-	-	-	-	-	-	-	
1-06	22.25	0.238	0.149	0.172	0.133	-	-	-	-	-	-	-	-	
3-05	23.51	-	0.211	0.229	-	-	0.249	-	-	0.264	-	-	0.216	
3-07	25.87	-	-	-	-	0.200	0.126	-	-	-	0.173	-	0.110	
5-01	21.23	0.762	0.573	0.599	0.535	0.800	0.625	0.680	0.682	-	-	-	-	
5-06	27.15	-	-	-	-	-	-	0.320	-	-	-	0.308	0.254	
7-01	23.57	-	-	-	0.332	-	-	-	-	0.446	0.551	0.466	-	
7-06	29.61	-	-	-	-	-	-	-	0.318	0.290	-	-	0.245	
7-08	32.00	-	-	-	-	-	-	-	-	-	0.276	0.226	0.174	
HRL Mixture No.		2P13	2P14	2P15	2P17	2P16	2P18	2P19	2P20	2P21	2P31	2P32	2P36	

^a See Table I.

Table III. Average Length and Nematic Range of R-OR' Mixtures^a

Mixture	Average Length, \bar{L} , Å	Average Carbons in R + R'	mp, °C		Clpt., °C	
			Calc.	Obs. ^b	Calc.	Obs. ^c
A	21.47	6.24	15.3	-	44.2	43.2
B	21.77	6.50	2.7	-	44.6	44.8
C	21.93	6.63	4.6	-	45.8	44.5
D	22.15	6.80	-0.2	-	43.5	43.0
E	22.16	6.80	17.6	-	45.0	44.6
F	22.38	7.00	6.4	-	46.3	45.6
G	23.13	7.60	10.1	-	48.6	49.1
H	23.89	7.59	10.3	-	48.9	49.5
I	25.31	9.45	7.8	-	51.1	51.5
J	26.29	10.28	13.8	-	52.0	53.0
K	26.58	10.51	9.0	-	54.3	55.3
M	27.67	11.42	3.3	(19.9) ^d	60.5	60.6

^a Calculated as eutectic compositions, with \bar{L} calc. from Table II.

^b All mixtures are nematic at room temperature.

^c Clpt. observed in viscometer bath.

^d Smectic to nematic transition obs. by DSC.

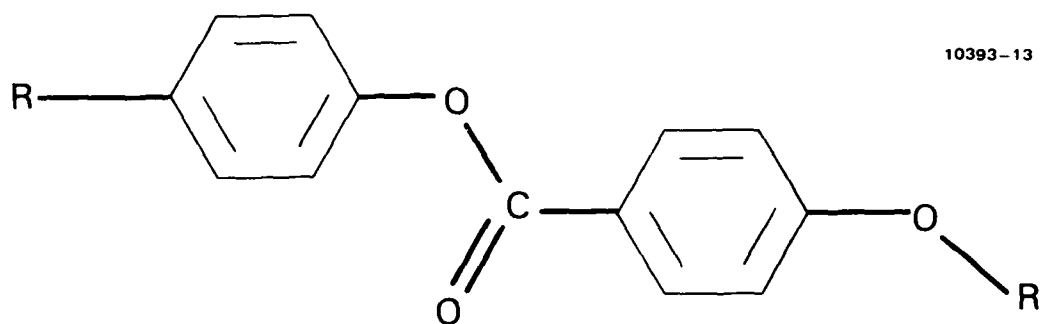


Figure 1(a). General structure of R-OR' LC mixture components.

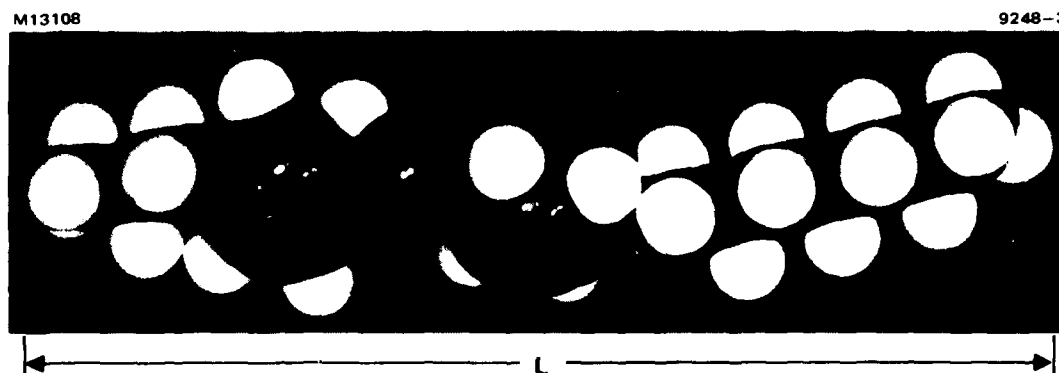


Figure 1(b). Model of 4-n-propylphenyl 4-n-heptyloxybenzoate (3-07) showing the molecular length used ($L = 25.87 \text{ \AA}$).

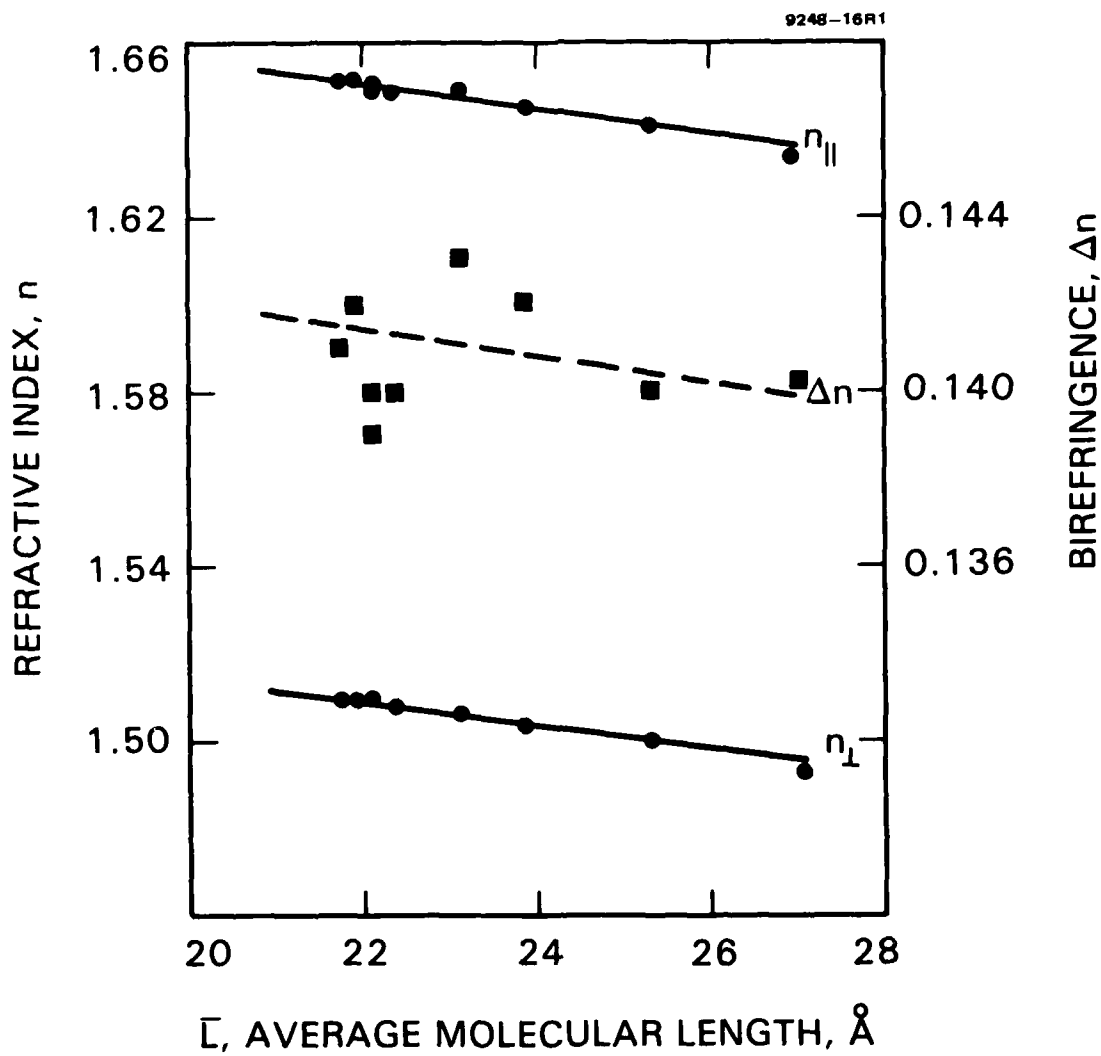


Figure 2. Refractive index and birefringence of R-OR' LC mixtures as a function of \bar{L} . (589 nm, 21°C).

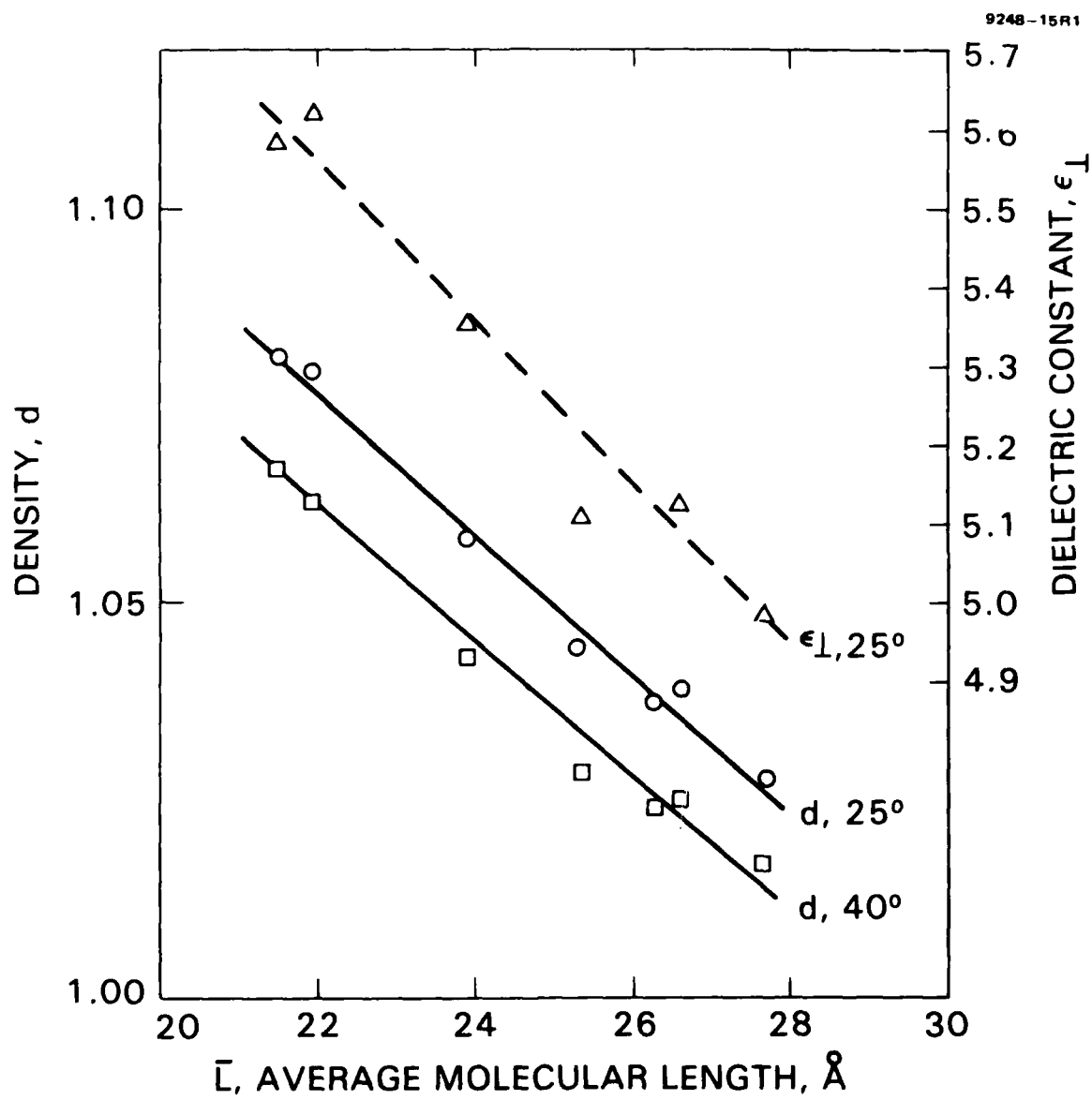


Figure 3. Effect of \bar{L} on density and dielectric constant of R-OR' LC mixtures.

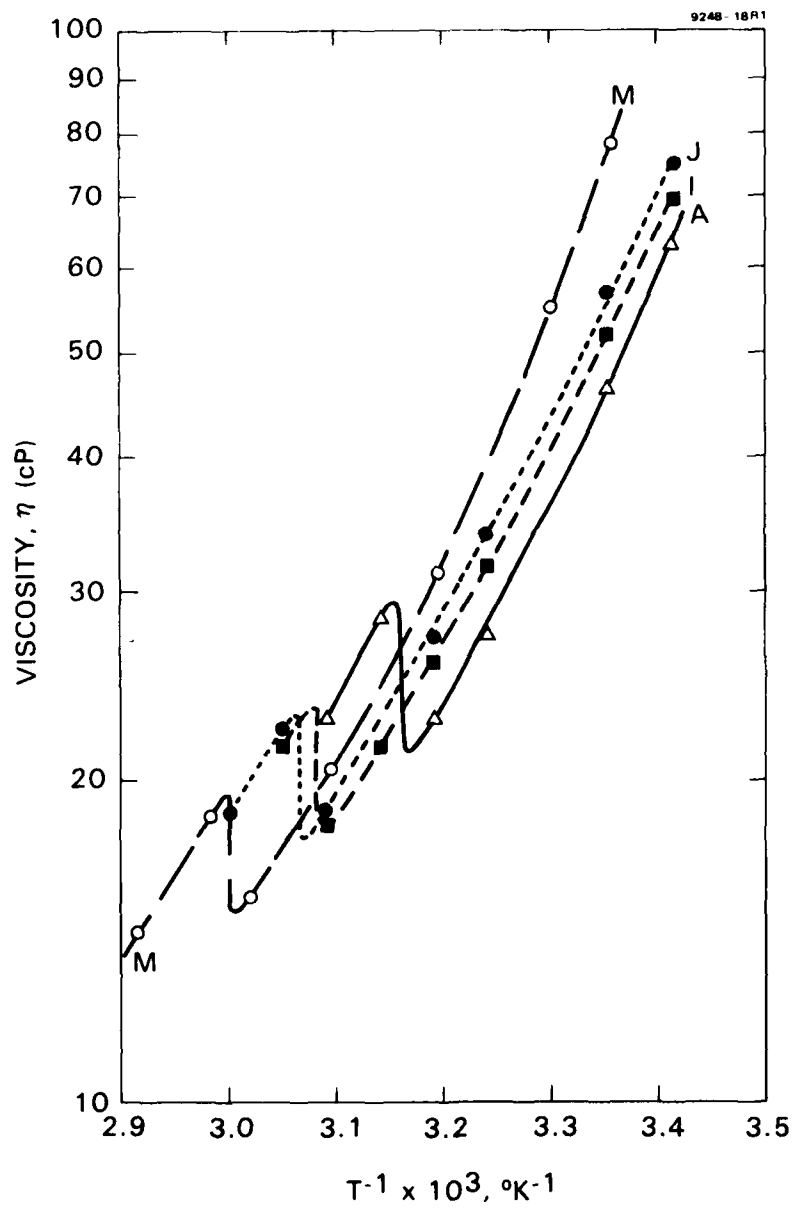


Figure 4. Temperature dependence of viscosity of R-OR' mixture.

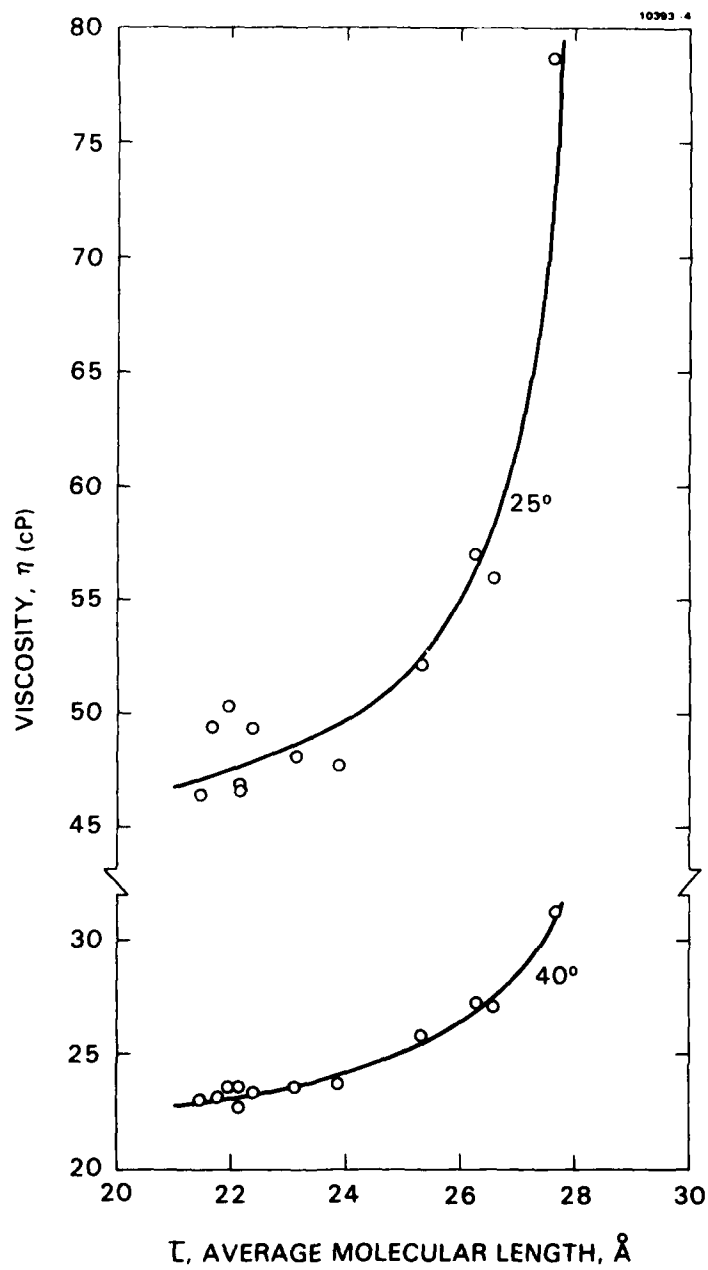


Figure 5. Effect of \bar{L} on flow viscosity of R-OR' LC mixtures.

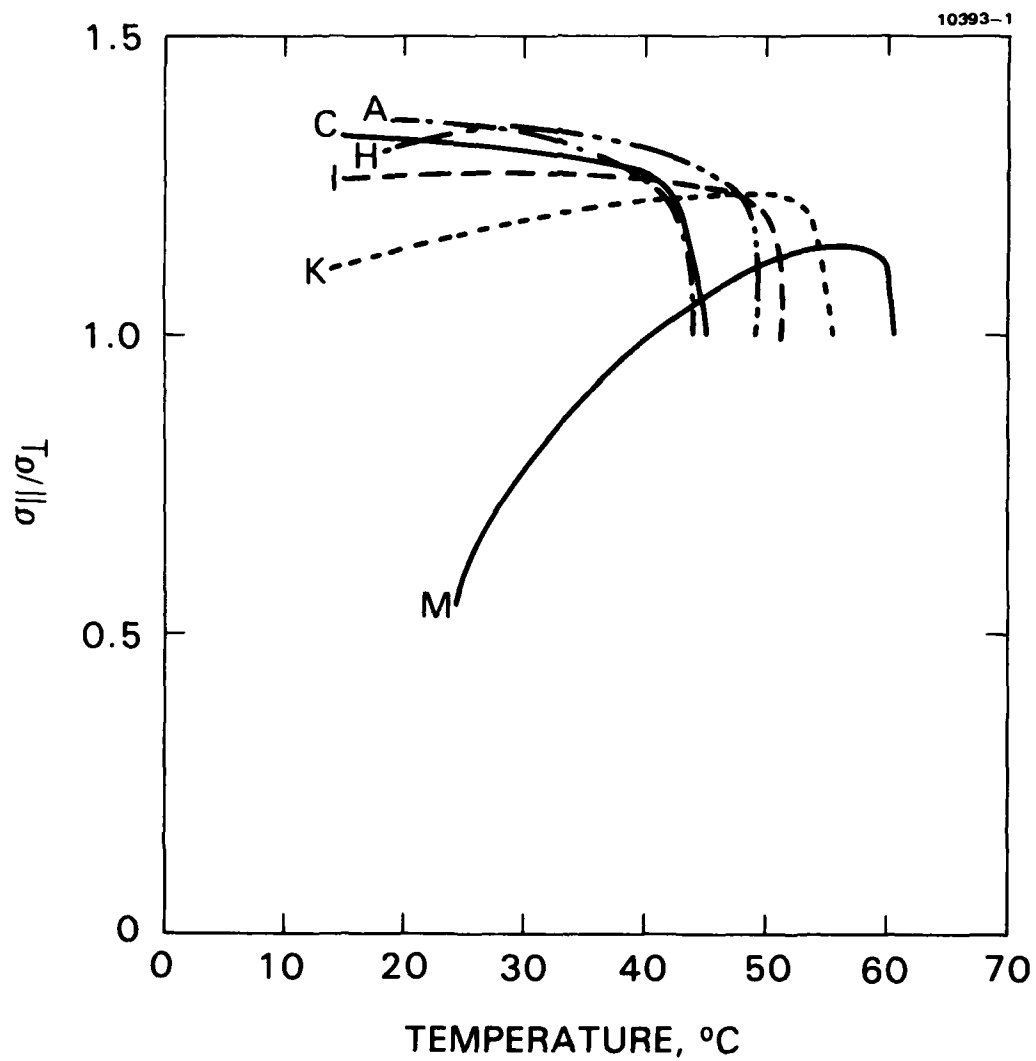


Figure 6. Effect of temperature on conductivity anisotropy of R-OR' mixtures with TBATPB dopant.

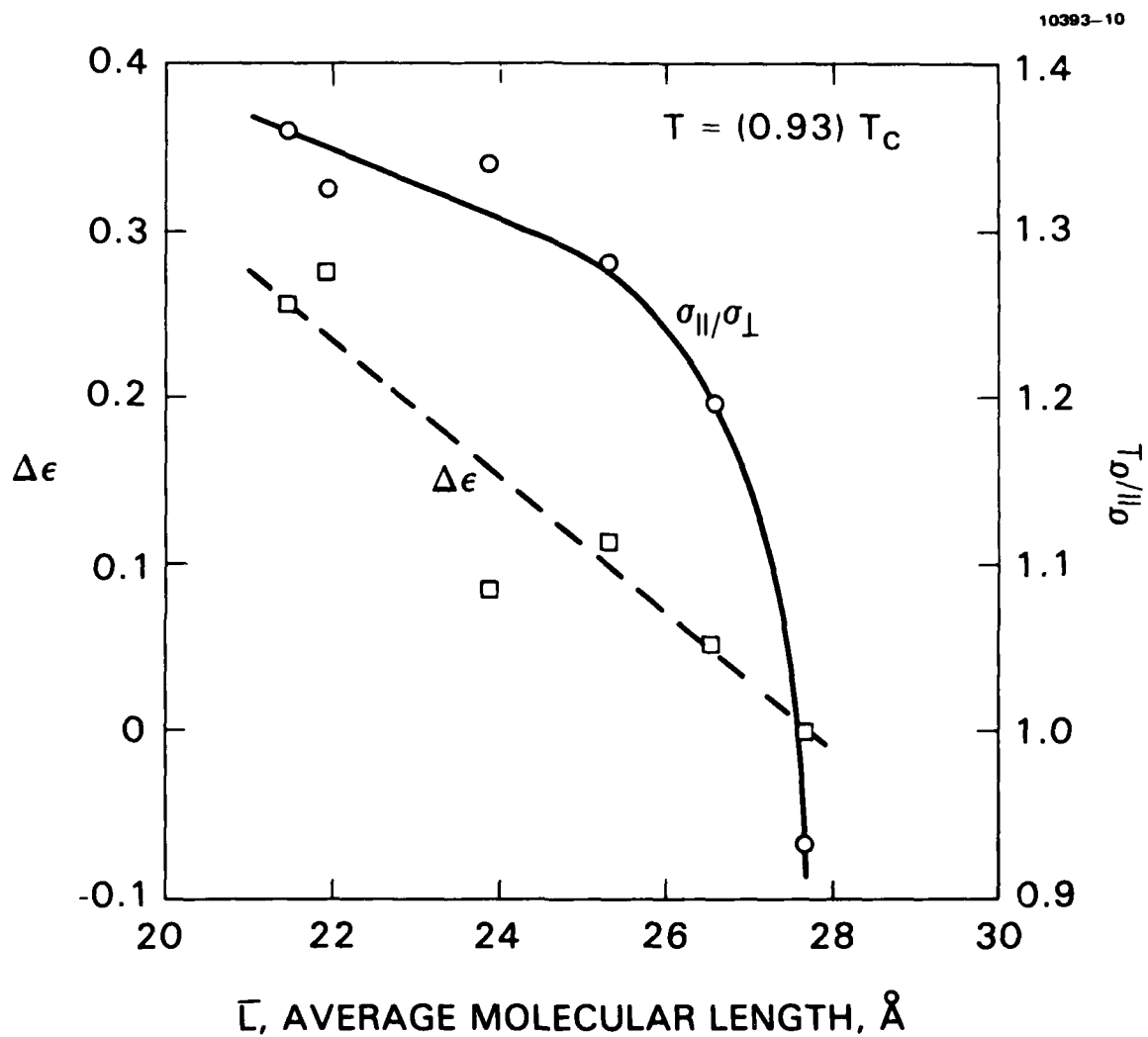


Figure 7. Effect of \bar{L} on conductivity anisotropy and dielectric anisotropy of R-OR' mixtures. (T = temperature, °K and T_c = clearpoint, °K).

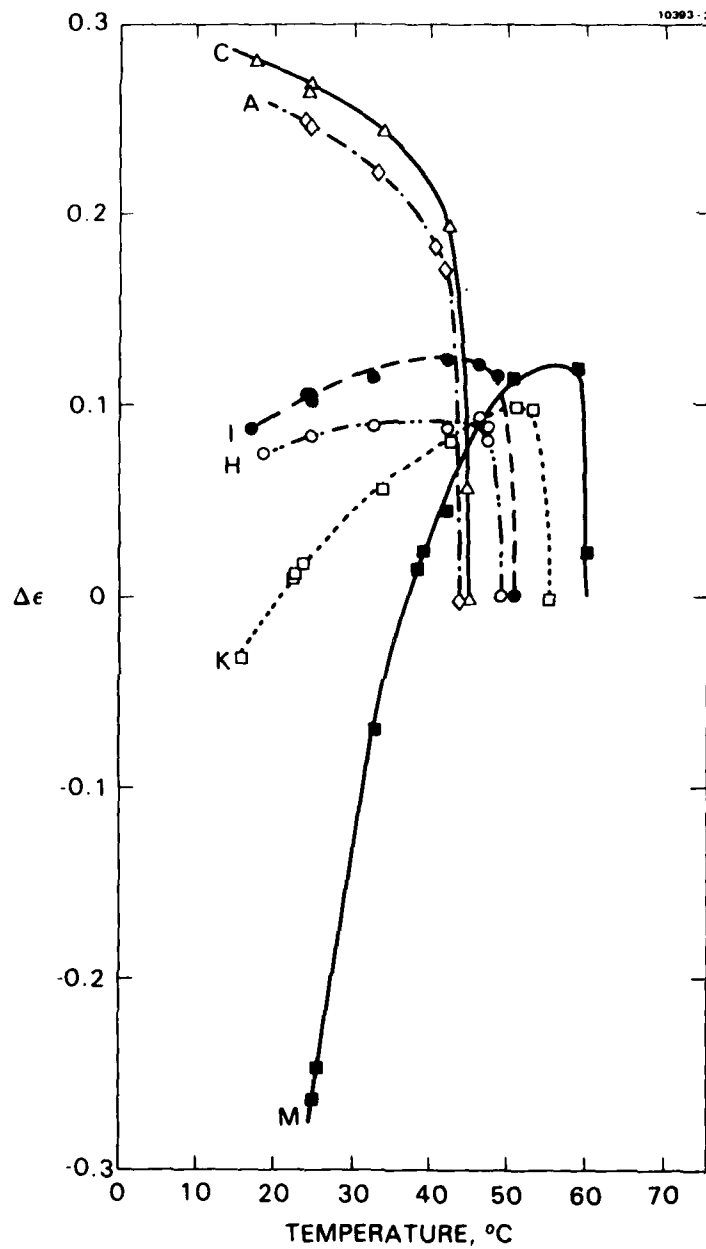


Figure 8. Effect of temperature on dielectric anisotropy in R-OR' mixtures.

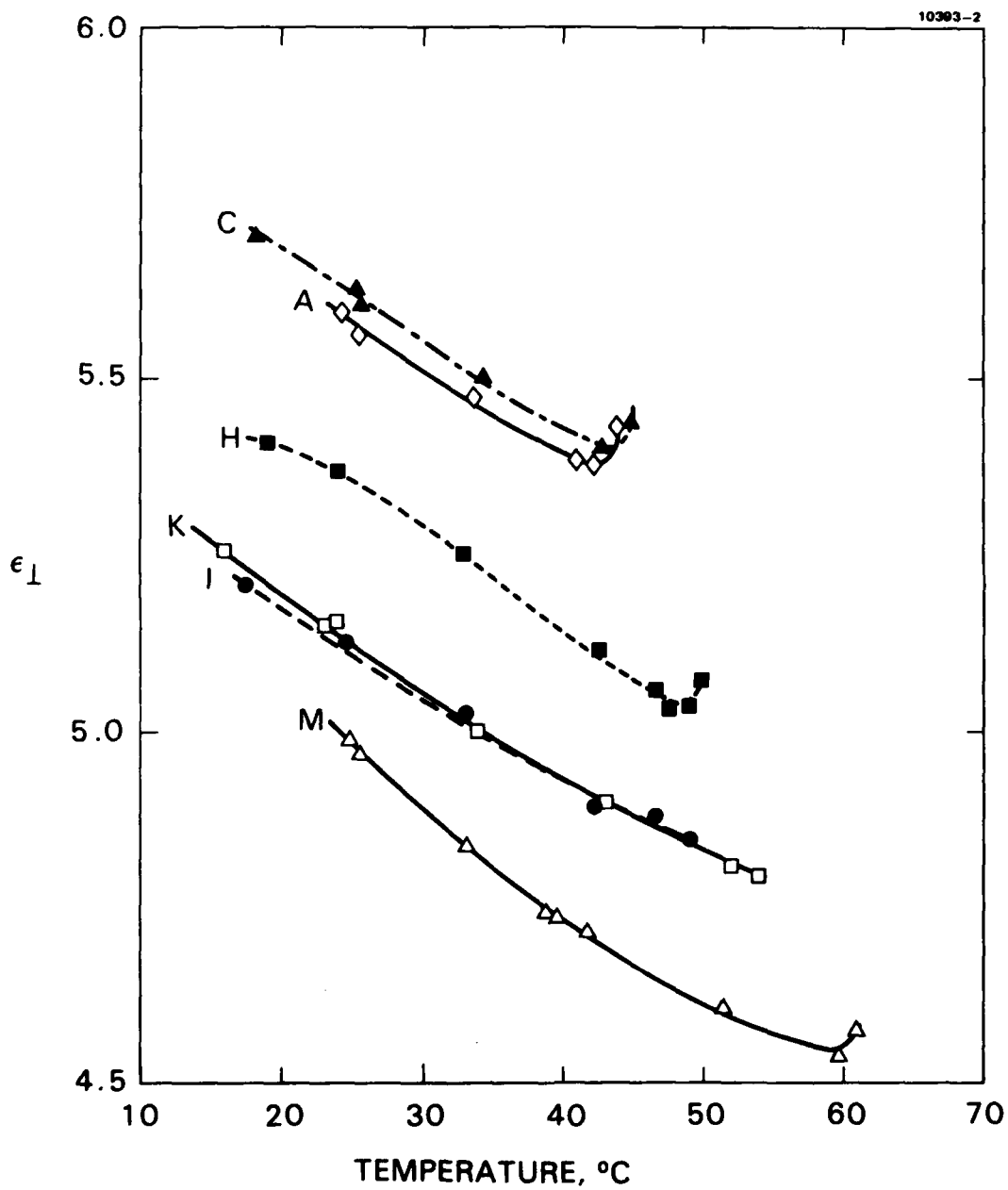


Figure 9. Effect of temperature on the ϵ_1 dielectric constant of R-OR' mixtures.

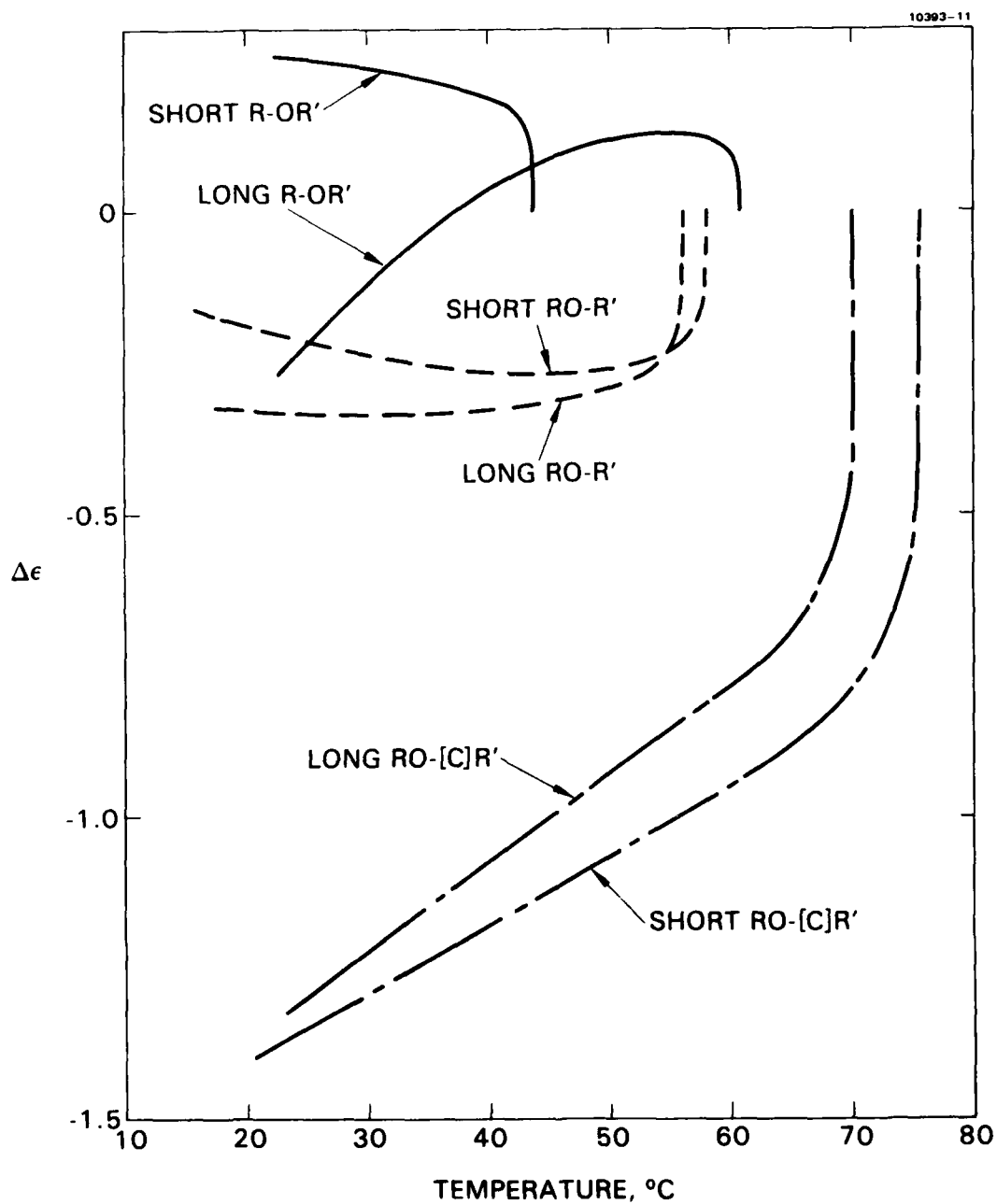


Figure 10. Comparison of \bar{L} and temperature effects on $\Delta\epsilon$ in three series of mixtures. The \bar{L} s for R-OR' are 21.47 and 27.67 Å, for RO-R' are 20.39 and 27.14 Å, and for RO-[C]R' are 21.20 and 26.15 Å.

APPENDIX V

EFFECTS OF MOLECULAR LENGTH ON NEMATIC MIXTURES. IV. STRUCTURE EFFECTS ON VISCOSITY OF ESTER MIXTURES.

J. David Margerum, Siu-May Wong, and J. E. Jensen

Hughes Research Laboratories
3011 Malibu Canyon Road
Malibu, California 90265

Abstract

The flow viscosity (η) of nematic ester mixtures is studied as a function of average molecular length (\bar{L}), chemical structure, and temperature. When \bar{L} is increased by use of longer alkyl end groups, the η of less polar mixtures increases while the η of strongly polar mixtures changes slightly or even decreases. However, when cybotactic nematic characteristics occur with increased \bar{L} , then η increases sharply. Studies of η are made for eighteen different classes of ester structures used as additives in 4-alkoxyphenyl 4-alkylbenzoate (RO-R') mixtures at fixed values of \bar{L} for both additive components and mixtures. Many interesting effects of structure on η are observed, and approximate class viscosities (η_{class}) at 25°C are assigned to each of the 18 classes. The η_{25° of other ester mixtures is estimated by summing η_{class} times the mole fraction of that class present in the mixture. These η_{calc} values are generally within 10% of the actual η_{25° for multicomponent ester mixtures containing some RO-R' components. Temperature variations often result in a non-linear plot for $\log \eta$ vs T^{-1} of ester mixtures. The apparent activation energy between 25° and 40°C generally increases strongly with the η of the mixture, ranging from 6.7 to 12.0 kcal/mole between η_{25° values of 16 and 118 cP.

I. Introduction

The flow viscosity (η) of a nematic liquid crystal (LC) is an anisotropic physical parameter which is relatively simple to measure and is often used to help characterize LC mixtures. It is often assumed that the electrooptical response time of a LC is faster for mixtures with lower η values. We have been studying the properties of ester LC mixtures for electrooptical applications, particularly in regard to dynamic scattering (DS) effects.¹⁻⁶ In each of three classes of ester LC mixtures, we found that their η values at a given temperature increased with the average molecular length (L) of the mixtures.¹⁻³ Mixtures within two of these classes of esters, 4-alkoxyphenyl-4-alkylbenzoates (RO-R') and 4-alkoxyphenyl 4-alkylcyclohexanecarboxylates (RO-[C]R'), showed DS. Their DS decay times increased with η in surface-perpendicular cells, although not in surface-parallel cells.^{1,2} However, in six different multiclass ester mixtures, the DS on-times and decay times in surface-parallel cells were generally longer for the LCs with the higher η values.⁴ When new mixtures are being considered for the optimization of various LC properties, it is important to understand the molecular structure effects of the components on η . There is also a need to predict the approximate η of mixtures, such as newly calculated eutectic LC mixtures formulated from several classes of nematic esters.

In this study, our main approach is to evaluate the viscosity contributions of various classes of LC ester structures by measuring the capillary flow viscosity of RO-R' mixtures which contain these other esters as added components. This permits us to study many different components in room-temperature nematics, to compare results at similar temperatures, to vary systematically the \bar{L} of several series, and to compare structural effects on viscosity by measurements

at fixed values of \bar{L} . Although these results are specifically related to the behavior of components in RO-R' mixtures, we find that very useful structural correlations are observed and that the η of new ester mixtures can be estimated with fairly good accuracy.

II. Experimental

The flow viscosity is measured in calibrated Cannon-Manning type viscometer tubes held in a temperature controlled water bath. The calibrated ranges are 3 to 15, 7 to 35, and 20 to 100 CS, respectively, in three different diameter tubes. In several cases, overlapping results from different size tubes are found to be in good agreement (i.e. there is no tube diameter effect on η). The density is measured in calibrated pycnometer tubes, at the same temperatures as the viscosity.

The class structures and the class code abbreviations for the LCs used in this study are shown in Figure 1. The structures are listed in decreasing class viscosities, as shown in the third column. These assigned η_{class} values are derived from the present studies, as described below in the section on results. The compounds used as additives are listed in Table I, where the numbers in the compound code refers to the number of carbons in each straight chain alkyl end group. For example, 7-6 is the abbreviation for 4-n-heptylphenyl 4-n-hexylbenzoate. The molecular lengths are measured using CPK molecular models in a fully extended configuration, as previously described.¹⁻³ The melting points listed are mostly crystalline to nematic transitions, except for a few crystalline to smectic transitions, and the clearpoints are nematic to isotropic transitions. The lower end of the transition temperatures are given, as determined from differential scanning calorimetry (DSC) analysis¹ or from a

hot stage attachment (Mettler FP5) on a polarizing microscope. Most of the LC compounds are synthesized at the Hughes Research Laboratories (HRL), and the preparation of some of them has been reported previously.¹⁻⁹ The commercial LC samples are used as received, except for EK-11650 which is recrystallized prior to use. Many of the other LCs in Table I are prepared by standard methods from the corresponding commercially available benzoyl chlorides and phenols (or thiophenols), e.g. the RO-OR', RS-OR', and R-R' compounds. The acid intermediates for the R- ϕ OR' compounds are prepared by hydrolysis of the commercially available (BDH) 4-alkoxy-4'-cyanobiphenyls according to the procedure of Byron et al.¹⁰ The phenol intermediates for the R-OOC ϕ R' compounds are prepared by refluxing the 4-alkylphenol with 4-hydroxybenzoic acid in toluene with sulfuric and boric acid added.¹¹ The resulting phenol is isolated and reacted with a benzoyl acid chloride to give the corresponding diester. The 4-butoxythiophenol intermediate for 40605 and 4063 is synthesized by the alkaline hydrolysis of the corresponding xanthate esters as described by Tarbell and Fukushima.¹² Thin-layer chromatography and liquid chromatography analysis are used to evaluate the purity of the recrystallized ester LCs. (Note that 7-4 is distilled, b.p. 220° at 0.05 mm.) The impurity content of the LC compounds is less than 0.5%, although the R(CN)- ϕ OR' compounds and some of the commercial samples may be slightly less pure. The LC eutectic mixtures used in these studies are listed in Table II. The component mole fractions are given here for those mixtures not previously reported in the literature. All of the HRL mixtures are formulated by calculations with the Schroeder-Van Laar equation, using heat of fusion and melting points data obtained by DSC analysis of the components.

III. Results and Discussion

III. A. Effects of Molecular Length

In three series of single class ester mixtures, namely RO-R', RO-[C]R', and R-OR', the η values in each series increases as the \bar{L} of the mixtures increase.¹⁻³ For comparison purposes, these results are summarized in Figure 2. In each series, \bar{L} was increased by an increase in the average length of just the R and R' alkyl end groups. The relationship between η and \bar{L} in the RO-R' series indicates that the increase in molecular length has a larger effect on η than the relative decrease in overall molecular polarity caused by the longer alkane groups. Similar effects are seen in isotropic liquids, such as n-alkyl acetates.¹³ We believe that the large (exponential) increases in the η of the RO-[C]R' and R-OR' series at longer \bar{L} is due to the strong cybotactic nematic (short range smectic) characteristics identified in these mixtures.^{2,3} The flow viscosity of a nematic LC usually corresponds approximately to the Helfrich viscosity η_2 (in which the director is parallel to the flow direction) when the temperature is well below the clearpoint.^{14,15} The short range smectic ordering in the longer \bar{L} RO-[C]R' and R-OR' mixtures impedes the flow parallel to the director and increases η . In the shorter \bar{L} (<23Å) of Figure 2 there are no cybotactic characteristics and the effects of molecular structure can be compared between the three series. Use of the cyclohexane ring in RO-[C]R', in place of the benzene ring in RO-R', substantially decreases η . This is probably largely due to the decreased polarity of the cyclohexane ester carbonyl as compared to the aromatic ring and its ester carbonyl group. On the other hand, when the alkoxy group is switched from the phenol side in RO-R' to the acid side in R-OR' the polarity of the molecules is increased and

increases. This is largely due to the electron-donating and conjugation effects of the p-alkoxyl group, which increases the polarity of the ester carbonyl in the R-OR' structure as compared to the RO-R' structure.

Since it is difficult to prepare room temperature nematics of most other single class ester mixtures, we studied the \bar{L} effects on the η of many ester structures as additives to the RO-R' mixtures. The data are given in Tables III, IV, V and VI, along with graphical summaries in Figures 3, 4 and 5. The 25° data with 25 mole percent additives are shown in Figure 3, where the effect of \bar{L} is found to vary with the structure of the additive ester. In the mixture with R-R' additives, η varies with \bar{L} as in the 100% RO-R' case. Mixtures with RO-OR' esters show slightly less dependence of η on \bar{L} . The shorter \bar{L} mixtures with NC-R additives behave similarly, but η increases sharply at longer \bar{L} values. The η of the mixtures with R-(Cl)OOC ϕ R' additive decrease slightly as \bar{L} increases. These effects can be understood better by examining Figure 4, in which the \bar{L} effects are shown on the calculated viscosity (η_{calc}) contribution attributed to the added ester in the RO-R' mixture. If x is the mole fraction of the additive, then we determine η_{calc} from equation (1) at the \bar{L} of the overall mixture:

$$\eta_{\text{obs}} = \eta_{\text{calc}}(x) + \eta_{\text{RO-R'}}(1-x) \quad (1)$$

Thus, η_{calc} is the apparent viscosity of the additive in the mixture. (We have found that the most consistent results are obtained when η_{calc} and $\eta_{\text{RO-R'}}$ are both taken at the \bar{L} of the overall mixture rather than at the \bar{L} of each class prior to mixing.) The η_{calc} values in Figure 4 are for mixtures in which x is only 0.25 or 0.10 so that the additive is in the presence of a large excess

of RO-R' molecules. The results are strongly dependent on the polarity of the additive ester structure. The η_{calc} of R-R' esters increases with \bar{L} slightly more steeply than does the η of the 100% RO-R' mixtures. The R-R' compounds are not very polar: the dominant effect on η_{calc} is the increased length of the end groups. With the more polar RO-OR' additives, η_{calc} is approximately constant: the increase in \bar{L} of the mixture is apparently offset by the dilution of intermolecular dipole interactions as the non-polar end groups are lengthened. The NC-R additives are strongly polar and their η_{calc} is independent of \bar{L} in the shorter mixtures; however, it increases sharply at longer \bar{L} where cybotactic nematic structures are formed. This is a behavior related to the induced smectic phases observed by others¹⁶⁻¹⁸ when strongly polar LCs are mixed with relatively non-polar LCs. In the mixtures with R-(Cl)OOC ϕ R' additives, the η_{calc} decreases as \bar{L} increases: presumably, decreased dipole interactions occur as the alkyl end groups are lengthened and this overrides the effects of longer \bar{L} .

IV. Effect of Additive Concentration

The η_{calc} value of R-(Cl)OOC ϕ R' at a constant \bar{L} strongly increases as its concentration in the mixture increases when more than 25 mole percent is used. This is shown by the data in Table VI and Figure 5. We believe that this is because the polar interactions between R-(Cl)OOC ϕ R' molecules is greater than those between R-(Cl)OOC ϕ R' and RO-R' molecules. As indicated below, we have observed similar effects in comparing η_{calc} for RO-OR' in 75% RO-R' versus the higher η_{obs} value of a 100% mixture of RO-OR' components, and also in the increase of η_{calc} for R(CN)- ϕ OR' when the RO-R' components are 75% instead of 90%.

V. Effects of Structure

We studied the effects of molecular structure by measuring the η of various ester additives (10 or 25 mole percent) with fixed \bar{L} in RO-R' mixtures of fixed \bar{L} . Three such series of measurements are shown in Tables VII, VIII and IX. Table VII is the main series, with each additive class averaging 27.03Å in length and 25% added to HRL-2N42. Some of the components are not soluble enough for 25% mixtures, so the Table VIII series uses 10% of such length additives (27.03Å) added to HRL-2N42. There is some overlap of classes in Tables VII and VIII in order to compare concentration and \bar{L} effects. The series in Table IX is measured to compare esters with the corresponding thioesters (of which we have available only relatively short length components) with 25% additives of 22.50Å added to HRL-2N42. In each table the additives are listed in decreasing η . The overall results are compared as η_{calc} values in Table X, and our assigned class viscosities are shown in Figure 1. These assigned η_{class} values are specifically for about 10 to 25% of the class structure in RO-R' mixtures with an overall average \bar{L} of 22Å.

Many interesting correlations of η_{class} with structural features are indicated in Figure 1, including some effects already known from other studies. These semi-quantitative results clearly show the following relationships for the η_{class} of the same length ester structures used in relatively short length RO-R' ester mixtures:

Factor Decreasing η_{class}	Examples (Relative Size of η_{class})
• Replace benzoate with cyclohexane-carboxylate	$\text{RO-R}' > \text{RO-[C]R}'$
• Replace <u>p</u> -alkoxy with alkyl	$\text{RO-R}' \text{ and } \text{R-OR}' > \text{R-R}'$ $\text{RO-OOCR}' > \text{R-OOCR}'$ $\text{RO-OR}' > \text{RO-R}' \text{ and } \text{R-OR}'$ $\text{ROSOR}' > \text{ROSR}' \text{ and } \text{RSOR}'$ $\text{R-}\phi\text{OR}' > \text{R-}\phi\text{R}$ $\text{R(CN)-}\phi\text{OR}' > \text{R(CN)-}\phi\text{R}'$
• Move <u>p</u> -alkoxy from acid to phenol side	$\text{R-OR}' > \text{RO-R}'$
• Replace aromatic with aliphatic groups	$\text{R}\phi\text{-R}' \text{ and } \text{R-}\phi\text{R}' > \text{R-R}'$ $\text{R-}\phi\text{OR}' > \text{R-OR}'$ $\text{R-OOC}\phi\text{R}' > \text{R-OOOCR}'$
• Replace <u>p</u> -CN by alkoxy or alkyl	$\text{NC-R} > \text{RO-R}' \text{ and } \text{R-R}'$
• Replace <u>o</u> -CN by hydrogen	$\text{R(CN)-}\phi\text{OR}' > \text{R-}\phi\text{OR}'$ $\text{R(CN)-}\phi\text{R}' > \text{R-}\phi\text{R}'$
• Replace <u>o</u> -Cl by hydrogen	$\text{R-(Cl)OOC}\phi\text{R}' > \text{R-OOC}\phi\text{R}'$
• Replace thiobenzoate by benzoate	$\text{ROSOR}' > \text{RO-OR}'$ $\text{RSOR}' > \text{R-OR}'$ $\text{ROSR}' > \text{RO-R}'$
• Replace benzoyloxy with phenyl	$\text{R-OOC}\phi\text{R}' > \text{R-}\phi\text{OR}'$
• Replace phenyl with acyloxy	$\text{R-}\phi\text{R}' > \text{R-OOCR}'$

These results are partially consistent with the general rule that η is increased by more polar structures. Thus large increases in η are observed from strong dipolar groups (e.g. cyano), and by groups which increase the molecular dipole and polarizability (e.g. alkoxy para to the ester carbonyl). On the other hand, different factors must be considered in other cases. For example, the p-alkylphenyl substituent in $\text{R-}\phi\text{R}'$ gives a larger η than does the more polar

p-acyloxy group in R-OOOR'. The relatively large effect on η by phenyl groups (i.e. biphenyl esters) may be due to a combination of effects such as a larger molecular volume, more of a bent-rod molecular shape, and increased intermolecular association as compared to acyloxy and alkoxy groups. The high η_{class} values of the biphenyl esters is seen on either end of the ester substrate, i.e.,: $R-\phi R' > R-OR' > R-OOOR' > R-R'$ and also $R\phi-R' > RO-R' > R-R'$.

VI. Predicting η of New Mixtures

We find that the η_{25° of short length ester LC mixtures can be estimated with fairly good accuracy by using equation (2), where x_i is the total mole fraction of each class.

$$\eta_{\text{mix}} = \sum (\eta_{\text{class}})_i \cdot x_i \quad (2)$$

The calculations from equation (2) are often more accurate than estimates made by taking the average of the actual η s of the pure components. For example, in mixing 25% of the R-(Cl)OOC ϕ R' LC HRL-2P37 with 75% of the RO-R' LC HRL-2N48 the η_{25° is 65.2 cP and the calculated η_{mix} is 65.2 cP, whereas the η_{av} is 95.0 cP. On the other hand, differences are noted between our assigned η_{class} values and the η of those single class mixtures with more with polar structures. This is shown in Table XI-A, where the η_{25° of 100% R-(Cl)OOC ϕ R' and of 100% RO-OR' is much larger than the η_{class} value determined from 10 to 25% of these structures in RO-R' mixtures. As noted above, the high η values of the 100% polar LCs is attributed to increased intermolecular effects as compared to their interaction when mixed with the less polar RO-R' esters. The less polar single class mixtures, such as R-OR', R-OOOR', and RO-[C]R' show better agreement with the η_{class} values.

Multiple class mixtures containing some RO-R' components have η_{25° values that are within 20% of the value predicted by our η_{mix} calculation. As illustrated in Table XI-B, the η_{mix} values are often quite accurate. We find that when the calculated and observed values are not very close, as in the HRL-26N4 and HRL-246N1 mixtures, the η_{mix} is generally higher than the η_{obs} . Thus, we use the η_{mix} as an approximate upper limit for estimating the η_{25° of new ester mixtures -- particularly those mixtures designed to have low viscosity and negative dielectric anisotropy.

VII. Temperature Effects

Although 100% mixtures of RO-R' esters showed a linear plot of $\log \eta$ versus T^{-1} , other ester mixtures studied previously²⁻⁴ as well as the ones in this study do not give a linear equation (3) plot. Instead,

$$\log \eta = \log A + E_\eta / RT \quad (3)$$

the η values above room temperature are larger than expected from the variations near 25°C. This is the case even well below the clearpoint. (The η increases sharply at the clearpoint, in a manner similar to changes observed for η_2 measurements.¹⁵) For comparison purposes, we have calculated the apparent E_η values from the slope of equation (3) curves between the fixed temperature of 25° and 40°C. These data are summarized in Figure 6 which includes results from prior papers.¹⁻³ The E_η values in the 100% RO-R' series (various \bar{L} s) does not vary appreciably. However, in the 100% RO-[C]R' series (various \bar{L}) and in the Table VII mixtures (constant \bar{L} , with 25% additive ester and 75% RO-R') the apparent E_η increases linearly with $\log \eta_{25^\circ}$. In fact, all of the data points for all of the short length mixtures in Figure 6 (the dark points)

are roughly correlated by this relationship, with apparent E_{η} ranging from 6.7 to 12.0 kcal/mole. This indicates that in the 25° to 40°C range the change of η with temperature is greatest for the most viscous ester mixtures and smallest for the least viscous esters. We have also calculated an apparent E'_{η} for the mixtures between fixed η values of 30 and 15 cP and the corresponding (variable) temperature. These E'_{η} values range between 7.7 and 9.6 kcal/mole, with an average value of 8.5 kcal/mole. We have found no obvious relationship between these apparent E'_{η} values and the component structures, nor the \bar{L} of the mixtures.

VIII. Conclusions

These studies give semi-quantitative values to the viscosity characteristics of 18 different classes of LC ester structures. When new LC mixtures are made from among these classes of esters, the η_{25° can be predicted with fairly good accuracy. The calculated value generally provides an upper limit for η , and is often within 10% of the actual value of the mixture. Our correlations of η_{class} with various structural features also provide a good basis for rough estimates of the η contributions of additional classes of ester LCs. The formulation of LC mixtures for electro-optical applications, generally involves trade-off of properties e.g. for a mixture with wide nematic range, low η , negative dielectric anisotropy ($\Delta\epsilon$) and high conductivity anisotropy for DS devices. In general the lowest η values are obtained with short \bar{L} mixtures of the less polar esters. Short \bar{L} mixtures also give less cybotactic nematic effects. The cyclohexanecarboxylates, $\text{RO}-[\text{C}]\text{R}'$, are one of the few structures with low η , negative $\Delta\epsilon$, and fairly high clearpoints. The acyloxy esters ($\text{R}-\text{OOCR}'$ and $\text{RO}-\text{OOCR}'$) have relatively low η s for polar structures of

negative $\Delta\epsilon$. In contrast, the *o*-cyanophenyl biphenylcarboxylates such as $R(CN)-\phi R'$ have strongly negative $\Delta\epsilon$ and high clearpoints, but they also have such high η_{class} values that even in small amounts they greatly increase the η of most mixtures. Relatively low η ester mixtures for DS are made by including components from classes such as $RO-[C]R'$, $RO-R'$, and $R-OO CR'$. The lower η mixtures also show less temperature dependence on η than do the higher η mixtures.

Acknowledgements

We are indebted to the Directorate of Chemical Sciences, Air Force Office of Scientific Research, Contract F49620-77-C-0017, for partial financial support of this research; to C.I. van Ast for assistance in component synthesis; and to W.H. Smith, Jr., for assistance in DSC measurements.

References

1. J. D. Margerum, J. E. Jensen, and A. M. Lackner, Mol. Cryst. Liq. Cryst., in press, 1981. (Paper I of this series.)
2. J. D. Margerum, S. -M. Wong, A. M. Lackner, and J. E. Jensen, Mol. Cryst. Liq. Cryst., in press, 1981. (Paper II of this series.)
3. J. D. Margerum, S. -M. Wong, A. M. Lackner, J. E. Jensen, and S. A. Verzwylt, (submitted to Mol. Cryst. Liq. Cryst. as paper III of this series).
4. J. D. Margerum and A. M. Lackner, Mol. Cryst. Liq. Cryst., in press.
5. H. S. Lim, J. D. Margerum, and A. Graube, J. Electrochem. Soc., **124**, 1389 (1977).
6. H. S. Lim and M. J. Little, U. S. Pat. 4129312 (Dec. 5, 1978).
7. F. G. Yamagishi, L. J. Miller, J. E. Jensen, and J. D. Margerum, U.S. Pat. #4,225,454 (Sept. 30, 1980).
8. Y. S. Lee, P. Y. Hsieh, and J. E. Jensen, U.S. Pat. #4,000,084 (Dec. 28, 1976).
9. S. -Y. Wong, U.S. Pat. #3,826,757 (July 30, 1974).
10. D. J. Bryon, G. W. Gray, and R. C. Wilson, J. Chem. Soc., **C**, 840 (1968).
11. W. W. Lawrence, Tetrahedron Lett., 3464 (1971).
12. D. S. Tarbell and D. K. Fukushima, Org. Synthesis, Col. Vol. III, (John Wiley, NY, 1955) p. 809.
13. Handbook of Chemistry and Physics, R. D. Weast, Ed. (CRC Press, Boca Raton, FL, 1979) 60th ed, pp. F52-57.
14. A. E. White, B. E. Cladis, and S. Torza, Mol. Cryst. Liq. Cryst. **43**, 13 (1977).
15. W. H. deJeu, Physical Properties of Liquid Crystalline Materials, (Gordon and Breach New York, 1980), p. 121.
16. C. S. Oh, Mol. Cryst. Liq. Cryst., **42**, 1 (1977).
17. G. Heppke and E. -J. Richter, Z. Naturforsch. **33a**, 185 (1978).
18. M. Bock, G. Heppke, E. -J. Richter, and F. Schneider, Mol. Cryst. Liq. Cryst., **45**, 221 (1978).

List of Tables

- Table I. Liquid Compounds Used as Additives in Viscosity Studies
- Table II. Liquid Crystal Eutectic Mixtures Used in Viscosity Studies
- Table III. Effect of \bar{L} on Viscosity: RO-R' With 25% R-R'
- Table IV. Effect of \bar{L} on Viscosity: PO-R' With 25% RO-OR'
- Table V. Effect of \bar{L} on Viscosity: RO-R' With 25% NC-R
- Table VI. Effect of Mole Percent and \bar{L} on Viscosity of Ester Mixtures With R-(Cl)OOC-R'
- Table VII. Structure Effects on Viscosity: Mixtures With 75% RO-R' and 25% Additives
- Table VIII. Structure Effects on Viscosity: Mixtures with 90% RO-R' and 10% Additives
- Table IX. Effects of Thiobenzoates Versus Benzoates on Viscosity of Mixtures With 75% RO-R'
- Table X. Calculated Viscosity of Additives When Used in RO-R' Mixture
- Table XI. Comparison of Calculated vs Observed Viscosities of Ester Eutectic Mixtures

List of Figures

- Figure 1. Structure, class code, and class viscosities of LC ester components. (The η_{class} at 25°C apply when 10 to 25% of these components are used in RO-R' mixtures with $\bar{L} \sim 22 \text{ \AA}$.)
- Figure 2. Effect of \bar{L} on the viscosity of three series of single class ester LC mixtures.
- Figure 3. Effect of \bar{L} on η_{25° of RO-R' mixtures and of RO-R' mixtures with 25% of other LC components.
- Figure 4. Effect of \bar{L} on η_{calc} of the 25% components in RO-R' mixtures.
- Figure 5. Effect of \bar{L} and concentration of a diester on its η_{calc} from η_{25° in RO-R' mixtures.
- Figure 6. Dependence of apparent activation energy of viscosity between 25 and 40°C on η_{25° .

Table 1. Liquid Compounds Used as Additives in Viscosity Studies

Class Code	Compound Code	Molecular Length, Å	Melting Point, °C	Clearpoint, °C	Source
R(CN)-φOR'	4(CN)-φ03	25.82	103	137	HRL ^c
	4(CN)-φ05	28.14	80	126	HRL ^c
R(CN)-φR'	7(CN)-φ5	31.50	44	103	Merck(S1014)
R-φOR'	4-φ03	25.82	118	196	HRL
	4-φ05	28.14	92	165	HRL
R-(C1)OOCφR'	2-(C1)OOCφ2	23.79	60	126	HRL
	5-(C1)OOCφ5	31.03	40	122	Kodak(11650)
R-OOCφR'	2-OOCφ2	23.79	143	190	HRL
	4-OOCφ4	28.31	88	186	HRL ^d
ROSOR'	10S04	21.20	74	107	HRL ^e
	10S06	23.90	65	100	HRL ^e
	40S05	26.40	84	104	HRL
RO-OR'	10-01	17.52	124	-	HRL
	10-04	21.09	92	79	HRL
	10-06	23.54	93	76	HRL
	20-01	18.72	97	93	HRL
	40-01	21.13	79	80	HRL
	40-05	26.03	71	84	HRL ^e
	60-01	23.60	55	77	HRL ^e
	60-05	28.50	55	84	HRL
NC-R	NC-4	20.18	68	39	HRL ^d
	NC-7	23.57	43	55	HRL ^d
R-φR'	5-φ5	28.98	96	176	Merck(S1011)

Table I. Liquid Crystal Compounds Used as Additives in Viscosity Studies (Cont)

Class Code	Compound Code	Molecular Length, Å	Melting Point, °C	Clearpoint, °C	Source
RO-OOCR'	40-OOC4	25.40	67	84	HRL ^e
	60-OOC5	28.92	51	86	HRL ^e
R ₂ -R'	34-4	25.55	93	182	Merck(S1013)
	54-4	27.95	97	172	Merck(S1012)
RSOR'	1S06	22.51	66	78	HRL
R-OR'	1-06	22.25	62	51	HRL ^f
	3-07	25.87	65	57	HRL ^f
	5-06	27.51	50	62	HRL ^f
I-OOCR'	3-OOC5	24.81	48 ^a	55 ^a	Merck(S1008)
	7-OOC5	28.88	42 ^b	61 ^b	Merck(S1008)
ROSR'	40S3	22.50	51	82	HRL
RO-R'	40-3	21.78	71	61	HRL ^g
	40-6	25.81	40	49	HRL ^g
	60-5	27.03	41	59	HRL ^g
R-R'	4-1	18.72	36	-	HRL ^h
	5-5	24.16	33	-	EMC ⁱ
	7-4	25.68	9 ^b	15 ^b	HRL
	7-6	27.92	32	23	HRL
RO-[C]R'	40-[C]4	23.84	40	70	HRL ^j
	60-[C]5	27.41	32	80	HRL ^j

^aLit. value.^bLit. value, R. Steinsträsser, *Z. Naturforsch.* 27b, 774 (1972).^cSee ref 7. ^dSee ref 8. ^eSee ref 4. ^fSee ref 3. ^gSee ref 1. ^hSee ref 9.ⁱElectronic Materials Corp. ^jSee ref 2.

Table II. Liquid Crystal Eutectic Mixtures Used in Viscosity Studies

Mixture No.	Components	Length \bar{L} , Å	Melting Point, °C	Clearpoint °C
HRL-2N25 ^a	20-3, 60-4, 60-01	24.48	0	54
HRL-2N40 ^b	10-1, 20-3, 20-5, 40-1, 40-6, 60-01	22.68	0	58
HRL-2N42 ^c	10-1, 20-3, 20-5, 40-1, 40-3	20.39	5	58
HRL-2N44 ^c	20-5, 40-3, 60-4	24.31	-8	51
HRL-2N46 ^c	40-3, 40-6, 60-5	25.92	16	55
HRL-2N48 ^c	60-3, 60-5, 80-3, 80-6	27.14	18	56
HRL-2N54 ^d	10-01, 10-04, 10-06, 20-01, 40-01, 40-05, 60-01	23.23	(25) ^g	(78) ^g
HRL-2P37 ^e	2-(Cl)OOCφ2, 5-(Cl)OOCφ5	28.05	(21) ^g	(124) ^g
Merck S1008 ^f	3-00C5, 7-00C5	26.12	20	56

^aComponent mole fractions are 0.132, 0.640, and 0.228 respectively.

^bSee ref 6.

^cSee ref 1.

^dComponent mole fractions are 0.045, 0.051, 0.033, 0.078, 0.118, 0.291, and 0.385 respectively.

^eComponent mole fractions are 0.412 and 0.588 respectively.

^fComponents mole fractions are reported to be 0.586 and 0.414.

^gCalculated values.

Table III. Effect of \bar{L} on Viscosity: RO-R' With 25% R-R'

R-R' Component	RO-R' Components	$\bar{L}(\text{\AA})$	Clearpoint °C	Mixture With 75% RO-R'	
				Viscosity (cP)	
				η_{25°	η_{40°
4-1	HRL-2N42	19.97	45	29.1	15.1
5-5	HRL-2N42	21.33	45	28.5	14.6
7-4	HRL-2N42	21.71	42	31.1	17.3
7-6	HRL-2N42	22.27	42	32.1	16.1
4-1	HRL-2N48	25.03	47	37.7	-
7-6	HRL-2N48	27.34	48	39.9	21.0

Table IV. Effect of \bar{L} on Viscosity. RO-R' With 25% RO-OR'

RO-OR' Components		Mixture With 75% RO-R'				
Compound	% In Mixture	RO-R' Components	\bar{L} (Å)	Clearpoint °C	Viscosity (cP)	
					η_{25°	η_{40°
{ 10-04	10.61 }	HRL-2N42	20.92	62	46.4	-
{ 10-06	14.39 }					
60-01	25.00	HRL-2N42	21.19	62	44.5	19.8
{ 40-05	15.00 }	HRL-2N42	22.05	65	49.3	21.9
{ 60-05	10.00 }					
60-01	(24.50) ^a	(HRL-2N40) ^a	22.68	58	46.4	20.8
{ 20-01	10.00 }	HRL-2N44	23.27	57	48.4	22.5
{ 40-01	15.00 }					
60-01	25.00	HRL-2N44	24.13	57	47.4	22.6
40-05	25.00	HRL-2N44	24.74	60	50.2	25.7
60-05	25.00	HRL-2N44	25.36	61	51.2	26.1
60-01	25.00	HRL-2N48	26.25	60	52.0	23.5

^aHRL-2N40 contains 24.5 mole percent 60-01; see ref 6.

Table V. Effect of \bar{L} on Viscosity: RO-R' With 25% NC-R

NC-R Components ^a Additive \bar{L} (Å)	RO-R' Components	Mixture With 75% RO-R'		
		\bar{L} (Å)	Density At 25°C	Viscosity (cP) η_{25°
20.39	HRL-2N42	20.39	1.087	45.6
21.86	HRL-2N42	20.76	1.070	45.6
21.86	HRL-2N44	23.70	1.048	49.3
21.86	HRL-2N46	24.90	1.044	55.3
21.86	HRL-2N48	25.82	1.038	64.8

^aOnly NC-4 and NC-7 are used as additives: The 21.86 Å length corresponds to this binary eutectic of 31.8 and 68.2 mole percent, respectively.

Table VI. Effect of Mole Percent and \bar{L} on Viscosity of Ester Mixtures With $R-(Cl)OOC\phi R'$

R-(Cl)OOC ϕ R' Components ^a		RO-R' Components ^b		Total Mixture		Viscosity of Components ^c	
Mole %	\bar{L} (Å)	Mole %	\bar{L} (Å)	\bar{L} (Å)	η_{25° (cP)	RO-R' η_{est}	R-(Cl)OOC ϕ R' η_{calc}
10	27.03	90	20.39	21.05	46.2	34.1	155
10	28.05	90	27.14	27.23	51.9	43.6	127
25	27.03	75	20.39	22.05	66.1	35.6	158
25	29.03	75	23.76	25.08	64.1	40.3	136
25	28.05	75	27.14	27.37	65.2	43.8	129
25	31.03	75	27.14	28.11	65.2	45.0	126
50	28.05	50	27.14	27.60	94.8	44.2	145
75	28.05	25	27.14	27.82	155.8	44.5	193
100	28.05	0	-	28.05	249.3	-	249

^aComponents are 2-(Cl)OOC ϕ 2 and 5-(Cl)OOC ϕ 5.

^bComponents are HRL-2N42 and/or HRL-2N48 mixtures.

^cThe RO-R' viscosities are estimated at the \bar{L} of the total mixture from the plot their η vs \bar{L} .

Table VII. Structure Effects on Viscosity: Mixtures With 75% RO-R' and 25% Additives

25% Additive Components ^a			Mixture With 75% HRL-2N42 ^b			
Class	Components	Mixture Mole %	Clearpoint °C	Density at 25°C	Viscosity, cP	
					25°	40°
R(CN)-φOR'	4(CN)-φ03	12.28	76	1.103	118.0	44.7
	4(CN)-φ05	12.72				
R-(Cl)OOCφR'	2-(Cl)OOCφ2	13.37	73	1.120	66.1	28.3
	5-(Cl)OOCφ5	11.63				
R-OOCφR'	2-OOCφ2	6.72	88	1.105	60.6	26.0
	4-OOCφ4	18.28				
RO-OR'	40-05	15.00	65	1.083	49.3	21.9
	60-05	10.00				
RO-OOCR'	40-OOC4	13.64	65	1.087	45.6	20.7
	60-OOC5	11.36				
Rφ-R'	3φ-4	5.00	92	1.079	45.4	20.6
	5φ-4	7.20				
R-φR'	5-φ5	12.80				
R-OR'	5-06	25.00	58	1.065	39.8	18.8
R-OOCR'	3-OOC5	14.65	56	1.080	38.0	18.1
	7-OOC5	10.35				
RO-R'	60-5	25.00	58	1.052	36.3	17.4
R-R'	7-4	15.07	42	1.058	31.7	16.6
	7-6	9.93				
RO-[C]R'	40-[C]4	2.82	62	1.056	31.1	15.5
	60-[C]5	22.18				

^aAdditives have $\bar{L} = 27.03 \text{ \AA}$,

^bMixtures with additives have $\bar{L} = 22.05 \text{ \AA}$; HRL-2N42 alone has $\bar{L} = 20.39 \text{ \AA}$ and $\eta_{25^\circ} = 32.6$,

^cThe R-OOCR' additives have $\bar{L} = 26.12 \text{ \AA}$, and the mixture $\bar{L} = 21.82 \text{ \AA}$.

Table VIII. Structure Effects on Viscosity: Mixtures With 90% RO-R' and 10% Additives

10% Additive Components ^a			Mixture With 90% HRL-2N42 ^b
Class	Components	Mole % In Mixture	Viscosity η_{25° , cP
R(CN)- ϕ OR'	4(CN)- ϕ 03	4.91	57.0
	4(CN)- ϕ 05	5.09	
R- ϕ OR'	4- ϕ 03	4.91	47.0
	4- ϕ 05	5.09	
R-(Cl)OOC ϕ R'	2-(Cl)OOC ϕ 2	5.35	46.2
	5-(Cl)OOC ϕ 5	4.65	
R-OOC ϕ R'	2-OOC ϕ 2	2.69	43.6
	4-OOC ϕ 4	7.31	
ROSOR'	40S05 ^c	10.00	41.3 ^c
RO-OR'	40-05	6.00	39.0
	60-05	4.00	
R ϕ -R'	3 ϕ -4	2.00	37.9
	5 ϕ -4	2.88	
R- ϕ R'	5- ϕ 5	5.12	
R ϕ -R'	3 ϕ -4	3.70	37.4
	5 ϕ -4	6.30	
RO-R'	60-5	10.00	34.8

^aAdditives have $\bar{L} = 27.03 \text{ \AA}$

^bMixtures with additives have $\bar{L} = 21.05 \text{ \AA}$

^cMixture contains 89.1% 2N42 and 0.9% 60-5 to give $\bar{L} = 21.05 \text{ \AA}$

Table IX. Effects of Thiobenzoates Versus Benzoates on Viscosity of Mixtures With 75% RO-R'

25% Additive Components ^a			Mixture With 75% HRL-2N42 ^b	
Class	Cmpds	Mole % In Mixture	Viscosity η_{25° , cP	Density at 25°C
ROSOR'	10604	12.96	49.0	1.106
	10606	12.04		
RO-OR'	10-04	10.61	46.4	1.098
	10-06	14.39		
RSOR'	1606	25.00	42.5	1.088
R-OR'	1-06	23.27	42.0	1.081
	3-07	1.73		
ROSR'	4063	25.00	34.9	1.079
RO-R'	40-3	20.53	34.7	1.073
	40-6	4.47		

^aAdditives have $\bar{L} = 22.50 \text{ \AA}$.

^bMixtures with additives have $\bar{L} = 20.92 \text{ \AA}$.

Table X. Calculated Viscosity of Additives When Used in RO-R' Mixture

Amount of Additives ^a	25%	25%	25%	10%	10 to 25%
\bar{L} of Additives, Å	22.50	27.03	Various	27.03	Various
\bar{L} of Mixture, Å	20.92	22.05	23.00	21.05	22
η_{calc} at 25°C	η_{class}^c				
R(CN)- ϕ OR'		363		257	310
R(CN)- ϕ R'			(209) ^b	(192) ^b	200
R- ϕ OR'				157	160
R-(Cl)OOC ϕ R'		156	152	149	153
R-OOC ϕ R'		134		~123	130
ROSOR'	92				92
RO-OR'	82	88	80	~77	82
NC-R			82		82
RO-OOCR'		74			74
R ϕ -R'; R- ϕ R'		73		~66	71
RSOR'	66				66
R ϕ -R'				~61	65
R-OR'	64	50			55
R-OOCR'		43			43
ROSR'	36				37
RO-R'	[35]	[36]	[37]	[35]	36
R-R'		18	22		19
RO[C]R		16			16

^aIn HRL-2N42.^bAddition of 7(CN)- ϕ 5, whose \bar{L} = 31.50 Å, gives a 25% mixture with 79.9 cP and 23.17 Å and a 10% mixture with 50.2 cP and 21.50 Å.^cAssigned class viscosity at 25°C in RO-R' mixtures.

Table XI. Comparison of Calculated vs Observed Viscosities
of Ester Eutectic Mixtures

A. Single Class Mixtures

Class	Mixture	\bar{L} (Å)	η_{25° (cP)	Assigned Viscosity ^a	
				η_{class}	Variation
R-(C1)OOC†R'	HRL-2P37 ^b	28.05	249	153	-39%
RO-OR'	HRL-2N54 ^b	23.23	106	84	-21%
R-OR'	HRL-2P15 ^c	21.93	50.3	55	+9%
R-OR'	HRL-2P17 ^c	22.15	46.6	55	+18%
R-OOCR'	Merck S1008 ^b	26.12	41.0	43	+5%
RO-R'	HRL-2N43	22.37	36.5	36	-1%
RO-[C]R'	HRL-6N7 ^e	21.20	16.3	16	-2%
RO-[C]R'	HRL-6N5 ^e	22.71	20.5	16	-22%

B. Multiple Class Mixtures

Mixture	No. Classes	% RO-R'	\bar{L} (Å)	η_{25° (cP)	Calc. Viscosity ^a	
					η_{calc}	Variation
HRL-2N25 ^b	2	77.2	24.48	48.5	47	-3%
HRL-2N40 ^f	2	75.5	22.68	46.4	48	+3%
HRL-2N52 ^g	3	38.4	24.90	64.2	63	-2%
HRL-25N4 ^g	4	42.0	23.92	59.2	58	-2%
HRL-26N3 ^g	4	26.6	26.41	47.8	49	+2%
HRL-26N4 ^g	4	22.8	23.29	49.3	54	+9%
HRL-246N1 ^g	4	18.1	26.28	66.6	80	+20%
HRL-256N5 ^g	6	14.9	23.32	58.2	59	+1%

^aUsing class viscosities calc. from η in RO-R' mixtures. ^bThis paper.

^cSee ref. 3. ^dSee ref. 1. ^eSee ref. 2. ^fSee ref. 6. ^gSee ref. 4.

STRUCTURE CLASS	CLASS CODE	APPROX CLASS VISCOSITY (η_{CLASS})
	R(CN) ϕ OR'	310
	R(CN) ϕ R'	200
	R ϕ OR'	160
	R (Cl)OOC ϕ R'	153
	R OOC ϕ R'	130
	RO-S-OR'	92
	RO-OR'	82
	NC-R'	82
	R ϕ R'	77
	RO-OOCR'	74
	R ϕ R'	65
	R-S-OR'	58
	R-OR'	55
	R-OOCR'	43
	RO-S-R'	37
	RO-R'	36
	R-R'	19
	RO-(Cl)R'	16

Figure 1. Structure, class code, and class viscosities of LC ester components. (The η_{class} at 25°C apply when 10 to 25% of these components are used in RO-R' mixture with L \sim 22 Å.)

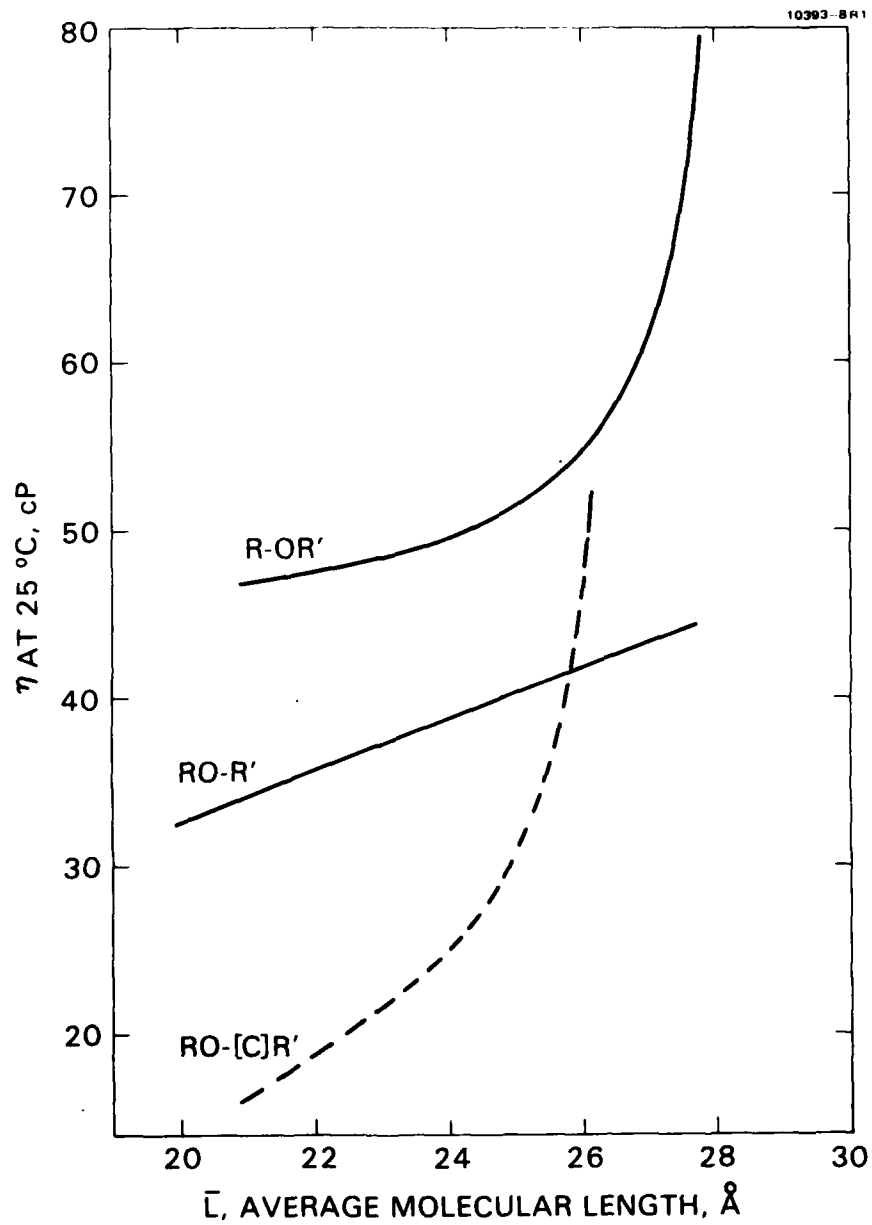


Figure 2. Effect of \bar{L} on the viscosity of three series of single class ester LC mixtures.

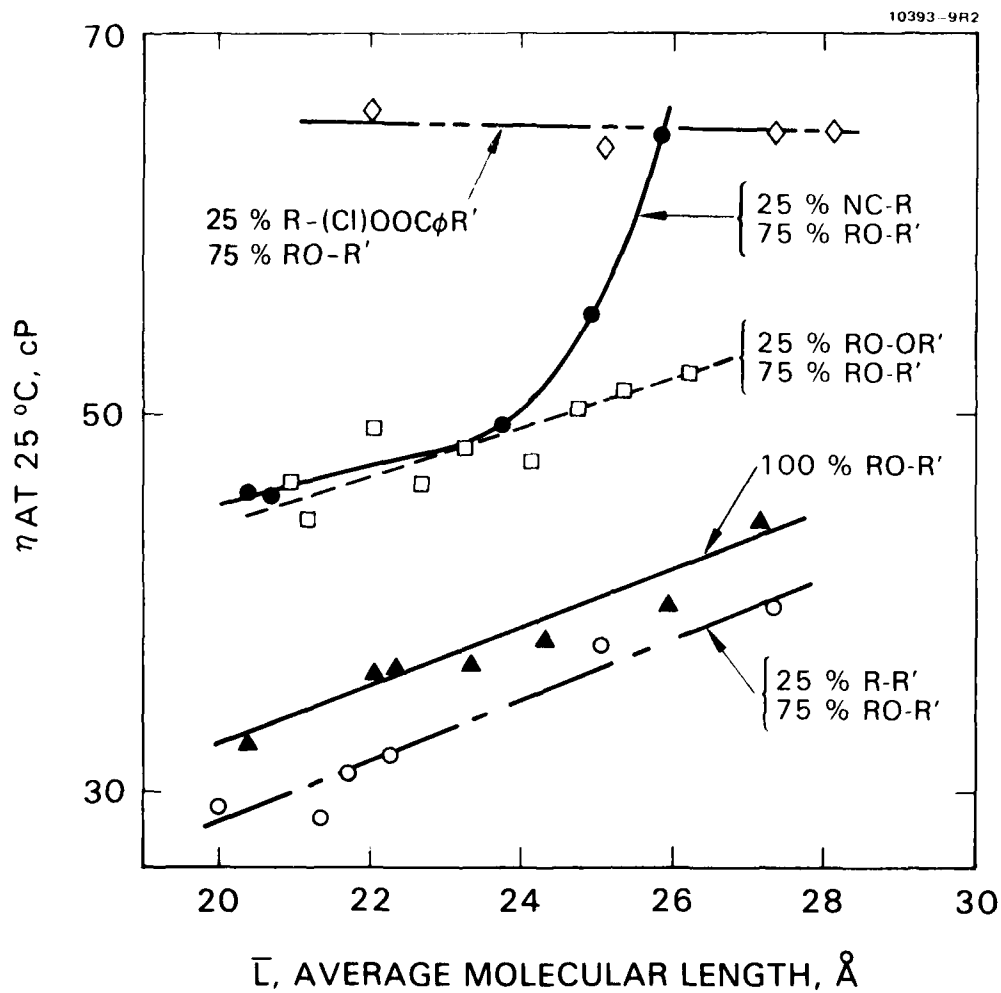


Figure 3. Effect of \bar{L} on η_{25° of RO-R' mixture and of RO-R' mixtures with 25% of other LC components.

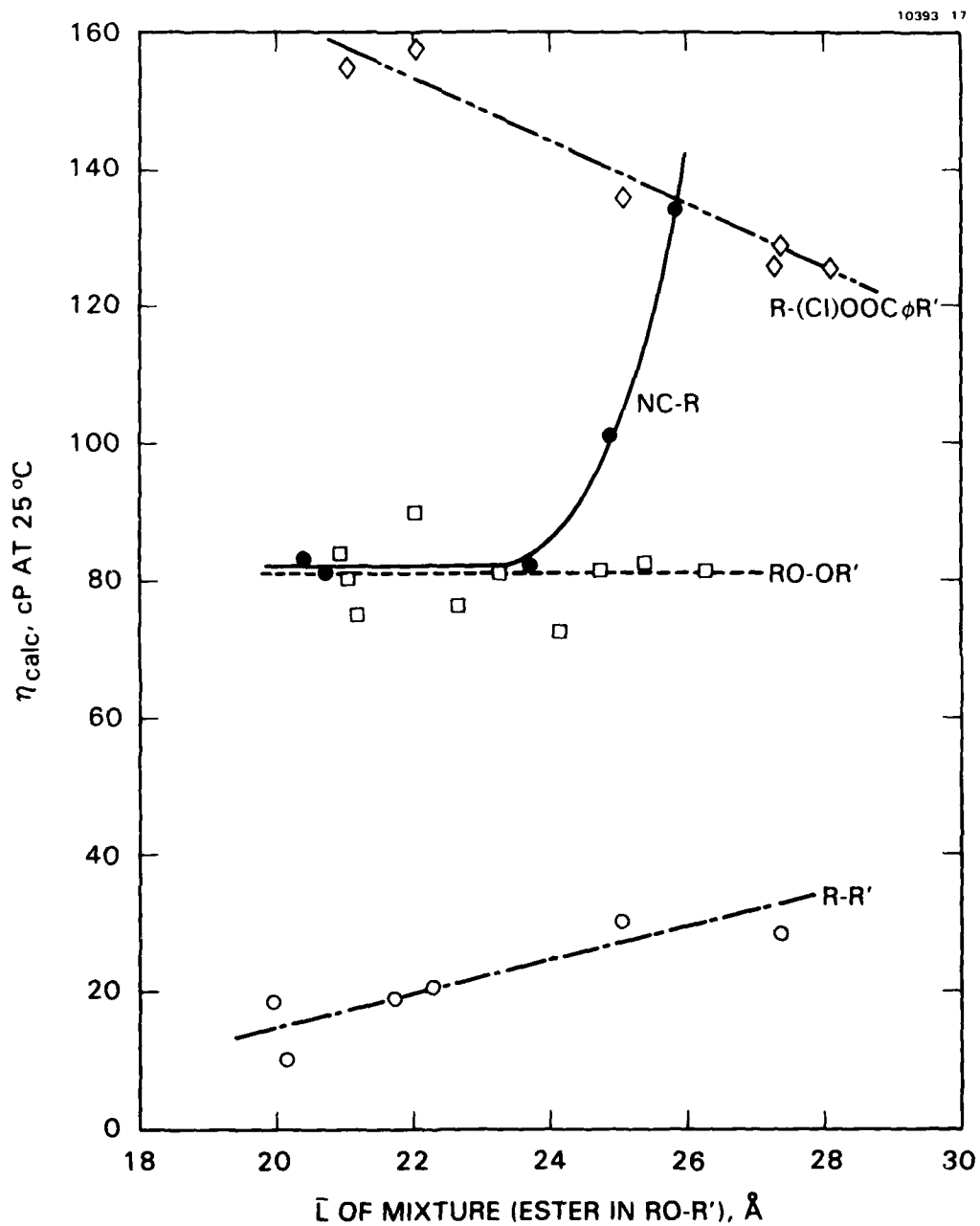


Figure 4. Effect of \bar{L} on η_{calc} of the 25% components in RO-R' mixtures.

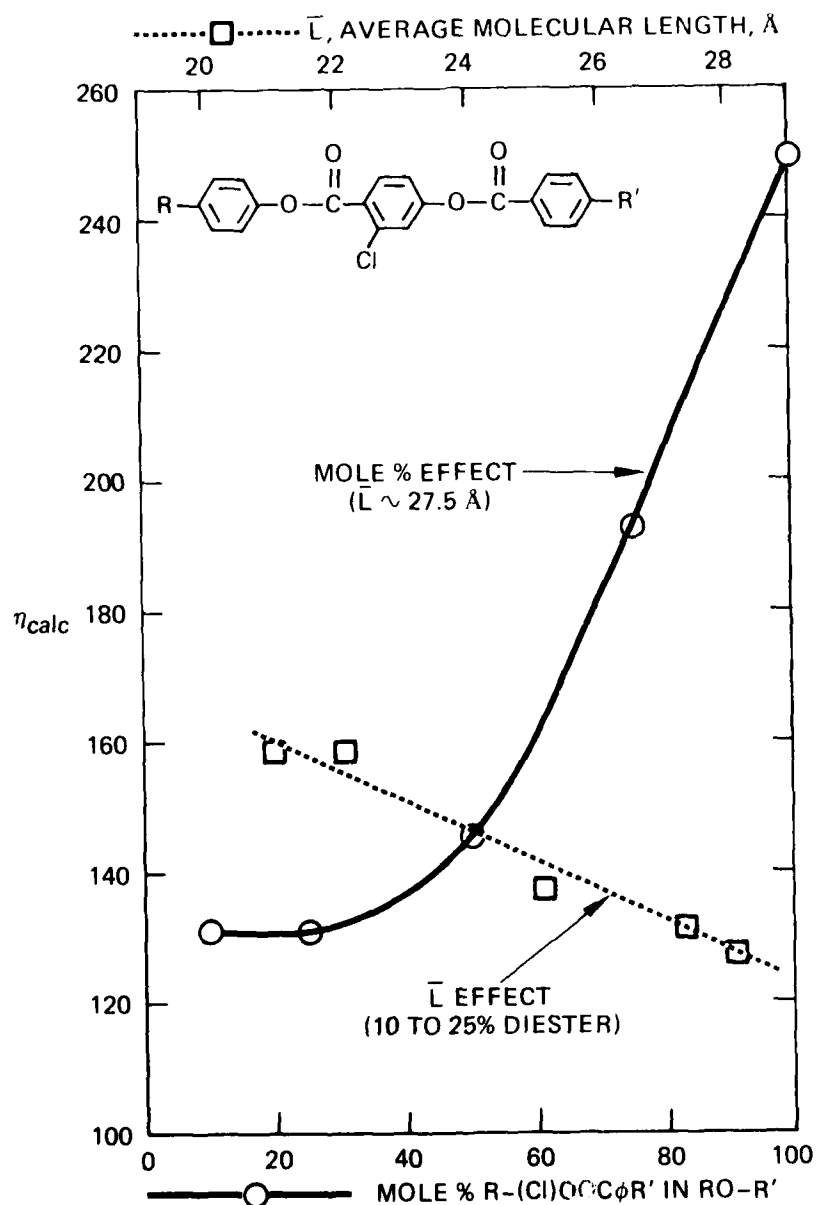


Figure 5. Effect of \bar{L} and concentration of a diester on its η_{calc} from η_{25° in RO-R' mixtures.

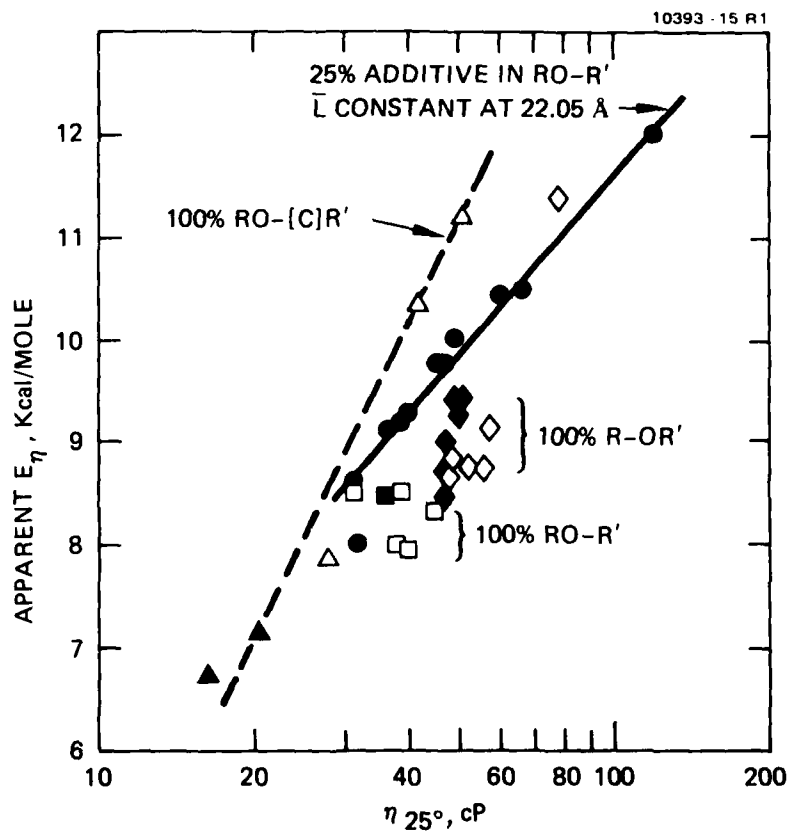


Figure 6. Dependence of apparent activation energy of viscosity between 25 and 40°C on η_{25° . (The dark points all have \bar{L} close to 22 Å, the open points have longer \bar{L} s)

APPENDIX VI

FACTORS AFFECTING THE DYNAMIC SCATTERING OF A NEMATIC ESTER MIXTURE

J. David Margerum, Anna M. Lackner, Hong S. Lim,
and John E. Jensen
Hughes Research Laboratories
3011 Malibu Canyon Road
Malibu, California 90265

Abstract

Various factors affecting the anisotropic and dynamic scattering (DS) characteristics of a 3-component eutectic mixture of phenyl benzoates are investigated in detail. The effects of dopant, surface alignment, signal, cell thickness, and temperature are studied. Variations in the conductivity anisotropy of the dopants has the largest effect on the DS threshold voltage at room temperature. However, cell thickness also changed the threshold slightly and has a large effect on the magnitude of the scattering obtained above threshold. Thinner cells give higher DS levels and higher multiplexing capabilities. The optical density of scattering increases linearly with the reciprocal of cell thickness. When the temperature is increased the DS threshold voltage decreases, indicating that changes in viscosity and elastic constants with temperature are more significant than the decrease in conductivity anisotropy.

I. Introduction

We are interested in using the dynamic scattering (DS) mode¹ in liquid crystal (LC) devices such as pictorial matrix displays^{2,3,4} reticle devices^{5,6} and automobile dashboard displays⁷. Phenyl benzoate ester mixtures of negative dielectric anisotropy are of interest for DS, because they are colorless, can be purified adequately for controlled doping⁸, show good dc stability when used

with redox dopants^{1,10}, and have relatively good thermal stability at elevated temperatures¹¹. In many of these applications it is desirable to have a low threshold voltage (V_{th}) for the DS mode. The present study is designed to evaluate, in detail, the factors affecting the V_{th} and scattering levels of a phenyl benzoate LC mixture. These factors include the conductivity dopant, resistivity, temperature, surface alignment, applied signal, and cell thickness. A simple LC eutectic mixture (HRL-2N25) containing just three phenyl benzoate components is used for these studies, and its properties are also characterized as a function of temperature.

II. Experimental

Most of the experimental techniques employed are described in recent publications^{11,12}. The ester LC components are synthesized and purified by standard methods. Liquid chromatography analysis indicates that these components have less than 0.1% impurity. The room temperature resistivity of the undoped LC mixture is greater than 10^{11} ohm-cm, typically about 4×10^{11} ohm-cm. The dopants are prepared as follows: Tetracyanoethylene (TCNE) from Aldrich is recrystallized from methylene chloride and then sublimed at 70°C; tetrabutylammonium trifluoromethanesulfonate (TBATMS) is prepared as previously reported⁸; ethylpyridinium tetraphenylboride (EPTPB) and tetrabutylammonium tetraphenylboride (TBATPB) are prepared in the manner described by Mann¹³, with recrystallization from acetone/water solutions before drying; dibutylferrocene (DBF) from Research Organic Chem. is distilled at 115°C at 0.3mm; (2,4,7-trinitrofluorenylidene)malanonitrile from Aldrich is recrystallized from acetonitrile; dodecyl(ethyl)dimethylammonium p-hexyloxybenzoate (ZLI-235) is used as obtained from E. Merck. The DS is measured⁹ in transmission and the V_{th} is obtained by

extrapolation back to the baseline of no scattering. Several different surface alignment techniques are used. Cells with surface-parallel LC alignment are made by rubbing ITO (indium tin oxide) electrode surfaces, or by rubbing a thin coating of polyvinyl alcohol (PVA) on ITO after drying in an oven, or by shallow angle ion beam etching of ITO, or by medium angle deposition (MAD) of SiO on ITO¹⁴. The surface-perpendicular LC alignment is made by bonding a long chain alcohol ($C_{18}H_{37}OH$) onto a thin (150Å) coating of MAD-SiO on ITO, except in the field effect measurements (no DS) where the C_{18} alcohol treatment is used on a SiO_2 (800 Å) coating in order to minimize the tilt angle.¹⁵ Cell thickness variations are made using various Mylar films as perimeter spacers for normal thickness. The actual thickness of the thinner LC cells is calculated from the resistance measurements of each cell and the resistivity of each LC sample in thicker cells (50.8 or 127 μm). The width of the Williams domains¹⁶ is measured with a Zeiss Standard WL polarizing microscope, using minimum applied voltages in the range of 1.04 to 1.23 times V_{th} .

III. Results and Discussion

III.A. LC Eutectic Mixture

A three component eutectic ester mixture, identified as HRL-2N25, is formulated using p-ethoxyphenyl p-propylbenzoate (20-3), p-hexyloxyphenyl p-butylbenzoate (60-4), and p-hexyloxyphenyl p-methoxybenzoate (60-01) as shown in Table I. The ratio of components is calculated with the Schroeder-van Laar equation. The actual nematic range, observed by differential scanning calorimetry, has both a lower melting point and clearpoint than the calculated values. Several other properties of the mixture are also summarized in Table I, including the average molecular length (\bar{L}) which is determined from measurements of

molecular models in the extended configuration¹⁷. The dielectric anisotropy (ϵ_a) is more negative than mixtures of 100% RO-R' (e.g. 20-3, 60-4, etc.) components¹⁷. The capillary flow viscosity (η) is relatively high due to the medium size \bar{L} and the presence of the RO-OR' (60-01) component, as shown by recent studies of RO-R'/RO-OR' mixtures¹⁷. The viscosity data fit the expression $\eta = A \exp (E/RT)$ quite well.

III.B Dopants and Conductivity Anisotropy

Purified mixtures are usually not conductive and will show DS effects only if ionic species are present or are generated by the applied field. Both the ionic conductivity and its anisotropy depend upon the structure of dopant as well as the LC^{8,18,19}. The six dopants in this study are chosen to provide a wide range of conductivity anisotropy ($\sigma_{\parallel}/\sigma_{\perp}$) values. In this ester mixture the $\sigma_{\parallel}/\sigma_{\perp}$ of each dopant except TBATMS is nearly independent of concentration, as indicated in Figure 1. Except for EPTPB, these dopants have been studied in various other LCs and similar results are found here. In HRL-2N25 at 25°C the $\sigma_{\parallel}/\sigma_{\perp}$ value is 4 to 6% higher for TBATMS, TBATPB, and DBF/TFM than in the HRL-2N10 ester mixture⁸, is 5% lower for ZLI-235 than in a Schiff base-ester mixture²⁰, and is 3% lower than TCNE in an azoxy LC²¹. Although changes in the dopant structure often have a larger effect on the $\sigma_{\parallel}/\sigma_{\perp}$ of nematic mixtures than changes in the LC structure, much larger variations of $\sigma_{\parallel}/\sigma_{\perp}$ are observed in other LC mixtures in which cybotactic nematic characteristics are present^{11,12,22}.

IV. Effects of Dopant, Alignment, and Signal on V_{th}

Figure 2 shows plots of V_{th} for ac-DS (30 Hz for both surface-perpendicular and surface-parallel cells) and for dc-DS (surface-parallel), each as a function

of the conductivity anisotropy of the six dopants in HRL-2N25. The dopants are identified by number, as indicated in Figure 1. In these samples the DS cut-off frequency is greater than 250 Hz, so that approximately constant V_{th} values are observed for dopants 2-6 in the 10-30 Hz range. In dopant 1 (TCNE) electrochemical reactions at 10 Hz are observed to lower the V_{th} value, and there also may be a slight effect at 30 Hz because of the high voltages. The $\sigma_{||}/\sigma_{\perp}$ has a very large effect on V_{th} in both of the surface alignments and with dc-DS as well as ac-DS. (The dc-DS measurements are less reproducible, but typical V_{th} values are shown here. The relatively high dc- V_{th} for dopant 6 may be due partly to its strong tendency to cause surface-1 alignment.) For a given dopant (i.e. $\sigma_{||}/\sigma_{\perp}$ value in Figure 2) the DS thresholds here follow the pattern: $ac-V_{th}(1) > ac-V_{th}(II) > dc-V_{th}(II)$. This supports some earlier observations discussed regarding other LC/dopant systems²³. Charge injection effects¹⁰ appear to play a dominant in the dc-activated cells. In contrast to ac-activation, the microscopic patterns of the instability under dc-activation vary with the individual dopants. The general appearance of these patterns are similar to a wallpaper pattern while the ac-activated Williams domains consist of many parallel line domains. The dc- V_{th} decreases with increasing $\sigma_{||}/\sigma_{\perp}$, but the values do not fit the correlation derived by Helfrich²⁴ for the Williams domain threshold variation with $\sigma_{||}/\sigma_{\perp}$, even though the expression was derived for dc fields. It should be noted that the values of $\sigma_{||}/\sigma_{\perp}$ are obtained with ac measurements at 100Hz. This gives the $\sigma_{||}/\sigma_{\perp}$ for the ionic species present in the bulk of the LC from the dopant under equilibrium conditions. It does not measure the conductivity anisotropy of electrochemically generated ionic species which are formed by dc activation, and such ions could have a larger anisotropy than the dopants. If the ionic transport in the dc cells is carried by both dopant ions

and de-generated ions of higher $\sigma_{\parallel}/\sigma_{\perp}$, then this could explain the observed dc results.

The qualitative expressions derived by Helfrich²⁴ for the V_{th} of Williams domains (corresponding here to the ac- V_{th} of DS) indicate that the correlations shown in equations (1) and (2) should be followed if small amounts of conductivity dopants in HRL-2N25 change only its $\sigma_{\parallel}/\sigma_{\perp}$, and do not affect the values of A, B, C and D.

• Surface- \parallel :

$$V_{th}^{-2} = A \left(\frac{\sigma_{\parallel}}{\sigma_{\perp}} \right)^{-1} + B ,$$

where

$$A = \frac{1}{4\pi^3 k_{33}} \left(\Delta\epsilon - \frac{K_1 \epsilon_{\parallel}}{\eta_1} \right); \quad B = \frac{K_1 \epsilon_{\perp}}{4\pi^3 k_{33} \eta_1}$$

• Surface- \perp :

$$V_{th}^{-2} = C \left(\frac{\sigma_{\parallel}}{\sigma_{\perp}} \right) + D ,$$

where

$$C = \frac{-1}{4\pi^3 k_{11}} \left(\Delta\epsilon + \frac{K_2 \epsilon_{\perp}}{\eta_2} \right); \quad D = \frac{K_2 \epsilon_{\parallel}}{4\pi^3 k_{11} \eta_2}$$

The expressions of V_{th} with ac activation^{25,26} contain extra terms of frequency dependence. However, these terms drop out if the frequency applied is substantially below the cut-off frequency, which is the case in the present studies. Using the ac data from Figure 2, there is a good fit of the surface-parallel data with Equation 1, and of the surface-perpendicular data with Equation 2, as shown by the least-square plots in Figure 3. These results indicate that in

each of these surface alignment boundary conditions the effects of various dopants on the $ac-V_{th}$ is determined largely by the $\sigma_{||}/\sigma_{\perp}$ values of the dopant in the LC.

V. Effects of Resistivity on V_{th}

Some effects of LC resistivity (ρ) on the ac and dc values of V_{th} are shown in Figure 4 for dopants 2, 4, and 5. In each case the $ac-V_{th}$ increases as ρ increases. In the TBATMS samples, the change in $ac-V_{th}$ is partially accounted for by the changes of its $\sigma_{||}/\sigma_{\perp}$ with ρ which are shown in Figure 1. However, the $\sigma_{||}/\sigma_{\perp}$ values of TBATPB and DBF/TFM are constant with ρ so some other (unknown) factor affects their V_{th} . The $dc-V_{th}$ effects vary with the electrochemical properties of the dopants. The $dc-V_{th}$ of TBATMS-doped samples decreases markedly as ρ increases. This dopant is more electrochemically stable than the LC, and the LC probably reacts under a dc field to give LC^+ and LC^- species^{9,10} which may have relatively high $\sigma_{||}/\sigma_{\perp}$ values. At a ρ of 10^9 ohm-cm the LC contains about 10^{-4} M TBATMS, giving an ionic concentration of approximately 10^{-5} M. As the ionic concentration is decreased, the concentration of the positive ions in the vicinity of the positive electrode and of the negative ions in the vicinity of the negative electrode will be decreased as a result of coulombic interaction. Thus, dc generated LC ions would be expected to contribute to the ionic transport current, and we believe that this becomes more significant as ρ is increased. The ρ of the TBATMS-doped cells under continuous, dc-DS decreases significantly only after hours of activation,⁹ presumably due to irreversible reactions of the LC^+ and LC^- species. On the other hand, the ρ of TBATPB-doped samples change fairly rapidly (in 10 minutes) with dc-activation, indicating that the dopant itself reacts readily and irreversibly at the electrodes. These reactions of TBATPB appear to result in species of high $\sigma_{||}/\sigma_{\perp}$, giving low $dc-V_{th}$ values for

the short lifetime period of the samples. The DBF/TFM dopant pair is a redox system chosen to protect the LC by reacting readily and reversibly at the electrodes^{9,10}. For a ρ of 10^9 ohm-cm the neutral DBF and TFM compounds are each added in about 3×10^{-2} M, so that there are larger concentrations of these redox dopants present than is the case with the salt dopants. Because of their electrochemical stability and the amounts of DBF and TFM present, the dc- V_{th} is relatively stable for very long periods of dc activation. The variations of dc- V_{th} for DBF/TFM in Figure 4 may be due to some differences in the surface adsorption of these dopants on the electrodes.

VI. Effects of Cell Thickness

The ac- V_{th} of DS is not constant with the thickness of the cell, as shown by the upper plot in Figure 5. There is a V_{th} minimum at thicknesses of approximately 25 μ m. In thicker cells the V_{th} increases appreciably, possibly due to the increase in the l/λ term as shown by the lower curve in Figure 5 (where λ is the Williams domain periodicity). However, in cells thinner than 25 μ m the V_{th} also increases while the l/λ term decreases. We do not know the reason for the increased V_{th} in thin cells. Cells with and without PVA coatings for surface- π alignment gave the same results, so the effect does not appear to be an artifact related to a voltage drop across the PVA. Also the resistivity changes have little effect in this range used: ρ between 6.15×10^8 and 1.36×10^9 ohm-cm.

The scattering level of DS (where % S = 100 - % T for cells measured in transmission) is higher in thinner cells. This is shown in Figure 6, where the % S is plotted versus cell thickness at $2 \times V_{th}$ at that thickness. The % S increases sharply in thin cells (we did not use cells thin enough to observe

the expected decrease in very thin cells.) We found a linear relationship between the optical density of scattering and the reciprocal of the cell thickness as shown in Figure 7. In Figures 6 and 7 the maximum multiplexing capability (N_{\max}) for 70% S is also shown. The N_{\max} increases greatly in thin cells, which of course also have the advantages of having much faster response times.

VII. Temperature Effects

The effects of temperature on several anisotropic and electro-optical properties of HRL-2N25 are shown in Figures 8 and 9. The Freedericks transition in Figure 8 refers to the field effect threshold in a surface-1 cell. The values of $(V_{th}')_{FE}$ and $\Delta\epsilon$ in Figure 8 are used to calculate the k_{33} elastic constant shown in Figure 9. The $\sigma_{\parallel}/\sigma_{\perp}$ and V_{th} values of DS are measured using TBATPB as a conductivity dopant. The most interesting result in Figure 9 is that the $DS-V_{th}$ values decrease with increasing temperature (at least up to 50°C) while the $\sigma_{\parallel}/\sigma_{\perp}$ decrease in the same temperature range. This is surprising considering the large effect that $\sigma_{\parallel}/\sigma_{\perp}$ has on the V_{th} (see Figure 2). It indicates that the temperature effects on other parameters such as elastic constants and viscosity anisotropies are large enough and in the opposite direction, to offset the decrease of $\sigma_{\parallel}/\sigma_{\perp}$. This is supported by the large decreases observed in k_{33} and n with increasing temperature.

ACKNOWLEDGEMENTS

We are indebted to the Directorate of Chemical Sciences, Air Force Office of Scientific Research, Contract F49620-77-C-0017, for partial financial support of this research; and to W.H. Smith, Jr., for assistance in the DSC measurements.

References

1. F. G. Heilmeier, L. A. Zanoni, and L. A. Barton, Proc. IEEE **56**, 1162 (1968).
2. M. H. Ernstoff, A. M. Leupp, M. J. Little, and H. T. Peterson, IEEE Electron Device Conf. Digest, Washington, D.C. (Dec. 1973).
3. J. D. Margerum and L. J. Miller, J. Colloid and Interface Sci. **58** 559 (1977).
4. M. Yoshiyama, T. Matsuo, K. Kawasaki, H. Tatsuta, and T. Ishihara, 8th Int'l Liq. Cryst. Conf. paper I-14, Kyoto, Japan (July 1980).
5. C. H. Gooch, R. Bottomley, J. J. Low, and H. A. Tarry, J. Phys. **E** **6**, 485 (1973).
6. R. P. Farnsworth, L. W. Hill, and S. -Y. Wong, U.S. Patent 3,885,861 (May 27, 1975).
7. Y. Ohsawa, T. Fujii, Y. Okada, and S. Kanabe, 8th Int'l Cryst. Conf., Paper I-26P, Kyoto, Japan (July 1980).
8. J. D. Margerum, H. S. Lim, P. O. Braatz, and A. M. Lackner, Mol. Cryst. Liq. Cryst., **38** 219 (1977).
9. H. S. Lim and J. D. Margerum, Appl. Phys. Lett., **28**, 478 (1976).
10. H. S. Lim, J. D. Margerum, and A. Graube, J. Electrochem. Soc. **124**, 1389 (1977).
11. J. D. Margerum and A. M. Lackner, Mol. Cryst. Liq. Cryst., (in press, 1981).
12. J. D. Margerum, J. E. Jensen, and A. M. Lackner, Mol. Cryst. Liq. Cryst., (in press 1981).
13. C. K. Mann, Electroanalytical Chemistry, A. J. Bard, ed. (Marcel Dekker, N.Y. 1969), **3**, p.132.
14. J. L. Janning, Appl. Phys. Lett. **21**, 173 (1972).
15. L. J. Miller, J. Grinberg, G. D. Myer, D. S. Smythe, and W. S. Smith, Liquid Crystals and Ordered Fluids, J. E. Johnson and R. S. Porter, eds. (Plenum Press, 1978), **3**, p. 513.
16. R. Williams, J. Chem. Phys., **39**, 384 (1963).
17. J. D. Margerum, S. -M. Wong and J. E. Jensen, to be submitted to Mol. Cryst. Liq. Cryst.

18. R. Chang, Liquid Crystals and Ordered Fluids, J. E. Johnson and R. S. Porter, Ed. (Plenum Press, 1974), 2, p. 367.
19. M. I. Barnik, L. M. Blinov, M. F. Grebenkis, S. A. Pinkin, and V. G. Chigrinov, Physics Letters, 51A, 175 (1975).
20. G. Heppke, F. Schneider, Z. Naturforsch., 31A, 611-14, (1976).
21. M. I. Barnik et al., Sov. Phys. - JETP 42, 550 (1976), Zh. Eksp. Teor. Fiz. 69, 1080 (1975).
22. J. D. Margerum, S. -M. Wong, A. M. Lackner, and J. E. Jensen, Mol Cryst. Liq. Cryst., (in press 1981).
23. M. J. Little, H. S. Lim, and J. D. Margerum, Mol. Cryst. Liq. Cryst., 38, 207 (1977).
24. W. Helfrich, J. Chem. Phys., 51, 4092 (1969).
25. Orsay Liquid Crystal Group, (a) Phys. Rev. Lett. 25, 1642 (1970); (b) Mol Cryst. Liq. Cryst., 12, 251 (1971).
26. E. Dubois-Violette, P. G. deGennes and O. Parodi, J. Physique, 32, 305 (1971).
27. P. M. Alt and P. Pleshko, IEEE Trans. Electron Devices, ED-21, 146 (1974).

List of Tables

Table 1. HRL-2N25 Eutectic Mixture

List of Figures

- Figure 1 Conductivity anisotropy of dopants in HRL-2N25 at 23°C as a function of resistivity (ρ_{\perp} at 100 Hz).
- Figure 2 Dynamic scattering threshold voltage as a function of the conductivity anisotropy and surface alignment of HRL-2N25 containing the dopants in Table 1. (23°C, $\rho = 2 \times 10^9 \Omega\text{-cm}$, 13 μm cells
■ - surface-I, ● and ▲ - surface-II).
- Figure 3 Helfrich equation plots for surface-dependence of ac dynamic scattering V_{th} on $\sigma_{\parallel}/\sigma_{\perp}$. (Data from Figure 2).
- Figure 4 Effect of resistivity (ρ_{\perp} at 100 Hz) on dynamic scattering V_{th} of doped HRL-2N25 in 12.7 μm thick cells with surface-II alignment, rubbed ITO.
- Figure 5 Effect of cell thickness of DS- V_{th} and on domain periodicity (λ), 30 Hz.
- Figure 6 The effect of cell thickness on %S and on N_{max} at 70%S (23°C).
- Figure 7 Reciprocal length plots for the optical density of scattering ($-\log T$) and the maximum multiplex capability.
- Figure 8 Temperature effects on dielectric properties and Friedericks transition of HRL-2N25 (undoped).
- Figure 9 Temperature effects on HRL-2N25, with TBATPB dopant.

Table I. HRL-2N25 Eutectic Mixture

Components					
Code	L, Å	mp, °C	clpt., °C	ΔH_f , K _{cal} /Mole	Mole Fraction
20-3	19.67	76	68	6.72	.132
60-4	25.78	29	48	4.20	.640
60-01	23.60	55	80	6.19	.228

Properties

Calc. nematic range: 13° to 57°C

Obs. nematic range: 0° to 54°C

Av. molecular length: $\bar{L} = 24.48 \text{ Å}$ Dielectric anisotropy: $\Delta\epsilon = 0.39$ (24°C, 1kHz)Birefringence: $\Delta n = 0.14$ (23°, 589nm)Freedericks transition: $V_{FT} = 7.0 \text{ V}$ (23°C)Flow viscosity: $\eta = 48.5 \text{ cP}$ (25°C)Viscosity activation energy: $\Delta E_{\eta} = 9.3 \text{ K}_{cal}/\text{mole}$

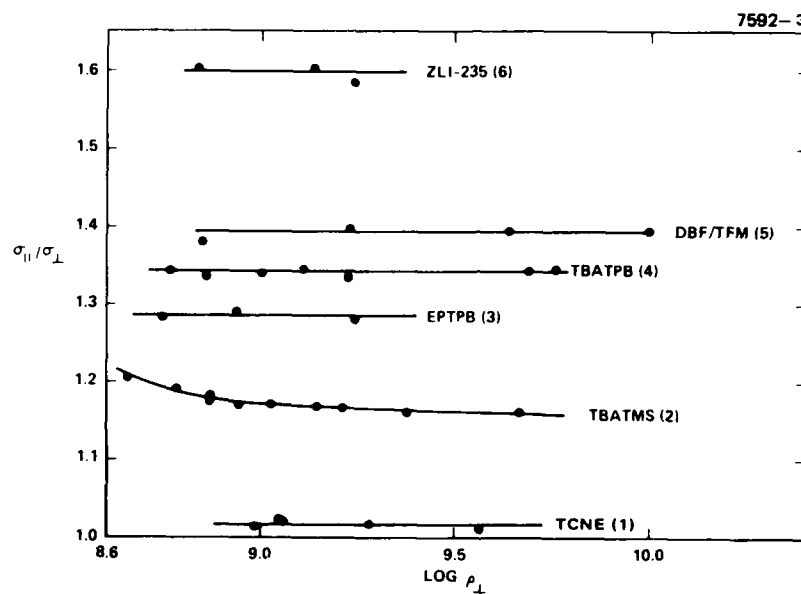


Figure 1. Conductivity anisotropy of dopants in HRL-2N25 at 23°C as a function of resistivity (ρ_{\perp} at 100 Hz).

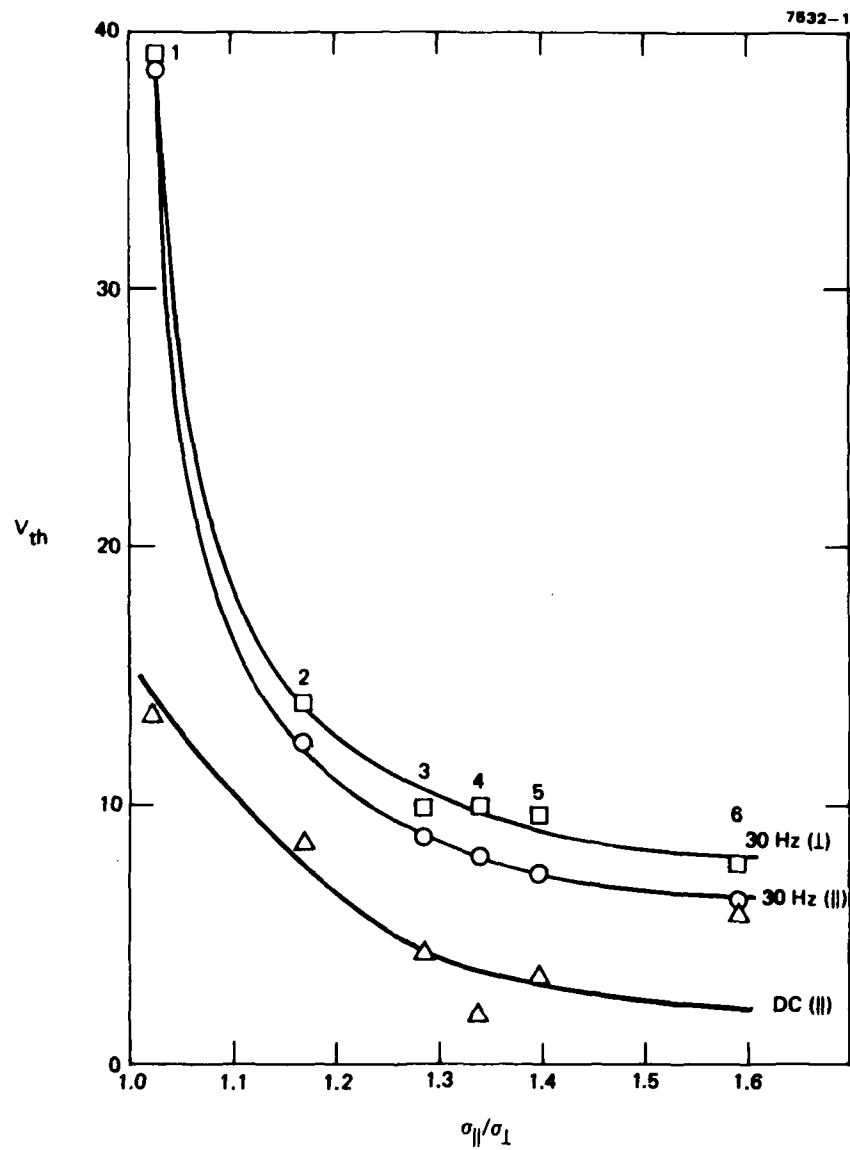


Figure 2. Dynamic scattering threshold voltage as a function of the conductivity anisotropy and surface alignment of HRL-2N25 containing the dopants in Table 1. (23°C , $\rho_{\perp} = 2 \times 10^9 \Omega\text{-cm}$, \square -surface-I, \circ and Δ - surface-II).

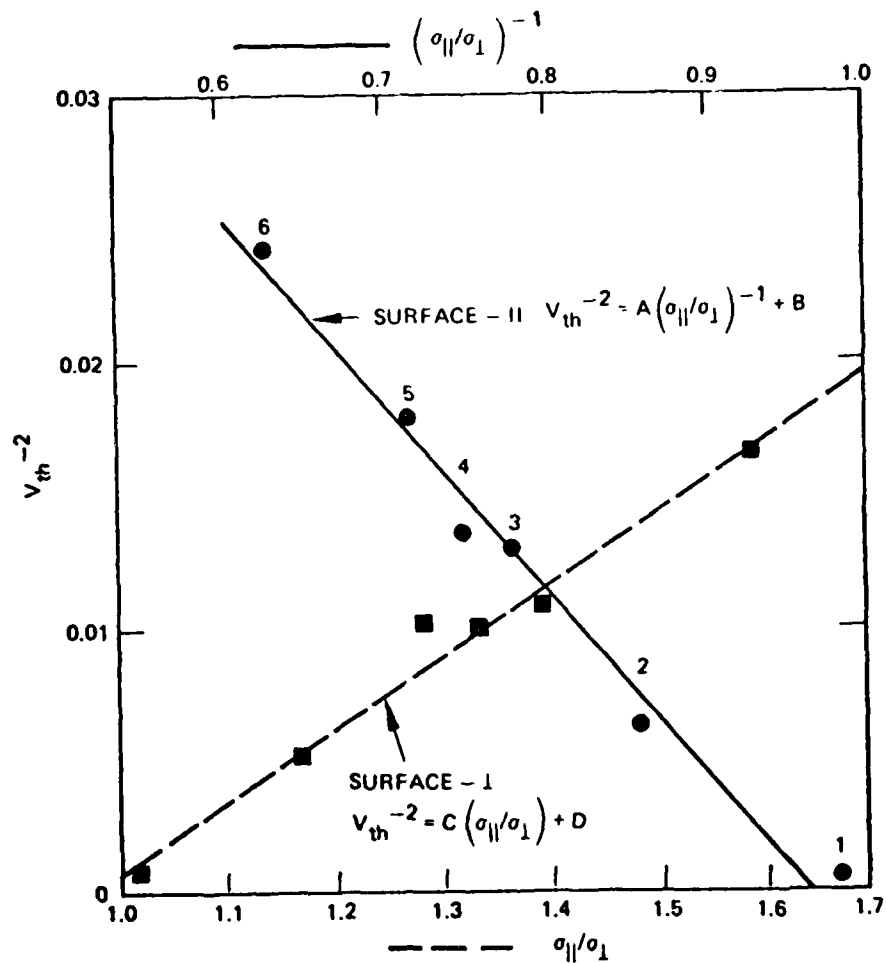


Figure 3. Helfrich equation plots for surface-dependence of ac dynamic scattering V_{th} on $\sigma_{||}/\sigma_{\perp}$.

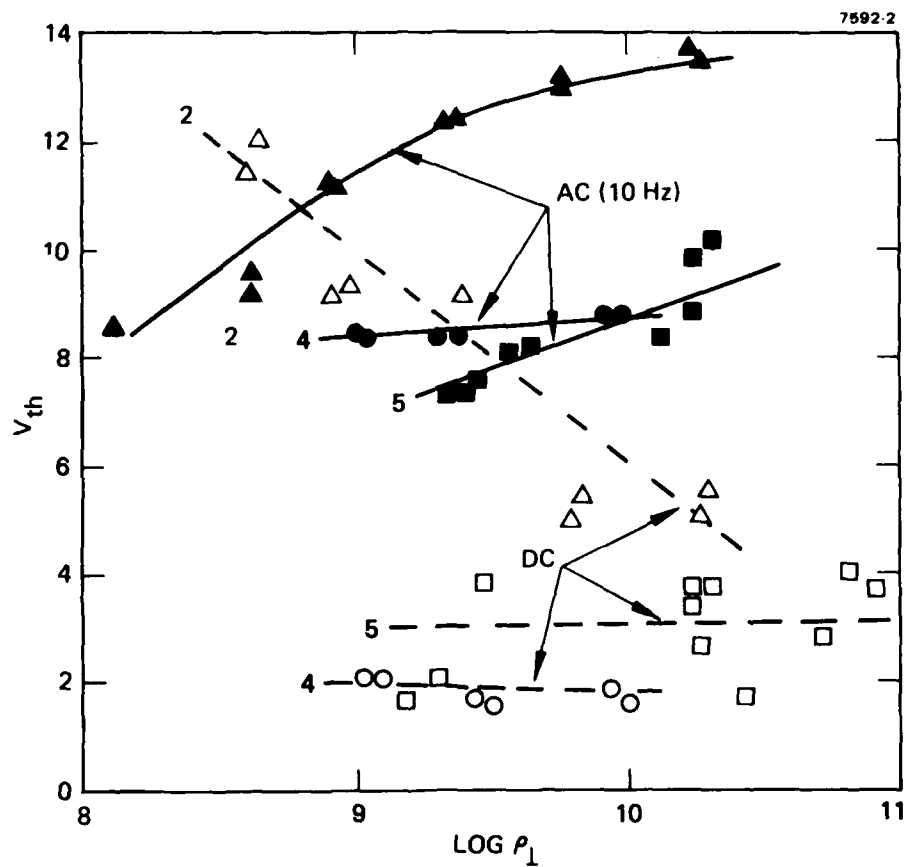


Figure 4. Effect of resistivity (ρ_1 at 100 Hz) on dynamic scattering V_{th} of doped HRL-2N25 in 12.7 μm thick cells with surface- \parallel alignment, rubbed ITO.
 O, ● - TBATPB(4); Δ , \blacktriangle - TBATMS (2); \square , \blacksquare - DBF/TFM (5).

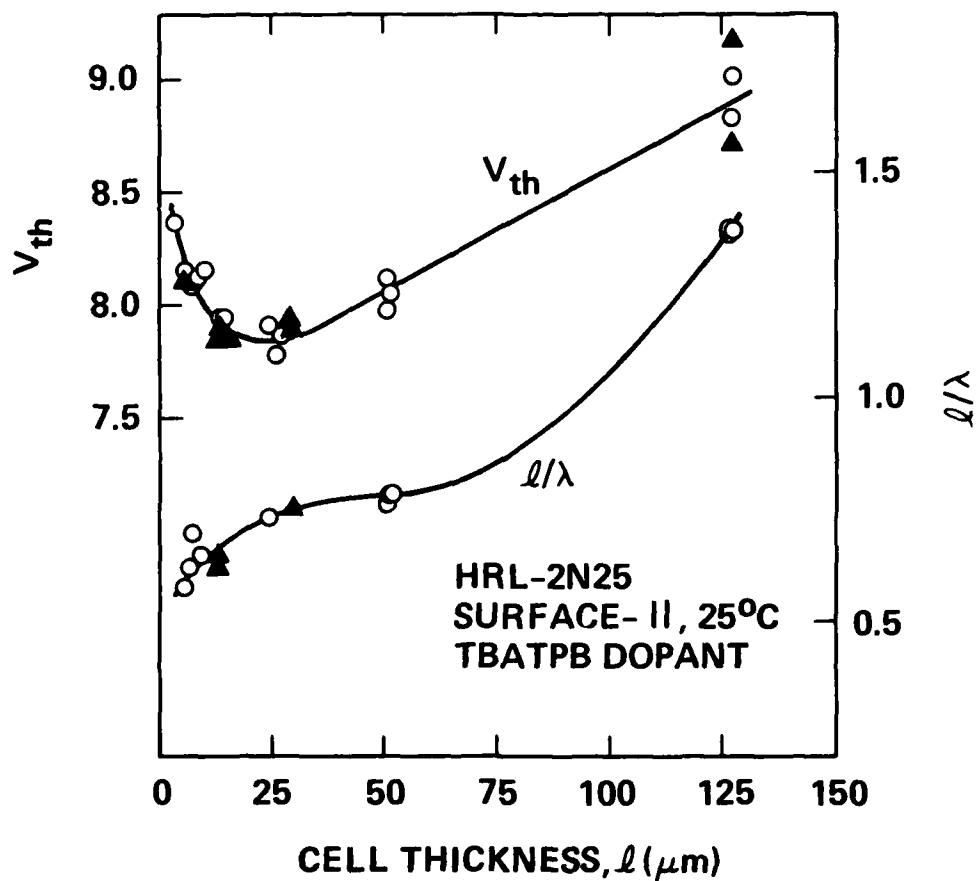


Figure 5. Effect of cell thickness on DS- V_{th} and on domain periodicity (λ), 30 Hz.

○ rubbed PVA on ITO

▲ rubbed ITO, or ion-beam etched ITO.

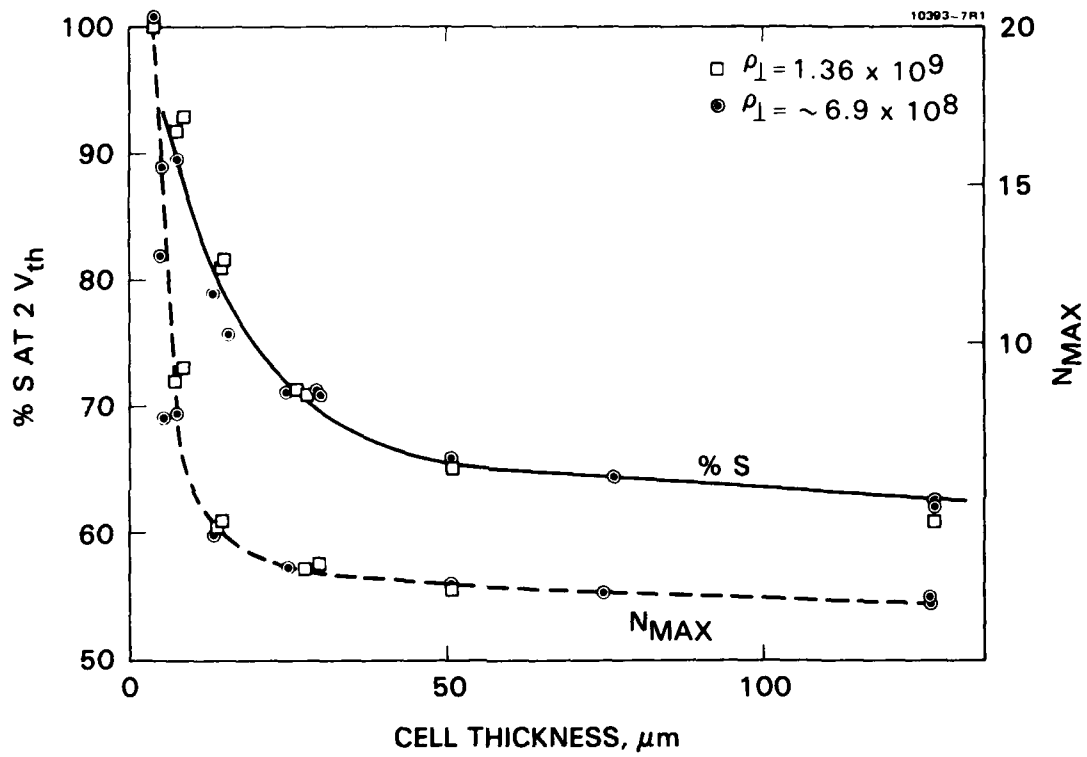


Figure 6. The effect of cell thickness on %S and on N_{max} at 70%S (23°C).

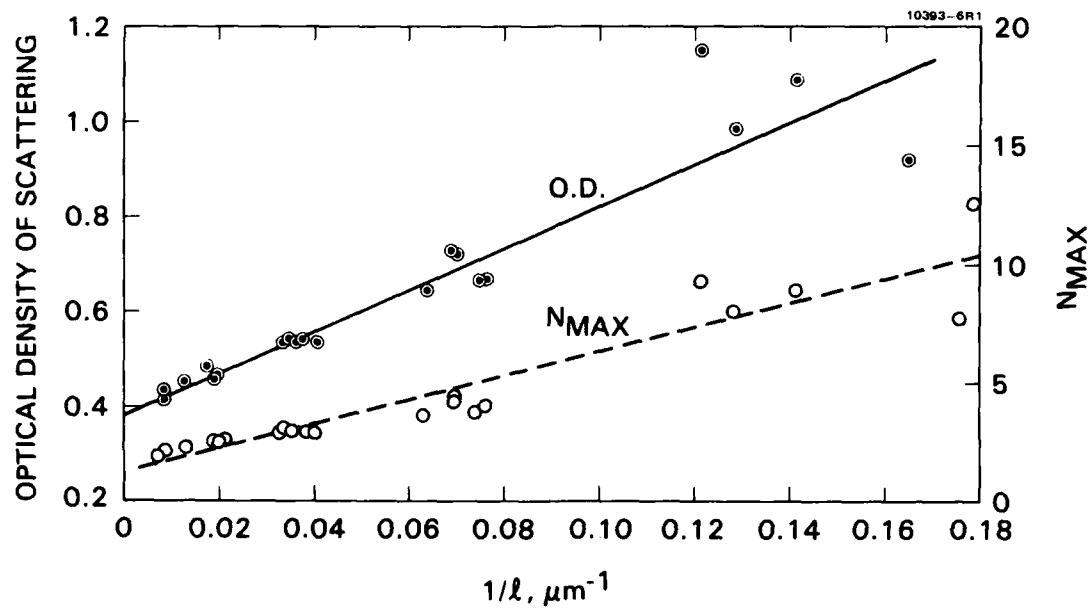


Figure 7. Reciprocal length plots for the optical density of scattering ($-\log T$) and the maximum multiplex capability.

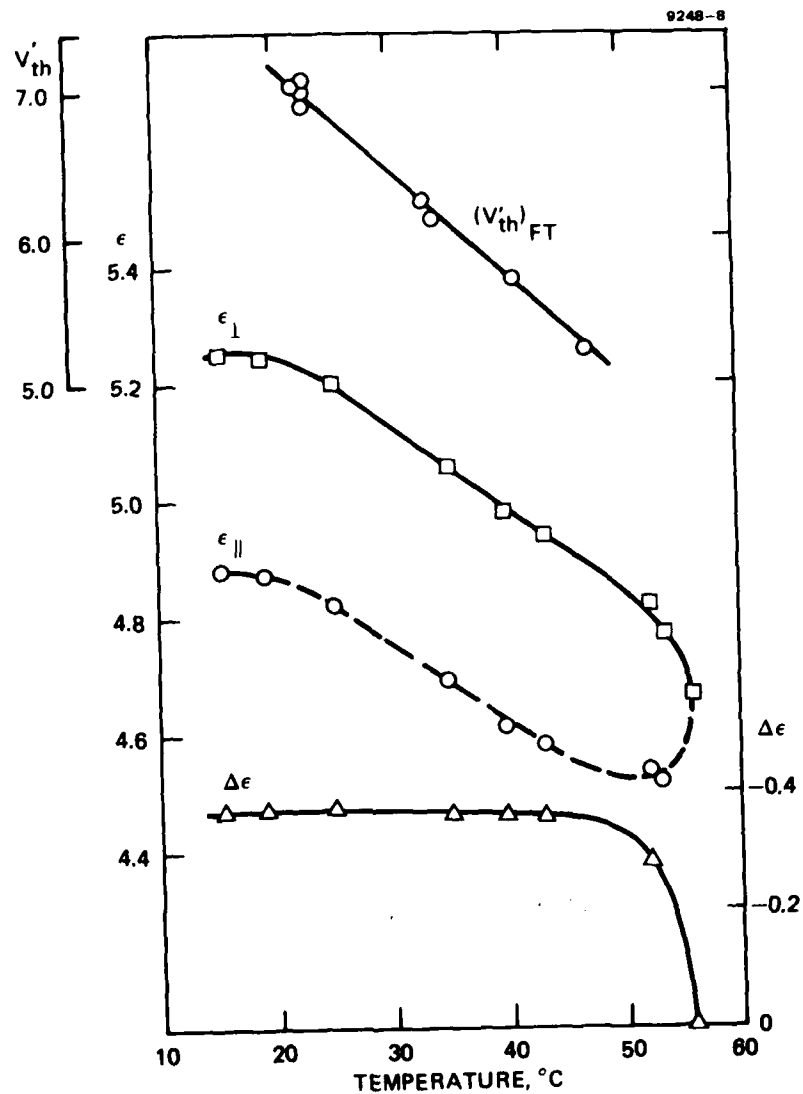


Figure 8. Temperature effects on dielectric properties and Fredericks transition of HRL-2N25 (undoped).

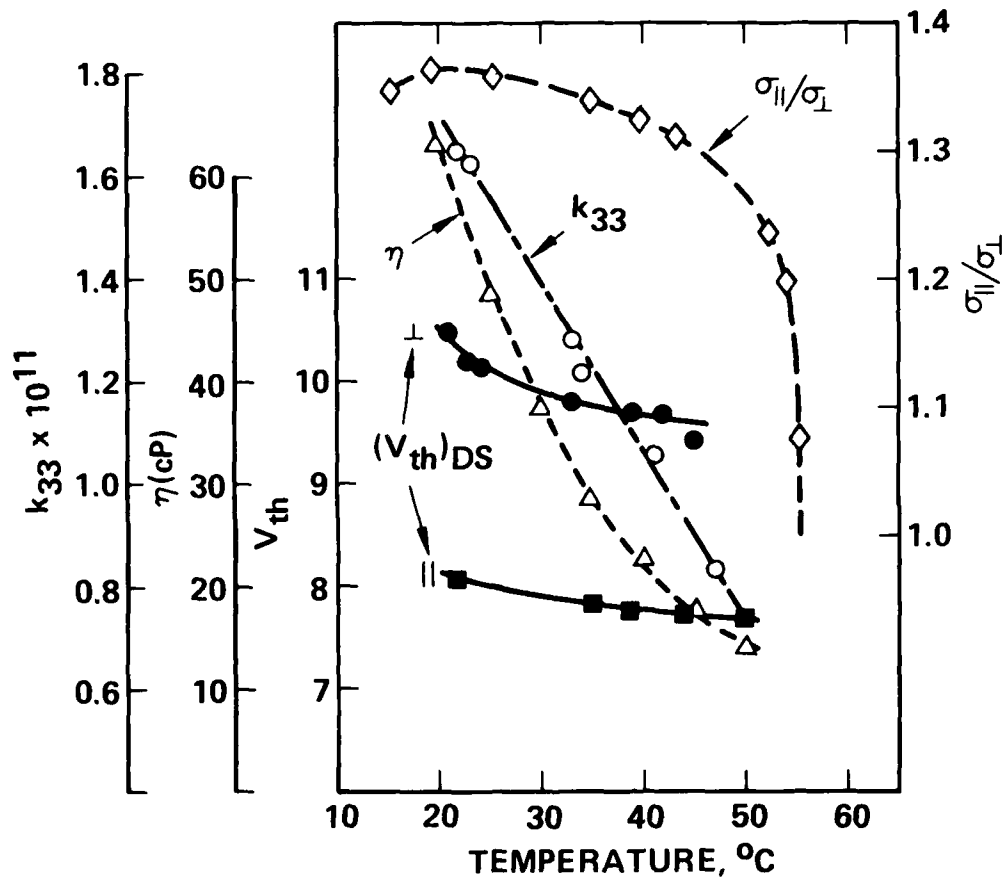


Figure 9. Temperature effects on HRL-2N25, with TBATPB dopant.

END

DATE
FILMED

10-81

DTIC